University
of Southampton

STRUCTURAL PERFORMANCE OF GRP TOP HAT STIFFENED MARINE STRUCTURES

ÖMER EKSIK

A thesis submitted for the partial fulfilment of the degree of
Doctor of Philosophy

FACULTY OF ENGINEERING AND APPLIED SCIENCE
SCHOOL OF ENGINEERING SCIENCES

JUNE 2005

UNIVERSITY OF SOUTHAMPTON

ABSTRACT

FACULTY OF ENGINEERING AND APPLIED SCIENCE

SCHOOL OF ENGINEERING SCIENCES

Doctor of Philosophy

Structural Performance of GRP Top-Hat Stiffened Marine Structures

by Ömer EKSİK

Top-hat stiffened composite structures are widespread in the fibre reinforced plastic (FRP) shipbuilding industry since they can be readily tailored to the complex curvatures of hulls, and provide built-in buoyancy by the fabrication technique of laminating over rigid polymeric foam cores. The longevity and survivability of these structures are affected by harsh conditions prevalent in the ocean environment such as humidity, temperature, impact, wave-slamming loads and cyclic loads. The work described in this thesis has aimed to investigate structural performance of two types of ship's components, namely: (i) top hat beam panels and (ii) cross-stiffened hat-shaped composite panels. These were tested experimentally and analysed theoretically using the finite element method.

As a first step a thorough background study was made to assess previous work in these fields. Current design practices were compared, and the history of their development was traced.

On the experimental side, first a number of coupons were tested to obtain stiffness and strength and fibre content of the layers of the composite structures. Then two types of ship's components have been tested under static loading conditions that may be encountered in service. Structural stiffness issues and their dependence on lay up have been explored. The progressive nature of failure, from matrix cracking through to final collapse was detailed. Numerous strain gauges and digital dial gauges were used to collect important information during the experimentation.

On the theoretical side, finite element models were generated by using the commercial finite element (FE) code ANSYS for these structures. The results have been validated against experimental results directly in the case of global load/deflection results. The finite element derived failure stresses were also compared with the material failure data, at experimental failure loads. This enables further understanding of the internal stress pattern and helps identify the regions of weakness within the structural element which are most susceptible to damage under a variety of loading conditions. Reasonable correlation was found on all accounts. A detailed parametric study has been conducted to examine the influence of geometric variables and material choice on the structural performance of top hat stiffeners.

Overall the results of this work form the first stage in enabling designers to draw up guidelines for scantling the frame systems of FRP boats.

Table of Contents

List of Tables

List of Figures

Acknowledgement

I would like to express my sincere gratitude my supervisors, Prof. Ajit Shenoi and Dr. Han K. Jeong for their supervision, support and encouragement during the period of my research.

Special thank goes to Prof. Stuart S.J. Moy for his consistent support, in my understanding and exploration of the experimental data.

I would like to thank Prof. W.G. Price Head, Department of Ship Science for making the departmental facilities available to me.

I would like to thank my colleagues in Lightweight and Composite Structures Research Group (Ship Science) Dr. A. K. Nayak, Dr. James I. R. Blake, Dr. Gleb Makarov Dr. Sampatkumar Narasimhan and Mr. Stephen Boyd for their stimulating supports and suggestions towards my research.

Thanks go to technicians of Civil Engineering Structural Laboratory for their assistance with the composite tests.

Finally, my deepest gratitude goes to my parents and my wife for love, support and encouragement have made the successful completion of this work possible.

Chapter 1 INTRODUCTION

1.1 Background

Composite materials play an ever-increasing role as a structural material in the construction industry, being used in a wide variety of strategic applications of which the shipbuilding industry has become one of the most important. The use of fibre-reinforced polymer (FRP) in marine fields dates back to late fifties as a result of research by both military and commercial interests. The materials used were almost entirely orthopthalic polyester resins with the E-glass chopped strand mat (CSM), with small amount of cloth used in highly loaded areas. The properties of such material and the overall structural consideration in the design of marine structures are well documented [1]. So far FRP hulls have been used for naval ships, underwater vehicles (submersible), lifeboats, passenger vessel, fishing vessels and pleasure boats [2]. The most significant naval application of FRP has been in the construction of mine hunter vessels. In 1973 a mine hunter vessel HMS WILTON up to 46.6 m was built entirely of glass-reinforced plastic (GRP) for the Royal Navy [3] in the UK. Today FRP ship hulls in naval applications have been produced up to about 72 m, [4] and an example of FRP hull for a sailing yacht approaching 75 m in length has been recently built in UK [5].

The success of FRP materials in becoming the most popular material for the boat building industry is due to a number of advantages [6]:

- Lightweight materials reduce weight directly, giving;
    - Increased payload for given overall dimensions
    - They allow higher speed to be achieved
    - They reduce the fuel consumption
- High strength-to-weight ratio of the material, which is ideal for the construction of ship hulls and makes it a cost-efficient material.
- The ability to fabricate large, complex shape in one piece
- The FRP is corrosion-resistant and has a low maintenance cost.
- The fact that it is non-magnetic

➢ Ability to tailor the stiffness and strength to specific design load

A major constraint to overcome in the design of FRP ships especially that using glass reinforcement is the relatively low modulus of the materials. In a structural context, the drawback from low material stiffness is overcome by employing an appropriate structural topology to give the desired structural stiffness. This is usually achieved by the inclusion of bulkheads and different types of open and close section stiffeners (Figure 1.1) [7]. Among them top hat stiffener is the most attractive alternative not only for its considerable torsional rigidity but also for its ease of construction. The primary task of top-hat stiffeners is to transmit shear stresses between the shell and frame flanges under local bending caused by lateral pressure or concentrated lateral loads. Figure 1.2 illustrates the configuration of the top hat stiffener.

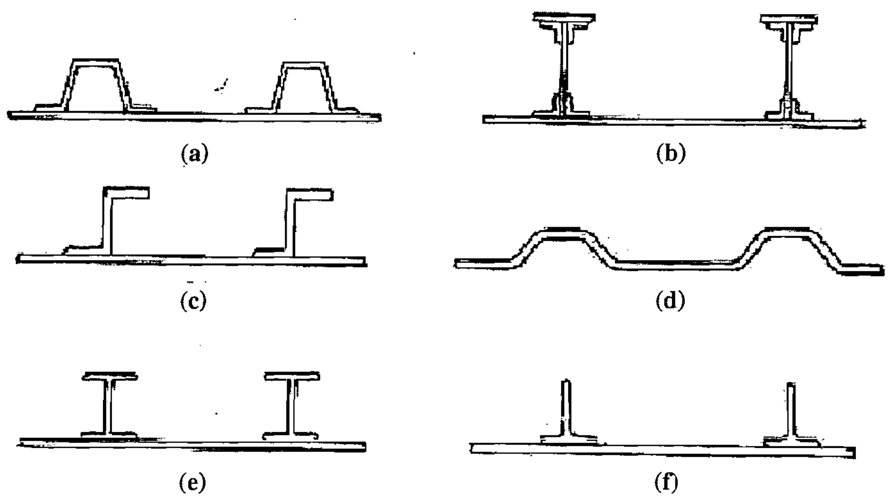

Figure 1.1 (a) hat-section (b)build-up I-section (c) fabricated Z-section (d) corrugated section (e) pultruded I-section (f) pultruded T-section

1.2 Characterisation of the Problem

Top-hat stiffeners are in widespread use in the FRP shipbuilding industry since they can be tailored readily to the complex curvature of hulls and provide built-in buoyancy by the fabrication method of laminating over rigid polymeric foam cores. The longevity and survivability of these structures are affected by harsh conditions prevalent in the ocean environment effects such as humidity, temperature, impact, wave-slamming loads and cyclic loads. The large difference in stiffness between the top-hat section and base panel results in the laminated connection between them being a highly loaded region. This is exacerbated due to orthogonality of the two members, which means the transfer of load from one member to the other being achieved in an out-of-plane mode. The weakness in this region is due to the lack of reinforcement across the connected surfaces. Therefore these structures were sustained damage at the stiffener flange/web corner and flange area in the form of delamination, which dramatically affects the integrity of the structure and hence the load bearing capabilities of the ship as a whole. Investigation into the structural performance of top hat stiffener can therefore provide huge insight into the characterisation of global structural strength.

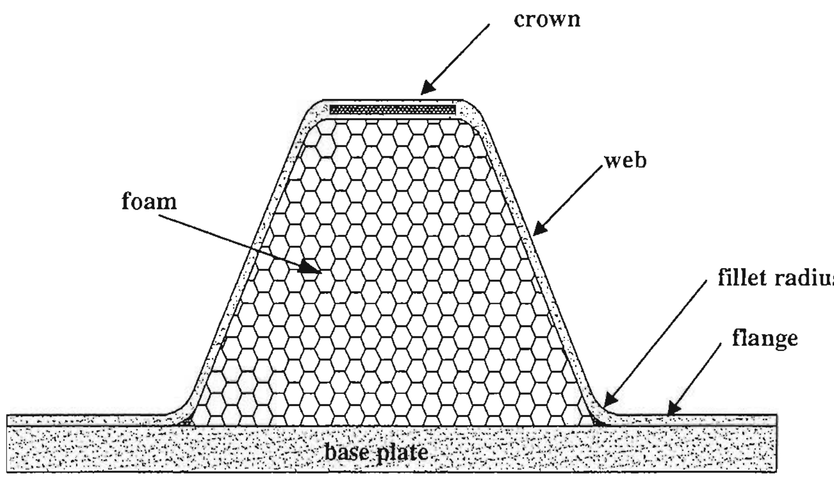

Figure 1.2 Top hat stiffener configuration

1.3 Research Aim

The research reported here includes a part of the test scheme and comprehensive theoretical study of typical ship types glass reinforced plastic (GRP) top hat stiffened structures. Two structural elements were considered: (a) top hat stiffener and (b) top hat stiffened panels. On the experimental side, these structures have been tested under static loading conditions. Numerous strain gauges and digital dial gauges were used to collect important information during loading. The objectives of the experimental works are: (i) to observe the failure mechanisms and (ii) provide validatory data for the numerical model. On the numerical side finite element analyses (FEA) were performed under representative static loading conditions. The results are used in a novel manner for these structures to provide a means of understanding and predicting the damage processes and failure mechanisms seen during the experimentation.

Thus the overall aims of this research are three fold;

1. To understand the flexural behaviour of two types of structural elements that are constructed using a top hat stiffened topology under static loading conditions and identify the failure mechanisms associated with different design parameters using experimental testing.

2. To assess the internal stress distribution within the two structural elements under representative static loading conditions, to determine load transfer mechanisms and thereby identify the most influential parameters which affect the structural performance of these structures.

3. To systematically vary these critical parameters, study the resulting stress distributions and correlate this information with experimentally derived failure mechanisms and their corresponding stress values.

Chapter 2 LITERATURE REVIEW

A typical stiffened single skin ship structure is shown in Figure 2.1 [7]. The structure comprises a large number of different out-of-plane connections including frame to shell, stiffener ends, stiffener intersections, deck edges and so on. This connection can be split into two main types. The first is the laminated tee joint where two orthogonally placed pre-fabricated panels are connected such as deck-to-bulkhead and floor-to-tank-top. The second is the top-hat stiffener joint where a hat section stiffener is connected to a panel.

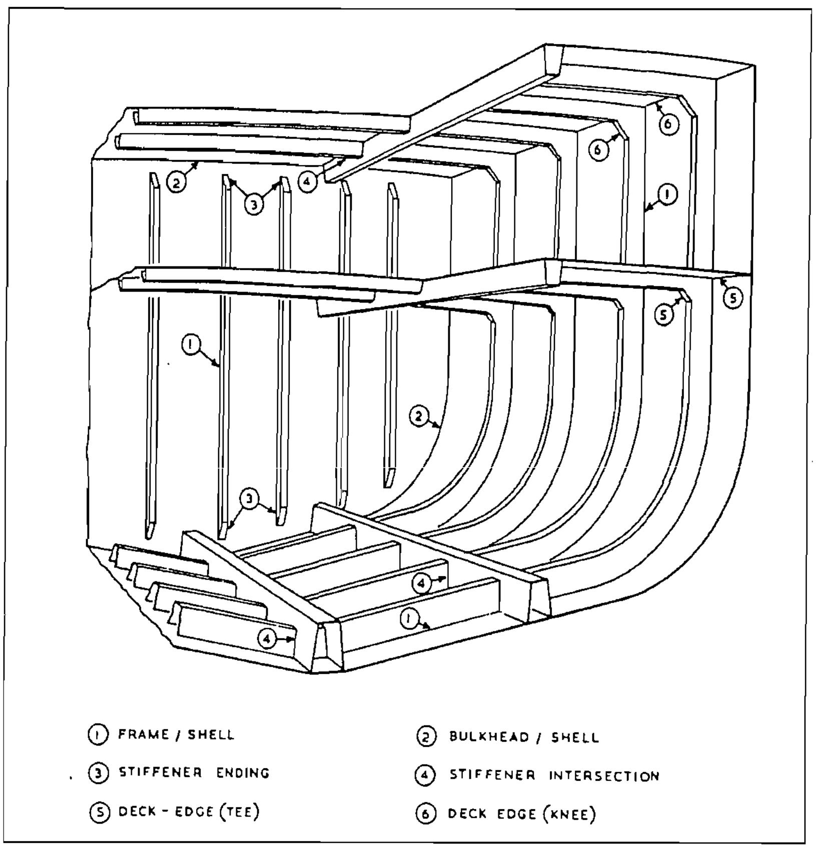

Figure 2.1 Typical GRP hull structural connection

A review was undertaken with the following intention

1) To determine the significance of the top-hat stiffener connections.

2) To define current practices for top-hat stiffened structures in different application.

3) To review previous work in this area, both experimental and theoretical.

4) To identify shortcomings in the existing knowledge base.

The published work could be categorized under three headings: (1) design guidelines, (2) theoretical modelling and (3) experimental programmes.

2.1 Design Guidelines and their Origins

One of the earliest approaches to FRP boat design is outlined in the manual of Gibbs and Cox [8]. This manual gives recommended arrangements of various joints and simple design examples. For the top-hat stiffener made of woven roving, design graphs of section modulus and moment of inertia are given to expedite the work of the designer. The design graphs for top hat stiffeners provide opportunities to the designer to vary stiffness and strength of the section simply by changing the cross-sectional dimensions. Tsouvalis and Spanopoulus [9] have produced design graphs, which could be used for selecting hat-type stiffeners that meet specific design requirement with respect to their moment of inertia, section modulus, cross-sectional area and shear area. They consider more than 4500 different cross-section which allows quick way to estimate the scantlings of the top hat stiffeners in the early stage of designing a frame system.

These guidelines were developed mostly from practical experience, with some confirmatory testing. No method of analysis or optimization is presented. Probably the most utilised sources of design guidelines are the various rules from the Classification Societies.

Lloyd's Register of Shipping (LRS) rules [10] state that for vessels greater than 30 m in length "the scantling is to be determined by direct calculation" For shorter vessels guidance is given on the design of both top-hat stiffener joints and tee joints. For top-hat stiffeners, LRS rules provide global modulus requirements. It is assumed that overlaminate of the joint will be formed by continuing the web of the stiffener around on to shell plating, and thus no recommendations are provided for fillet radius or overlaminate thickness. Although the length of the overlaminate is given to be 25 mm + 12 mm per 600 g/m^2 of reinforcement in the stiffener webs or 50 mm whichever is the greater.

American Bureau of Shipping (ABS) rules [11, 12], specify maximum height (h) and width of the top-hat stiffener. The minimum overlap of the angle is given as 0.2 h or 50 mm whichever is greater, with the condition that if the overlap exceeds 50 mm then it needs not be greater than 6t, where t is the thickness of the web of the stiffener. In addition overlapped must down over a length of 3t at its edge (See Figure 2.2). This thickness of the overlaminate should be t mm, whether the stiffener is laminated in position (where the web forms the over laminate) or is pre-formed (where the overlaminate is formed by separate boundary angle). Section modulus moment of inertia and shear area requirements also are given for the hat-type stiffener subjected to static pressure. However no guidelines are given for the fillet radius or composition.

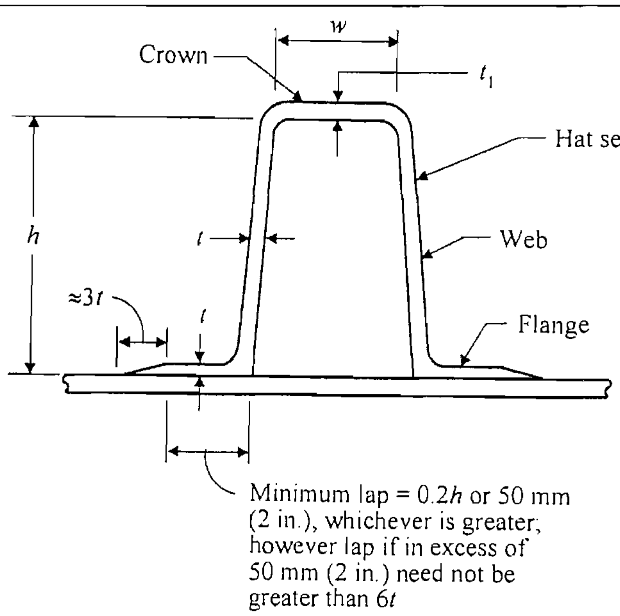

Figure 2.2 Geometry of a hat-type stiffener [10]

Det Norske Veritas (DNV) rules [13] adopt a similar approach to the design of top hat stiffeners as to the design of boundary angles in that tables of maximum allowable stresses and deflections are presented. In addition, formulae are given to derive the necessary section modulus and effective flange widths. However these apply to the overall stiffener design and not to detail of the out-of-plane joint, which is left undefined.

The extensive program of analysis conducted by the UK Ministry of Defence (UK MoD) in support of its mine hunter program has resulted in a naval engineering standard being developed NES140 [14]. Standard NES140 gives detailed guidelines on the design of structural intersections. It specifies that the thickness of the overlaminate, t, is to be at least half, and preferably two-thirds, the thickness of the thinnest member being joined (The geometric variables associated with this joint are shown in Figure 2.3). The length of the overlaminate overlap should be at least 100 mm and preferably 150 mm. The radius of the fillet is specified as t + 20 mm and the gap between members being joined is specified as less than t except over short lengths. In addition, guidelines are also given on lay-up and stacking sequence. It states that the overlaminates are to be made up of two layers of CSM plus one layer of woven fabric reinforcement, repeated as necessary such that, with the addition of at least two layers of woven reinforcement to the outside of joint, the desired thickness is achieved.

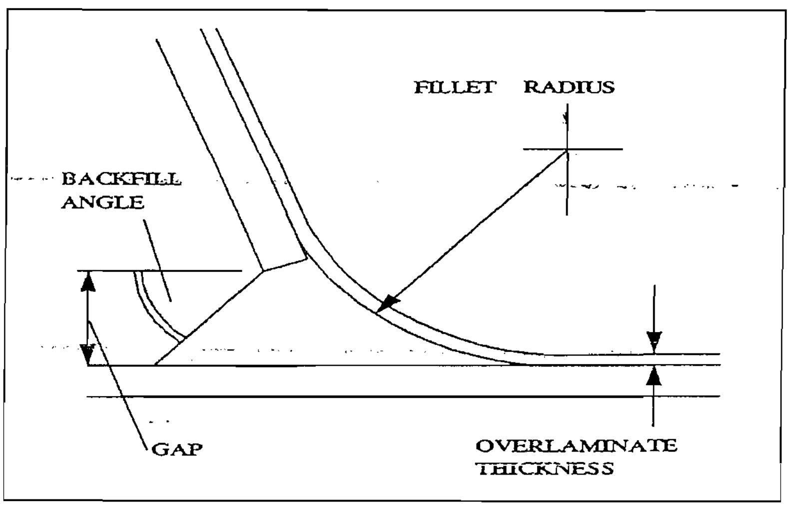

Figure 2.3 Top-hat joint design variables

It is noteworthy that no specific procedures concerning joint design are elaborated in the design rules above. Another common characteristic of all the rules issued by the different classification societies is that of conservatism in scantling of the structures through the application of high safety factors. The principal thrust of the rules is the provision of high stiffness in the region of the joint. Implicitly the rules are geared to result in adequate in-plane strength of boundary angle laminates. Significantly, the weak area, i.e. the out-of-plane properties, is not addressed in an explicit manner. The criticisms affecting such rule-based design are three fold:

- little encouragement and almost no direction is given for alternatives in the choice of material;
- no explicit mention is made of the potential failure modes ("Root Whitening" or "Delamination is frequently seen in top hat stiffeners), which is important for ship operators to enable repairing of the defects.
- no indication is given of the possible influence of varying design parameters (fillet radius, overlaminate thickness) on structural performance.

2.2 Theoretical Modelling of Static Structural Response

2.2.1 Laminated Plate Theories

The need for more accurate computational models for multi-layered laminated plates has led to the development of a variety of 2-D shear deformation theories. Together with the conventional 3-D elasticity theory, these theories can be grouped into three general categories [15]:

- Theories based on replacing the laminated plate by an equivalent single-layer anisotropic plate and introducing global displacement, strain and/or stress approximations in the thickness direction.
- Discrete layer theories based on the piecewise approximations in the thickness direction;
- The full 3-D elasticity theory which is of course the most general theory for assessing the stress state of the laminate.

The equivalent single layer theories are those in which a heterogeneous plate or shell is treated as a statically equivalent single layer, having complex constitutive behaviour, thus reducing 3-D continuum problem to a 2-D one. This first category includes the classical laminated plate theory (CLPT). Because of its simplicity, the CLPT is widely used in composite structure design and analyses. The CLPT can predict with reasonable accuracy the displacement and in-plane stresses of thin composite plates. However, the CLPT is based on the Kirchhoff Hypotheses. The Kirchhoff Hypotheses imply that the straight line normal to the mid-plane of the plate remains straight and normal to the mid-surface after deformation [16]. As a result of this assumption both transverse shear and normal deformation are neglected. This is why the CLPT can not predict accurate response characteristics of thick laminated plate in which transverse shear stress and normal deformation can be significant. Shear deformation theories aim at incorporating these effects.

Several approaches have been proposed to account for the transverse shear flexibility, and the other non-classical factors neglected in the classical laminated plate theory such as transverse normal strain. First-order shear deformation theory (FSDT) is extension of Reissner-Mindlin type theory for isotropic plates [17, 18]. In the FSDT, the Kirchoff hypothesis is relaxed by assuming that the transverse normal does not remain perpendicular to mid-surface after deformation. Since in this theory the transverse shear strains or stresses are assumed to be constant through each layer thickness of the laminate the theory requires shear correction factor to account for the discrepancy between the constant state of shear strains and stresses in the FSDT and the quadratic or higher-order distribution of shear strains and stresses in the elasticity theory. These coefficients are dimensionless quantities which have been calculated for homogeneous and isotropic plates by various static and dynamic methods [19-21]. For composite laminates they are difficult to determine since they depend on number of different parameters, such as constituents ply properties, the lamination scheme, and type of structure (i.e. geometry and boundary conditions). Restated first-order shear deformation theory by Knight and Qi [22] assumes physically that only in some average sense does a straight line originally normal to the mid-plane straight and rotates relative to the normal to the mid-plane after deformation. Hence, the in-plane displacement is still approximated, in an average sense, as linear and the transverse deflection as constant through the plate thickness. The associated nominal-uniform transverse shear strain, which is directly derived from these displacement fields assumptions, is identified as the weighted average value of shear strain through the plate thickness with the corresponding transverse shear stress as the weighting function. Likewise, the average rotation is identified as the weighted-average value of rotation, rather than the simple average one, which is obtained from the linear regression of in-plane displacement with the least-square method. In contrast to the first-order shear deformation theory, this theory allows the transverse shear-strains to vary through the plate thickness and satisfies the continuity requirement of the transverse shear stress at the layer interfaces. Therefore Knight and Qi's restated FSDT does not require shear correction factor. Knight and Qi's restated FSDT yields excellent agreement for both global and local response parameters (deflection, transverse shear strain and stress distribution) when compared to exact elasticity solution for cylindrical bending problem of symmetric cross-ply laminated plates

To overcome some of the disadvantages of the first-order-shear deformation theory the through thickness distributions of the displacement functions are assumed to be higher order polynomials of the thickness co-ordinate. Quadratic, cubic or higher polynomials have been assumed in higher-order shear deformation theory (HSDT). HSDT is based on a nonlinear distribution of the displacements and strains in the thickness direction [23]. In this theory it is possible to expand the displacement field in terms of the thickness co-ordinate up to any desired degree. However, due to the algebraic complexity and computational effort involved theories higher than third order have not been attempted. The reason for expanding the displacement up to cubic term in the thickness co-ordinate is to have quadratic variation of transverse shear strain and transverse shear stresses through the thickness. This avoids the need for shear correction. There are many papers on third order theories. Amongst them Reddy's refined higher order deformation theory is the most commonly used [24]. Reddy used an expression for in-plane displacement which satisfied the free surface zero shear conditions. The theory accounts not only for transverse strains but also for a parabolic variation of transverse shear strain through the thickness, and consequently, there is no need to use shear correction factors in computing the shear stresses. Furthermore, the theory contains the same number of dependent variables as the first-order shear deformation theory. HSDT in general yield more accurate results than the FSDT when compared to three-dimensional elastic solution.

The major drawback of the shear deformation theories arises from the assumption of continuous functions for in-plane displacement components. These mean strains are continuous through the thickness and therefore laminates made of dissimilar material layers can not be accurately modelled. This poor assumption subsequently results in: (a) The incapability of presenting zigzag distribution of in plane displacement through the laminate thickness, (b) The erroneous double valued interlaminar stresses on the laminate interfaces. In order to remove this fundamental defect, it is necessary to describe each composite laminate as an assembly of individual layers. Theories based on this layer-assembly technique are called Layer-wise plate theory (LWPT). LWPT utilises piecewise interpolation functions (first-order or higher-order) through the plate thickness for displacement fields and permit transverse shear strain discontinuity at layer interfaces in an attempt to satisfy both continuity of interlaminar transverse shear stresses and constitutive equation simultaneously [25]. Reddy proposed a layer wise displacement plate theory [26] in which the three-dimensional displacement field is expanded as a linear combination of the thickness coordinate and undetermined functions of position within each layer.

The finite element models of layerwise theories are capable of achieving the same level of solution accuracy and require the same number of degrees of freedom as conventional 3-D finite element model. Thus it is most often impractical to model an entire laminate with layerwise elements [27].

Three dimensional elasticity theories are required for the determination of three-dimensional stress state. Three-dimensional elastic models have been applied to calculate stress and to study buckling problem of laminated orthotropic rectangular plates. A finite element model based on the 3-D elasticity theory requires, ideally, at least one element through the thickness of each layer. To keep the element aspect ratios within the reasonable limits to avoid numerical problems of "locking", a large number of 3-D elements is required to model laminates, where and the thickness of individual lamina dictates the aspect ratio of an element. The cost of analysis precludes the sole use of 3-D elements in practical problems. Compared to layerwise theory 3-D elasticity theory provide more accurate means to calculate the stress fields at free edges, cut-outs, bolted joints.

Several theoretical approaches have been offered that are able to analyse the behaviour of curved composites similar to top hat stiffeners web/flange corner (accurate modelling of the stiffener's web/flange corner is particularly important, since it is this region that fails first in current ship type joints). These take one of two forms, either as developments of commercial finite element formulations or they are based on different plate theories.

An example of the former is the work of Chang and Springer [28]. Taylor et al [29] developed two dimensional 4-noded isoparametric element formulation which is based on the "non conforming" element formulation. This is basically a flat plate formulation in the local coordinate system, with the transformation to global coordinates incorporating the rotation around the bend. As a result, the displacement function is the same through the thickness as in the plane of the laminate, with all the limitations this imposes though coupling between in-plane and out of plane components is included. The method is limited to the analysis of symmetric laminates curved in two dimensions where the width is much greater than the thickness (displacements along the bend are ignored allowing a two dimensional analysis). Thus model definition need only be high in the through-thickness direction to achieve good results. The results from the FEM formulation were compared to two-dimensional elasticity solutions and exact correlation was found. A parametric study was then undertaken examining the effect of geometry and material lay-up on the ultimate strength of a CFRP bend this work also been applied to wooden bends [30].

Example of the latter including the work done by several authors of [31, 32] based on the " generalised layer-wise plate theory" of Reddy [26, 33-35] and the sub laminate analysis method described by Flanagan [36]. The basic premise of the generalised layer-wise plate theory is that the displacements on the interface between each layer of a laminate can be represented by a two-dimensional displacement function in the plane of the interface, with a one-dimensional function through the thickness of the each layer. The separation of the displacement function in the through- thickness direction allows it to be varied from layer to layer. These are then summed through the thickness of the laminate ensuring displacements are continuous, but allowing shear strains to be discontinuous. Thus the element is "non conforming" in that the normal to each layer need not remain normal once the element is loaded, allowing precurved surfaces to be modelled if suitably coupled in-plane displacement functions are used.

This theory has been developed and applied to a variety of problems and has been shown to give good results. In-plane displacement functions have been linear or quadratic without coupling terms to model curvature, and thus curves have been modelled by using many elements around the radius of curvature. The flexibility of this formulation has been shown by its ability to model the initiation and propagation of failure, since every interface between layers is modelled, even when the definition is coarse.

The sub laminate analysis method is not strictly a finite element formulation as it is an exact solution method, but the formulation is novel, applicable to the out-of-plane joint problem, and could easily be adapted to the FE method. Interconnecting higher order plates are used to represent the cross section of a structure. The plate can be both stacked, and linked end to end, to form complex shapes such as out-of plane joints. The stresses and strains at the interfaces between plate can be calculated to allow predictions of delamination initiation and propagation. The formulation is based on the Whitney-Sun plate theory [20] developed by Pagano [37] to model interlaminar normal stresses. Each layer of the laminate is represented by a continuous higher order displacement field in the plane of the layer, with a linear variation in the through-thickness direction. This ensures displacement continuity between layers and allows the plate to be shear deformable in this direction, but where displacements are not linear, such as around a delamination, increased definition is required. Coupling terms representing cylindrical curvature are included.

The plate equations are derived by combining the layer equations (similar to the global stiffness matrix assembly in FE), and the overall equations are assembled from the plate equations in the same way. This inevitably results in a formulation with insufficient boundary conditions to allow a closed form solution, so certain assumptions are made. Symmetry of the laminate is assumed and displacements are taken to be separable functions in the in-plane directions. The displacement in the principal direction are complex exponentials, with only the first order terms included This then allows an exact solution to be determined, but this could also be achieved using the FE method without this assumption being made.

This method has been shown to give excellent results when compared to other analysis methods, such as FE for a wide range of problems. Care must be taken to use an appropriate level of plate definition, as mentioned above, but, since results can only be computed on plate interfaces a reasonably high definition is required to show detailed stress distributions. The formulation developed to allow the rapid modelling of small sections of structures in cases where delamination resistance was a concern, and thus this limitation, which would make its general application to larger structures cumbersome, is not problematic.

2.2.2 Single Skin Top-Hat Stiffener Joints

A key characteristic of top-hat stiffener joints is that because of a lack of continuity of reinforcing fibres across the joints, it is susceptible to failure by peel or delamination well before the ultimate in-plane material stress is reached. Furthermore, its dependence on interlaminar properties makes the joint somewhat sensitive to material imperfections such as voids and to minute changes in geometry in the laminate. It is well known that main purpose of this connection is to transmit shear stresses between the shell and frame flanges under local bending caused by lateral pressure or concentrated lateral loads. Design of the connection requires evaluation of an envelope of maximum shear forces in each frame from the shear force distributions obtained by the finite element analysis of a hull compartment.

In the early days of the UKMoD development programme an attempt was made to predict the peeling stress along the secondary bond line in a tee joint to determine whether it was practical to remove the reinforcing bolts [38]. Two dimensional finite elements were used to model half of the joint which was subjected to both tensile and bending loads. A similar analysis was completed on a top hat stiffener to shell connection. Different lengths of overlaminate were modelled but it was concluded that results were very sensitive to the form of the applied load and until this was known no design recommendations could be made.

To identify key variables that controls and governs the transfer of load from the panel to the stiffener and vice versa, Dodkins et al [39] and Shenoi and Hawkins [40] carried out a study of the problem of a top-hat stiffener joint. The variations considered by them are radius of fillet (25-125 mm), thickness of overlaminate (1-12 laminate), gap between base panel and stiffener (10-50 mm) and fillet backfill angle inside the stiffener (0^0-45^0). The boundary conditions applied to models were centre-clamp loading and two clamps loading (See Figure 2.). Centre-clamp loading is the most severe in terms of minimum load at failure, as this mode places direct tensile loading on to the fillet. However this form of loading does not result in the initial delamination seen in practice, so two clamp loading has also been considered. The finite element analysis was conducted taking into account possible non-linearities in the material properties as well as those due to structural geometry. The main conclusion from this work as follows:

- For both loading modes, through-thickness stress in the overlaminate shows a minimum value with a thickness of two laminations, rapidly increases as laminations are added, then remains reasonably constant at thicknesses above five laminations.
- For two-clamp loading, the stress in the fillet increases slightly as overlamination is added and the joint become stiffer. This reduction in stress does not occur in single-clamp loading because the joint stiffness is little affected by an increase in overlaminations.
- For both loading methods, the stress in the fillet is a minimum at gap of 30 mm, although for single-clamp loading the stress value drops again as gap increases above 40 mm.

Junhou and Shenoi [41] reviewed papers about out-of-plane joints in FRP ship structures such as tee joints and top hat stiffener configurations. The paper focused on the design synthesis considerations, structural static response analysis and response under impulsive loading and creep and fatigue characteristics. They made suggestion for future research to improve an understanding of mechanical behaviour of out of plane joints. Phillips et al [42] have studied assessment of damage tolerance of a top hat stiffener to plate connection. They performed numerical analysis to determine the internal load transfer characteristics and failure mechanism in top hat stiffener under static loading and results showed that damage prone areas in top-hat stiffener are located in the curved region of the overlaminate close to the outer surface. Results also showed that delamination is likely to be due to excessive through-thickness stresses and damage which occurs in the flange is likely to be due to excessive in-plane stresses in the case of three-point bending loads and due to excessive through-thickness stresses in the case of reverse bending loads.

Blake et al [43] have carried out static structural response of a new type composite top hat stiffener containing a viscoelastic insert. They performed numerical and experimental analysis to understand effects of viscoelastic insert on the structural response of the joint. Their numerical work is based on a progressive damage methodology. The finite element models have been validated against experimental results by comparing finite element derived failure stresses with material failure data at experimental failure load. Good correlation was found.

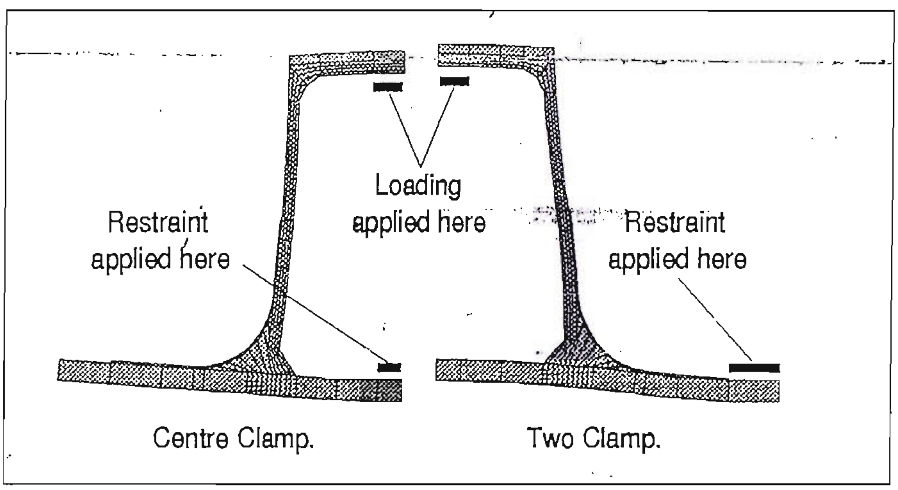

Figure 2.4 Schematic loading arrangementt for centre clamped and two clamped [40]

2.2.3 Single Skin Top-Hat Stiffened Panel

Design of panels reinforced by top hat stiffeners must clearly include careful consideration of elastic instability. Smith [7, 44] comprehensively examined compressive buckling of longitudinally stiffened panel and compressive buckling of the transversely stiffened panels using folded plate, finite strip and finite element analyses. In the case of compressive buckling of longitudinally stiffened panels two distinct forms of failure was observed. In the first case, collapse was precipitated by debonding of stiffeners caused by large local buckling deformation of the shell laminate. In the second case collapse was caused by compressive material failure in the tables of stiffeners resulting from overall column-like buckling of stiffeners. Folded-plate calculations were carried out for a wide range of transversely framed top-hat panels have indicated that the lowest buckling stress usually corresponds to local, interframe mode having one of the three forms shown in Figure 2.5. Data curves suitable for initial design purposes have been developed for each of the forms of buckling indicated in this figure.

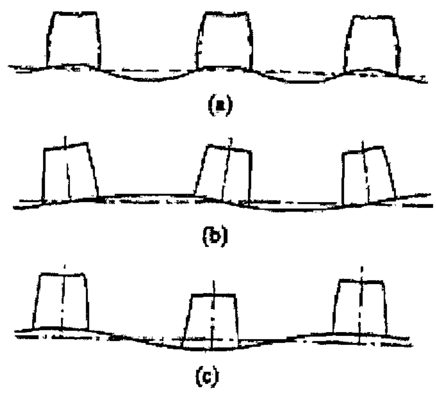

Figure 2.5 Interframe buckling modes for top-hat stiffened panels [7]

Ray and Satsangi [45] analysed composite plates stiffened with hat-shaped stiffener by the finite element method. An eight-nodded isoparametric quadratic plate-bending element was used for the plate element and three-noded beam element for the stiffener element formulation. The torsional rigidity of the top-hat stiffener has been taken into consideration. In order to validate the FE formulation they compared their results with those in the published literature.

Prusty [46] has developed finite element formulation for the linear static analysis of laminated composite stiffened plates with stiffeners top hat shape under transverse loading and various boundary conditions. Eight-noded quadratic isoparametric element was used for the shell and three-noded beam element was used for the stiffeners. His formulation is based on the first order shear deformation theory. Accuracy of the formulation has been carried out by using the general purpose commercial software package NISA.

Paul and Sinha [47] have developed computer code for the design of axially compressed stiffened composite panels. Their computer code has a capability to predict ultimate failure strength. They performed parametric study on a hat stiffened structural element made up of composite and aluminium alloy and they found that composite panels exhibit higher structural efficiency based on the buckling stress and overall panel strength.

Top hat stiffened structures are extensively used in aerospace industry where the structure is large, highly loaded and weight sensitive. Considerable amount of work has been completed on the behaviour of top hat stiffened structures. Agarwal and Davis [48] developed mathematical model including both strength and stability effects for hat-stiffened compression panels in order to generate optimum design for these structures. They used their model to generate optimum designs for both graphite epoxy and aluminium panels. They found that optimisation results for hat-stiffened graphite-epoxy panels show a 50% weight saving over optimised aluminium panels. Ko and Jackson [49, 50] have investigated buckling behaviour of hat stiffened panels under shear and compressive loading. They investigated both local and global buckling analytically and compared those results with FE (finite element) analysis and good agreement was found.

Vitali et al [51] studied structural optimisation of a hat stiffened laminated composite panel concept for the wing body of an aeroplane structure. They formulated a structural optimisation problem using the panel weight as the objective function, with constraints on stress and buckling. Lamberti et al [52] have developed analysis method for performing global optimization of stiffened shell structures by using PANDA2. They compared their analysis method with finite element solutions and good accuracy was obtained while their analysis method provides low computational cost. Collier [53] has presented formulation for equivalent plate stiffness and thermal coefficient for top hat stiffened plates, which are used in a hot structure on high speed aircraft in order to capture 3-D panel thermo elastic response. The formulation provides capability to model stiffened composite panels of any cross sections. The formulated values were compared to 3-D FEA and good agreement was found.

2.3 Experimental Modelling of Static Structural Response

While numerical analyses of stresses in out-of-plane joints provide insight into joint performance and may be used as a means of improving joint geometry, purely theoretical estimates of joint strength are unacceptable as a basis for design because of uncertainty about imperfections, local stress concentrations and material failure under multi-axial stresses within a connection. Reference must therefore be made to test data and development of new high performance designs includes through test programme of tests on all important joints for evaluation of static, fatigue, creep and impact strength.

2.3.1 Single Skin Top-Hat Stiffener Joints

When using top-hat stiffeners, it is vitally important that a good bond is achieved. The conventional fabrication method involves the lamination of the hull shell and flat or gently curved deck and bulkhead panels. Rigid foam cores are bonded to these unstiffened structures where stiffness required and FRP laminations are built up around the cores. When constructing a large hull, it is not uncommon for a substantial delay to occur between shell lamination and addition of the stiffeners. Early exploratory work [3] established that a delay of greater than seven days prior to stiffener lamination led to an excessively weak secondary bond between hull shell and the flanges of the stiffener, if no special precautions were taken. Surface treatments for the hull immediately prior to stiffener lamination have evolved, this involving abrasion, wiping with solvent and the use of peel plies.

A large experimental programme was conducted prior to the construction of the first of the UKMOD's mine hunters HMS Wilton with regard to many aspects of GRP construction. The results of static and fatigue test on top hat stiffener connection as follows:

- Visible damage in the form of resin crazing and delamination occurred in some of the tests at loads much less than those to cause final failure.
- Fatigue loading caused significant and progressive loss of stiffness in some but not all of the tests; and
- Fatigue testing had no significant effect on subsequent static strength even in those cases where resin crazing and/or delamination were apparent after fatiguing.

Elliott [54] performed a series of experiments (3-point bending, Reverse 3-point bending and Pull-off load test) on top-hat stiffener to investigate the failure mechanisms of these structures under different load conditions. For the three-point bending test, there was an initial debond of the fillet from the overlaminate interface followed by through skin thickness delamination of the overlaminate. For the reverse three-point bend, test failures consisted of through-fillet cracking and fracture of the fibre in the outer plies of the base plate on the tension surface. In the case of the pull-off load test, the failure was very simple, with overlaminates being peeled of the base plate.

2.3.2 Single Skin Top-Hat Stiffened Panels

A large amount of experimental work has been carried out on the study of top hat stiffened panel. Funatogawa et al [55, 56] have carried out experimental as well as analytical work on the stiffening effect of hat shaped stiffeners on a plate. In their first study, they performed experiments on the bending of panels with a single hat stiffener under uniform lateral load. The measurements were made on the deflection and surface strain in different points. Experimental results were compared to calculation based on the theoretical analysis and good agreement was obtained in terms of the bending deformation of the structure. They also carried out experiments to investigate the buckling deformation of orthotropic plate with a single hat shaped longitudinal stiffener under uniaxial compression.

Smith [44] investigated the collapse behaviour of transversely stiffened large scale GRP panels having stiffeners of hat section under longitudinal compressive load. From the test results, he found that compressive failure of transversely framed GRP panels occurs by local instability which is catastrophic and would result in loss of ship if it occurred in a ship's bottom shell or strength deck. His theoretical analysis results also confirmed that the reason of the compressive failure of the structure occurs by local instability.

Choqueuse et al [57] have tested top hat stiffened sandwich panels under uniform pressure. They also performed numerical analyses by using different finite element codes. Although the input parameters (boundary conditions and material properties) are identical they found significant difference between finite element predictions and a measured strain value. Reichard and Lewit [58, 59] performed experiments on PRISMA™ frame system (hat section beam panel) under three point loading to evaluate the flexural behaviour of this structure and compared this property with those of similar structures built using sandwich and solid laminate construction. They found that the PRISMA™ beam panels with unidirectional cap had the highest stiffness, with values greater than double that of other panels.

Mouring [60, 61] has tested GRP panels stiffened by preform frames with different laminate orientation of the fibre for the frames under in-plane uniaxial compressive loads. Biaxial [0/90], quadaxial [0/90/±45] and triaxial [±45/0] laminates were used in the frames. It was observed that all the panels started to fail with a local buckling of solid laminate panels. The panel with triaxial heavily laminated frames gave the highest local buckling and best overall strength.

Lee et al [62] investigated structural analysis and manufacturing techniques for hat stiffened composite panels. They performed experimental and numerical work to understand initial buckling and post buckling behaviour of hat stiffened composite panel under compression load. It was found that the predicted and experimental initial buckling and the failure load and buckle modes were in good agreement. Jiang et al [63] performed numerical work on bending and buckling of unstiffened, sandwich and hat-stiffened orthotropic rectangular plate. Based on this work, Roberts et al [64] have carried out experimental and analytical work to investigate the behaviour of top hat stiffened panels under buckling and uniform pressure load. They found reasonable agreement between FEA, analytic and experimental buckling stresses. On the other hand, in the pressure case there was a poor agreement between FEA and experimental results from stresses and deflections.

Falzon and Steven [65] have carried out experimental and numerical buckling and post buckling investigation of hat-stiffened carbon fibre composite panel. Good correlation between experimental and numerical strain and displacement results was achieved in the prebuckling and initial post buckling region of the loading history. Falzon [66] studied damage tolerant hat-stiffened thin-skinned composite panels with and without a centrally located circular cut-out under uniaxial loading experimentally and numerically. He found that both panels exhibited good post buckling strength and failed by the local buckling failure of the hat stiffeners. Non-linear finite element analysis was able to accurately represent the behaviour of these panels. Baker and Rousseau [67] studied mechanically fastened joint for the carbon-rod-reinforced hat-section stringer of the aircraft wing component experimentally and analytically. They found that the use of prefabricated pultruded carbon-epoxy rods has reduced manufacturing complexity and cost of stiffened composite panels while increasing the damage tolerance of the panels.

2.3.3 Response Under Impulsive Loading

In the case of naval minesweepers and mine hunters, the hull experiences not only static loading but also dynamic loads from hull motion, slamming and possibly explosive loads. Under explosive loading, a top-hat stiffener joint may be exposed to substantial through-thickness tensile stresses in both single skin [68] and sandwich cases [69]. These are caused both by reflection of a transmitted shock wave through the laminate and by differential inertia forces associated with overall dynamic response of stiffened panels to impact load. Even though the surface preparation of the hull prior to stiffener lamination yields a secondary bond, whose transverse tensile strength equals the interlaminar tensile strength of the woven glass roving/polyester resin laminate of the hull, there could be a tendency for stiffeners to debond from the hull during explosive loading at or just below the secondary bond line.

A large experimental program was conducted by the UK Ministry of Defence (UKMoD) in support of its mine hunter programme [3, 6, 70, 71]. Considering the out-of-plane joints, early experiments involved producing stiffened 10' × 10' panels and subjecting them to shock loading. This highlighted the weakness of the out-of-plane joints as the frames debonded from the shell. The solution adopted to overcome this problem was to through-bolt the connections using pretensioned bronze bolts. The initial failure occurred in the same way as before, but ultimate failure was delayed by the bolts. A 2/3 scale section representing the ships structure was built and similarly tested. Thus the structural agreement of HMS Wilton was arrived at.

This production method was less than ideal, however, since the bolts were expensive both to buy and to fit. The problem was exacerbated by the need to change to titanium bolts for the larger Hunt class of MCMV's [72]. Thus a concerted effort was applied to improve the joint performance [54, 73-77]. This centred around the replacement of the fillet with a flexible urethane acrylate fillet. Two-dimensional slices representing the boundary angles and top hat stiffener sections were subjected to pull-off tests (at 45^0 in the case of boundary angles to represent a tank under hydrostatic pressure and vertically for the top hat stiffener sections, with a variety of clamping conditions). This was followed by full scale tests in a tank structure subjected to explosive loading. This was correlated with a similar size section of the ship's structure. It was found that an initial delamination still occurred, the final failure load of the flexible fillet samples was equivalent to the bolted samples but significantly the energy absorbed to failure (the area under the load/deflection curve) was greatly increased due to the increased flexibility of the joint. This increased energy absorption was considered to be reason for the increased resistance to shock loading despite the static failure loads being similar. The results from the test programmes were sufficiently promising that bolts were removed from the Sandown class of SRMH's .This type of joint was also used in some cases for building the Hunt class mine countermeasures vessels HMS Brecon in 1980[72]

2.4 Summary of Literature Review

Summary of the literature review, which are given in Tables 2.1 to 2.3, has shown that considerable amount of work has been completed in various industries to try to improve structural efficiency of composite top hat stiffened structures. From these several conclusions can be drawn:

- The equivalent single layer theories provide sufficiently accurate description of the global response of thin to moderately thick laminates. However, as mentioned in section 2.2.1, the equivalent single layer model have several serious limitations that prevent them being used to solve whole spectrum of composites laminates problems. Compared to single layer theories, 3-D elasticity theory provide more accurate means to calculate the stress fields at free edges, cut-outs, bolted joints,... Since it is very important to calculate the stress state when developing models for composite behaviour the 3-D elasticity theory will be used in this research.

- There is currently very little design information available for top hat stiffened composite structures. The review of the previously published work showed that these structures have been recognised by design authorities as being a problem area. However, the design methodology proposed by these authorities does not quantify of the load transfer and failure mechanisms exhibited by these structures.

- The current knowledge of flexural behaviour of top hat-stiffened structures has been based largely on empirical evidence. There is currently very little numerical modelling information available. The experimental work carried out in support of the minehunter programmes, for example, has been relatively simple in nature with only failure loads being recorded.

- A theoretical study of these structures requires the use of a numerical model such as FEM, as analytical methods would be unable to model the complex geometry. In some literatures comparison with experimental results has not been reported. For practical applications of numerical model, it is essential that numerical model is validated against the test results. Correlation of numerical results (such as deformation, strain and damage patterns) with the experimental value would give an added robustness to the numerical model.

- There is significant body of evidence relating the out of plane behaviour of joints and buckling analyses of stiffened plates experimentally and numerically. It is also evident that only limited systematic investigation has been conducted with regard to shear load transfer and shear induced failures in the web of the top hat under different static load conditions for top-hat stiffened structures.

In summary there is a clearly a need to develop a more complete understanding of the behaviour of the top hat stiffened structure under out-of-plane loading. Since exact results are not available for the top hat stiffened composite structures, experimental and numerical modelling such as FEM are to be carried out to understand the flexural behaviour of top hat stiffened structures. This work will analyse these structures for stiffness and strength with particular attention to failure modes in order to determine optimum structures for out-of-plane loading conditions. Comparison of results from numerical model with results from structural testing series of top hat stiffened structures will quantify any modelling error. The information gained should be helpful developing an optimal framing system for the recreational boating industry.

Table 2.1 Comparative assessment of plate theories

Theory	Constraint conditions on stress	Through the thickness displacement assumption	Total number of generalized displacement parameters
Classical laminated plate theory	$\sigma_{13}=\sigma_{23}=\sigma_{33}=0$	Neglected	5
First-order shear deformation theory	$\sigma_{33}=0$	*Linear u_α Constant w	5
Higher-order theory Lo et al. [23]	None	Cubic u_α Quadratic w	11
Higher-order theory Reddy [24]	$\sigma_{33}=0$ $\sigma_{3\alpha}=0$ at the top and bottom surface	Cubic u_α Constant w	5
Discrete Layer Theory	$\sigma_{33}=0$	Piecewise linear u_α constant w through out thickness	2*NL**+3
Simplified Discrete Layer theory	$\sigma_{33}=0$ continuity of $\sigma_{3\alpha}$ at layer interfaces	Piecewise linear u_α constant w through out thickness	5

*Many of the cited theories can be considered as a special case of a general theory based on the following through-thickness displacement assumptions[15]:

$$u_{\alpha}(x_{\beta},x_3)=u_{\alpha}^{0}(x_{\beta})+U_{\alpha}(x_{\beta},x_3), \quad 2.6$$

$$w(x_{\beta},x_3)=w^{0}(x_{\beta})+W(x_{\beta},x_3), \quad 2.7$$

where u_{α}^{0} and w^0 are the displacement components of the reference plane of the plate ($x_3=0$), U_α and W are the function of x_3 which vanish at $x_3=0$, $\alpha,\beta=1,2$.

**NL: Number of layer for laminated plate. Typical geometry of the laminated plate (NL=4) is given in Figure 2.6.

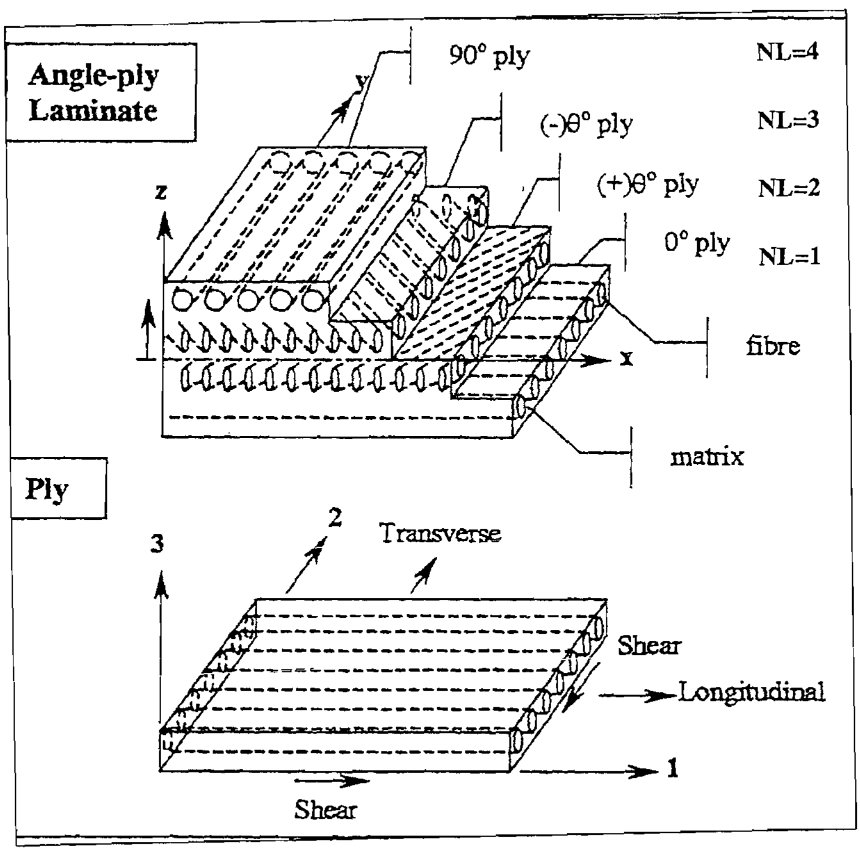

Figure 2.6 Composite laminate geometry

Table 2.2 Comparative assessment of experimental modelling of top hat stiffened structures

Structural Configuration	Loading Type		Failure Mode
Top Hat Slice	Pull off test***	Centre Clamp Loading [75,76,77]	Catastrophic failure which was complete separation of one stiffener flange from the base panel along the secondary bondline
		2 Clamp Loading [76,77,54]	Catastrophic failure which was complete separation of one stiffener flange from the base panel along the secondary bondline
		3 Clamp Loading [76,77]	Rapid crack growth along secondary bondline leading to separation of a stiffener flange from the base panel
	3-point bending***	[54]	Initial debond of the fillet from the overlaminate interface followed by through skin thickness delamination of the overlaminate
		[43]	cracks in balsa propagate into viscoelastic insert resin. Final failure characterized by separation of flange and overlaminate
	Reverse Bending***	[54]	Failure consisted of through fillet cracking and fracture of the fibres in the outer plies of the base plate on the tension surface
Top Hat Stiffener	Fatigue Loading	[3]	Delamination at curved part of the overlaminate (web/flange corner)
	3-point bending	[3,56,57]	Buckling of the side wall under the center loading nose
	4-point bending	[3]	NA
Top Hat Stiffened Plate	Uniaxially compressive loading	[44,49,50,60,61,62-66]	Local buckling of the hat stiffener Disbonding and delamination at the stiffener plate interface Lateral skin buckling of the skin
	Uniform Pressure	[56,57]	Local instability in the web and crown
	Shock Loading	[3]	Local failure at web flange corner

***: Schematic loading condition are given for three-point bend, reverse bend and pull-off test in Figure 2.7

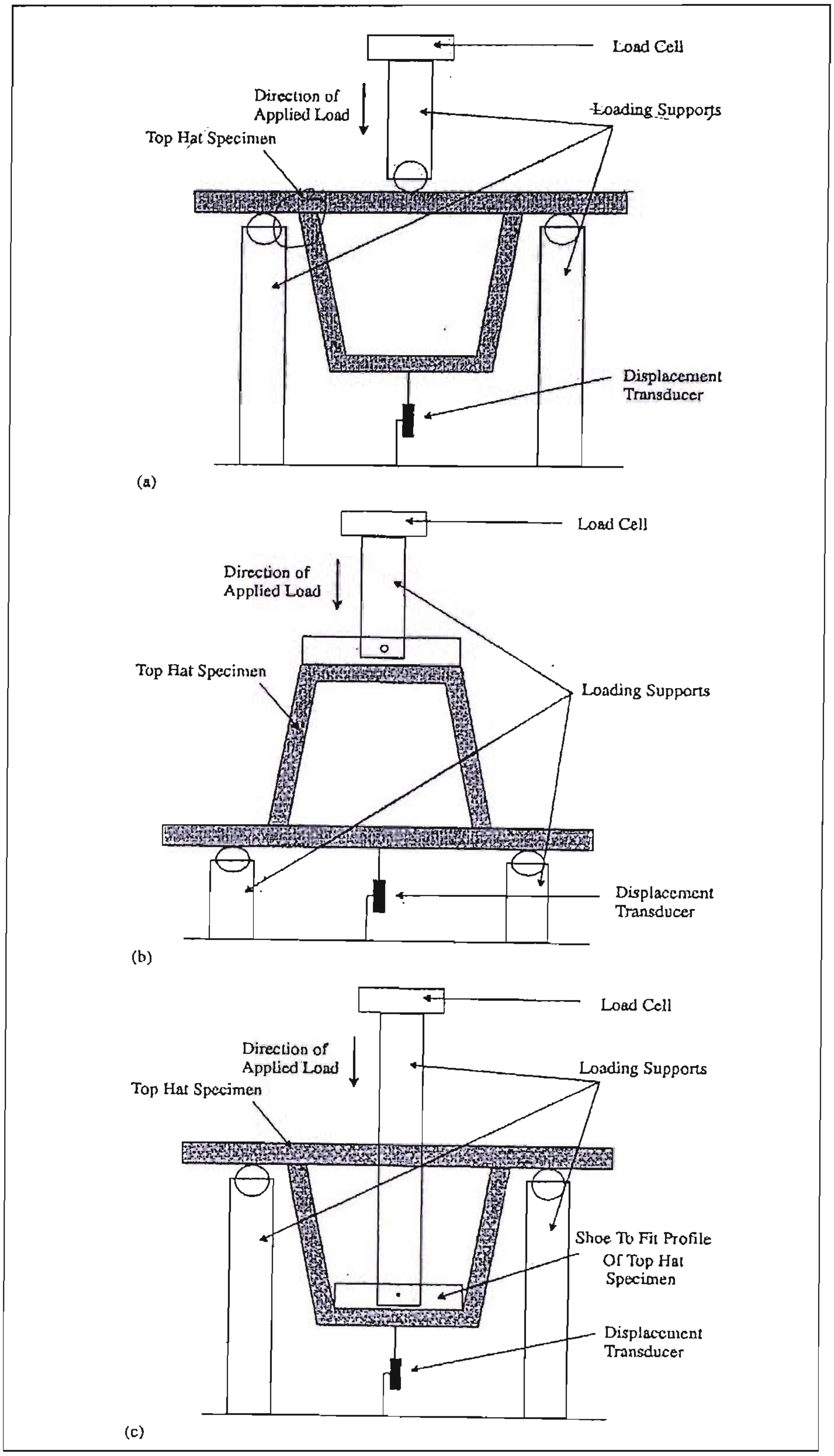

Figure 2.7 Loading configurations for the experiments: (a) three-point bend; (b) reverse bend; (c) pull-off [42]

Table 2.3 Comparative assessment of numerical modelling of top hat stiffened composite structures

Structural Configuration	Loading Type		Failure Mode
Top Hat Slice***	Pull off test	Centre Clamp Loading [39,75]	Separation of one stiffener flange from the base panel Failure across the fillet from internal side in tension to the flange base secondary bond
		2 Clamp Loading [37]	Delamination at boundary angle in the web to shell
	3-point bending	[42]	Delamination at interface between fillet and overlaminate Tensile failure of flange
		[43]	Shear failure propagates throughout balsa core Fibre failure occurring in frame radius
	Reverse Bending	[42]	Debond between overlaminate and fillet
Top Hat Stiffener	NA		NA
Top Hat Stiffened Plate	Uniaxially compressive loading	[44,49,50,60,61,62-66]	Failure mode shapes captured (Local instability of stiffener, local skin buckling)

***: Typical top hat slice geometry is given in Figure 2.8

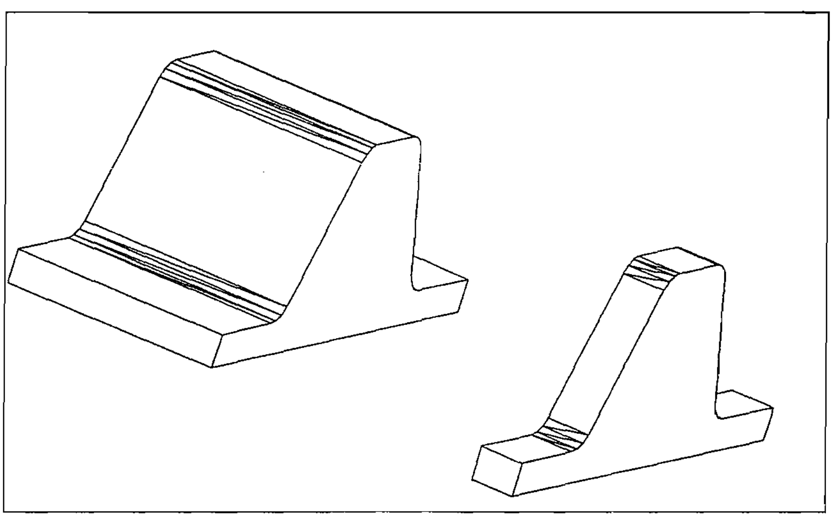

Figure 2.8 Top hat stiffener is sliced off.

Chapter 3 RESEARCH METHODOLOGY

3.1 Introduction

Nowadays design is more and more performance oriented. Indeed the tendency is to produce lighter, faster and more economically efficient ships without compromising their structural integrity. During their operating life, ship structures subjected to harsh conditions prevalent in the ocean environment, effects such as humidity, temperature, impact, wave-slamming loads and cyclic loads. Consequently theoretical analysis needs to be carried out at the design stage, in order to accurately optimize the design of ship's structural members. The main focus of this research has involved a comparative investigation of structural performance of two types ship's components, top hat stiffeners and top hat stiffened panels under different static loading conditions. The logic behind the ensuing methodology a part of the test scheme and comprehensive theoretical study of these structures are outlined as follows:

- On the experimental side, fully detailed experimental studies are to be carried out on top hat stiffeners and top hat stiffened panels to assess the strength and stiffness and their dependence on lay up. Failure mechanisms of these structures will be detailed and their linkage to lay up and topology will be discussed. Four point bending loading is chosen for top hat stiffeners. In four-point bending the stiffener subjected to constant bending moment, which allows investigating shear induced failure at the support. On the other hand uniform pressure is chosen for top hat stiffened panel which more likely to representative of uniform bending caused by hydrostatic pressure. Finally coupon tests are to be conducted to investigate the material properties of the top hat stiffened panels' constituents which would be useful input data for FE analyses. Figure 3.1 shows the background of the experimental programme. Chapters 4 and 6 are devoted to this part
- On the theoretical side analytical and finite element analyses are to be carried out. The results will be validated against experimental findings directly in the case of global load/deflection results. The finite element derived failure stresses shall be compared with the material failure data, at experimental failure loads in order to validate the model and further understand the internal stress patterns within the

structural elements when subjected to a selection of static loading conditions. The loading condition is chosen so as to represent as closely as possible the actual modes of loading present in boats. These include, (i) four point bending load for top hat stiffener and (ii) uniform pressure for top hat stiffened panels due to hull bending under hydrostatic loading. The internal stress distribution will allow the regions within the structures which are most likely to damage to be identified. These studies are discussed in chapters 5 and 7.

Finally Figure 3.2 shows a flowchart of the research programme.

(a) Pleasure boat

(b) Internal structure of the pleasure boat

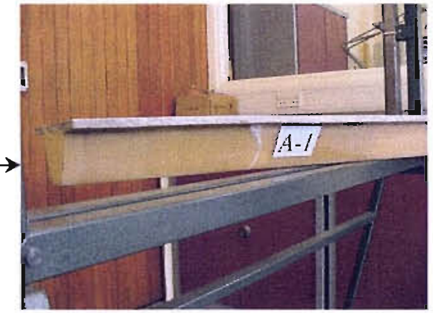

(c) Structural element-1 (top hat stiffener)

(d) Top hat stiffened panels

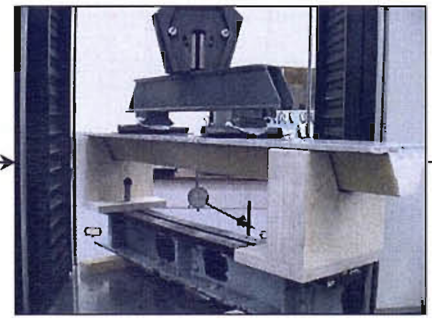

(e) Experiment on Top hat stiffeners

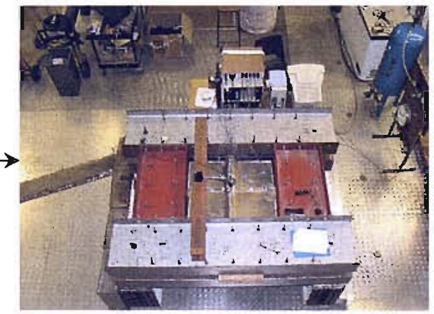

(d) Experiment on Top hat stiffened panels

(d) Coupon Test on material constituents of both structural element

Figure 3.1 Background of the experimental programme

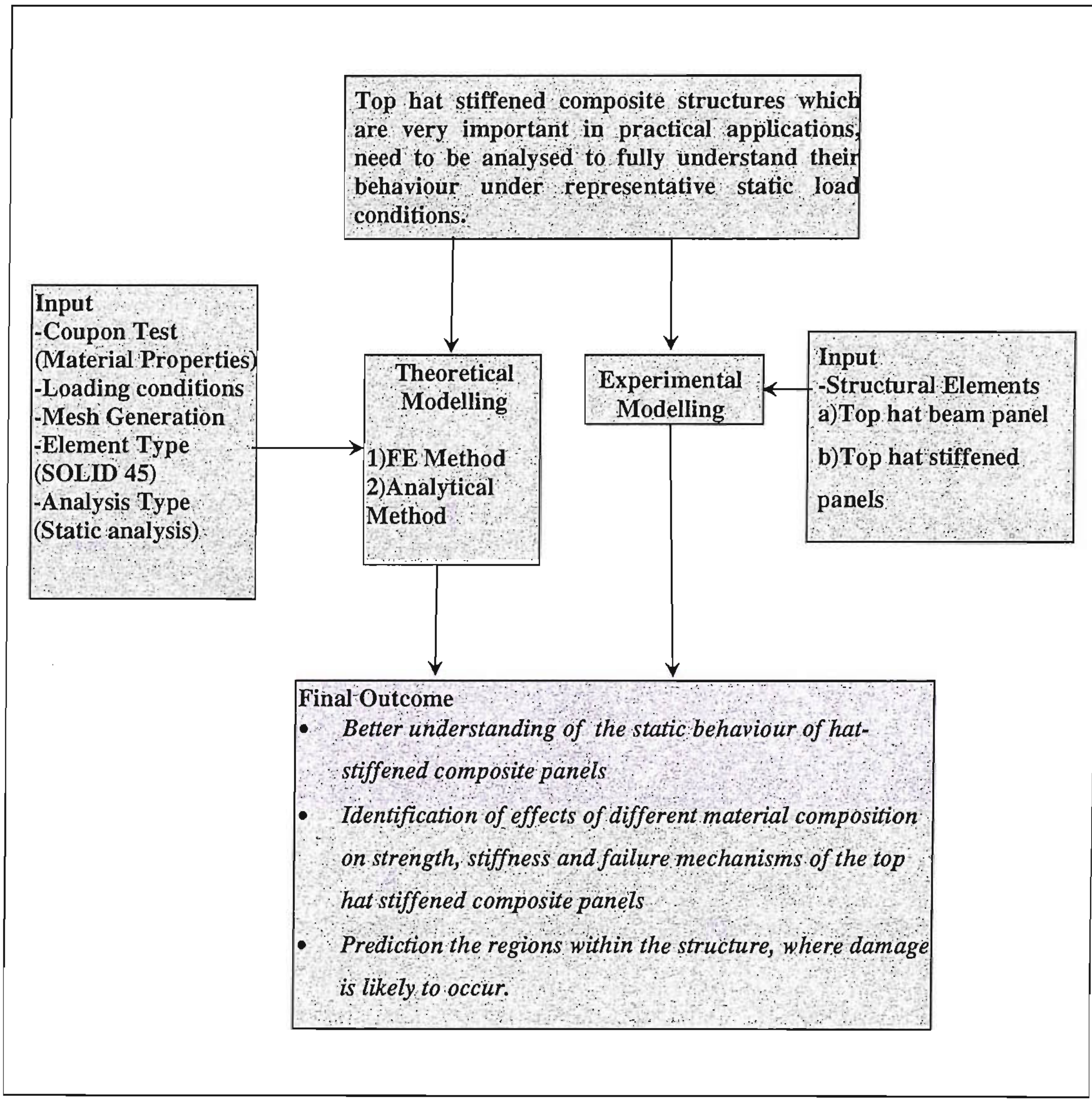

Figure 3.2 General overview of the proposed approach (novelty and contribution to knowledge highlighted in italics)

Chapter 4 EXPERIMENTS ON TOP-HAT STIFFENERS

4.1 Introduction

It is clear that from the literature review discussed in chapter 2, there is significant body of evidence relating to the behaviour of out of plane joints and buckling analyses of stiffened plate experimentally and numerically. It is also evident that only limited systematic investigation has been conducted with regard to shear load transfer and shear induced failures in the web of the top hat under panel loading, spanned along the stiffener. This bending case therefore forms the topic of this chapter.

Top hat stiffeners provide shear stress transmission between the shell and frame flanges as a result of local bending forces. The work presented in this chapter, is the result of systematic experimental programme investigating the structural performance of top hat stiffeners under four point bending loading configurations. Two different types of top hat stiffeners were used, which are referred to as stiffeners A and B. They have been tested under four point bending load. There were three specimens of each type (denominated 1, 2 and 3). All stiffeners were 1.25 m long. The stiffeners are made up from glass fibre reinforced orthopthalic and isopthalic polyester resin. The sequence of construction involves first laying and curing the base plate. A light non-structural foam former is placed at the appropriate location, where stiffness is desired and filleting resin placed adjacent to the former and base plate. An appropriate number of overlamination plies is then placed on the foam former and consolidated and cured to form the top hat stiffener.

Isophthalic resin is used with the 300g/m^2 CSM layer whereas orthopthalic polyester resin is used for the remainder of the laminate. This is because isophthalic resin provides more stiffness and superior interface between glass fibre and matrix and naturally costs more. Therefore it is used for the first ply against the gel coat for environmental protection while cheaper resin (orthopthalic) is used for the bulk laminate. The base plate of the stiffeners consists of 10 layers and its stacking sequence is the same for all type of stiffener. Both stiffeners have non-structural trapezoidal polyurethane foam with density 28 kg/m^3. The main difference between the two types of top hat stiffener is the over foam lamination scheme which is given in Table 4.1. While the overlamination of the group stiffener A was made up of 3 layers of 600 g/m^2 CSM with orthapthalic resin, its counterpart (group stiffener B) is made of lightweight 225 g/m^2 CSM stitched to 600 g/m^2 Bias material with orthopthalic resin. Hence group stiffener A is approximately 14 % heavier than group B. The geometries of two types of top hat stiffeners are given in Figures 4.1. Dimensions are given in mm.

Table 4.1Lamination scheme for stiffeners A and B

		Layer No	Stiffener A	Stiffener B
Base Plate		1	300 g/m^2 CSM	300 g/m^2 CSM
		2	600 g/m^2 CSM	600 g/m^2 CSM
		3	600 g/m^2 WR	600 g/m^2 WR
		4	600 g/m^2 CSM	600 g/m^2 CSM
		5	600 g/m^2 CSM	600 g/m^2 CSM
		6	600 g/m^2 WR	600 g/m^2 WR
		7	450 g/m^2 CSM	450 g/m^2 CSM
		8	600 g/m^2 CSM	600 g/m^2 CSM
		9	600 g/m^2 WR	600 g/m^2 WR
		10	450 g/m^2 CSM	450 g/m^2 CSM
Foam		11	Trapezoidal PU Foam	Trapezoidal PU Foam
Over Foam Lamination	Flange	12	600 g/m^2 CSM	225 g/m^2 CSM
		13	600 g/m^2 CSM	600 g/m^2 Bias
		15	600 g/m^2 CSM	225 g/m^2 CSM
		16		600 g/m^2 Bias
	Web	12	600 g/m^2 CSM	225 g/m^2 CSM
		13	600 g/m^2 CSM	600 g/m^2 Bias
		15	600 g/m^2 CSM	225 g/m^2 CSM
		16		600 g/m^2 Bias
	Crown	12	600 g/m^2 CSM	225 g/m^2 CSM
		13	600 g/m^2 CSM	600 g/m^2 Bias
		14	1600 g/m^2 UD	1600 g/m^2 UD
		15	600 g/m^2 CSM	225 g/m^2 CSM
		16		600 g/m^2 Bias

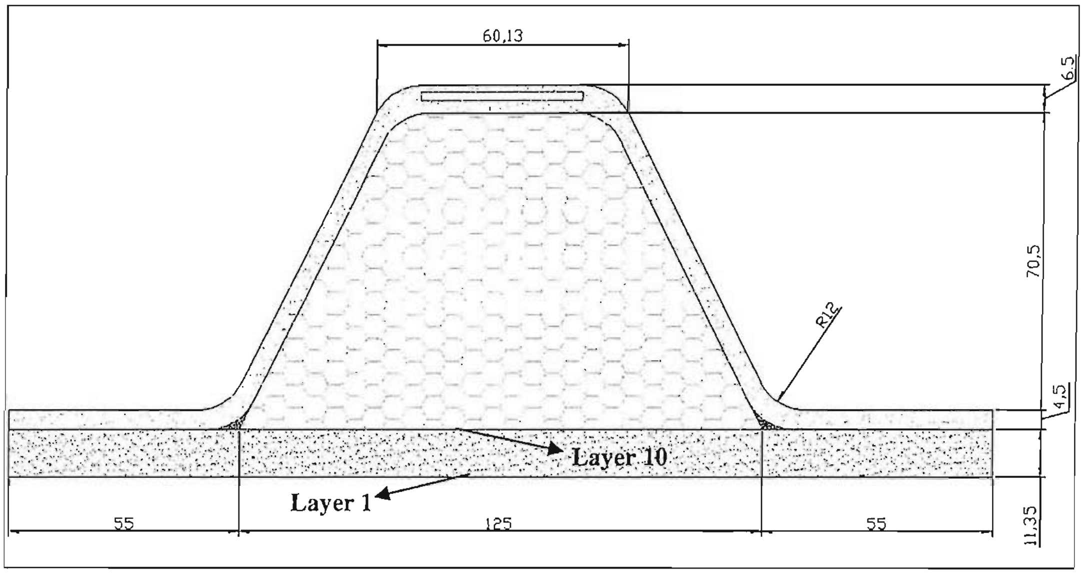

a) Group Stiffener A

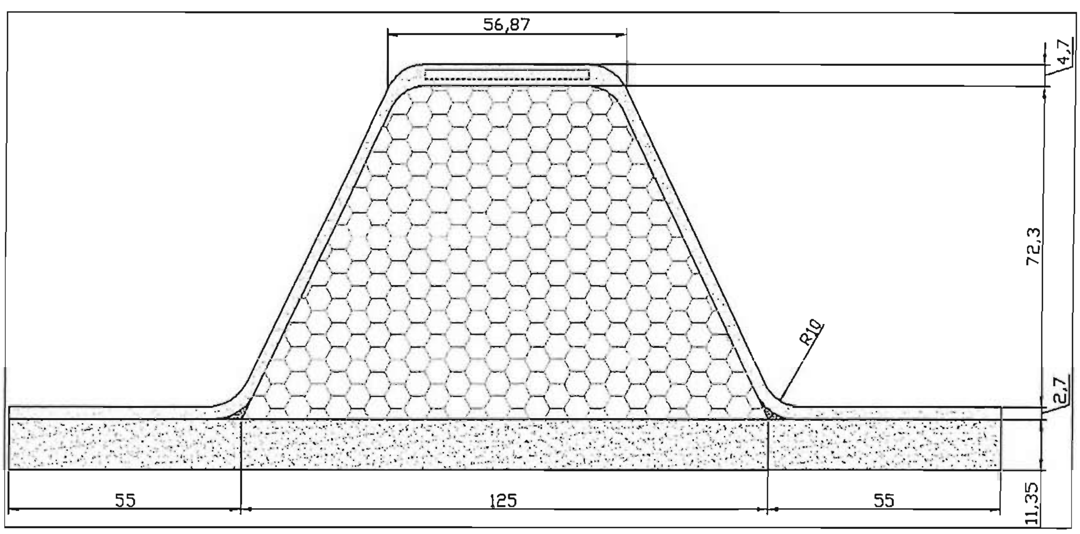

b) Group Stiffener B

Figure 4.1 Geometry of group stiffeners A and B

The three principal objectives of experimentation were:

1. Observe the failure pattern
2. Identify the implication of varying overlamination lay-up
3. To provide a validatory data for the theoretical analyses described in chapter 5

4.2 Experimental Setup

Due to the large and complex shape of these top hat stiffener sections and the possible high loading required to fail them a 250kN Instron 1196 Universal test machine based in the Material Engineering Laboratory at the University of Southampton with in the School of Engineering Sciences was employed. The four point bending test set up allows the measurement of two quantities directly from the test machine, reaction load and crosshead displacement. A dial gauge was also mounted at the mid-span of the top hat stiffener to measure mid-span deflection. The tests were carried out under displacement control to pick up stress relief, with a crosshead speed of 2 mm/min.

Replicating the in-service loading conditions experimentally is complex. Ideally, the boundary conditions should be identified from the global stiffener response and transferred to the top-hat stiffener section edges. Because of this complexity the experimental test setup was designed to primarily validate the numerical model so that more appropriate loading conditions could be numerically applied and structural responses better understood.

In the experimental programme, only one type of boundary condition is applied at the ends of the top hat stiffener sections: simply supported. The simply supported condition is not a physical representation of the in-service problem but allowed for a rapid determination of stiffener response to help validate the numerical model without delay for design and manufacture of end fixtures.

The tests were carried out in the test rig shown in Figure 4.2 (a). Two wooden supports were produced and tightly bolted to the heavy steel I-stiffener. Loads are applied across the stiffener width via rollers of 25 mm diameter on the outer surface of the top-hat stiffener and equivalent in length to the width of the stiffener. The applied load roller separation is considered a function of support spacing, with a ratios 0.6 (load spacing divided by support spacing). For the current boundary condition the support positioned 180mm from the stiffener ends. This is shown in Figure 4.2 (b) and Table 4.2 respectively

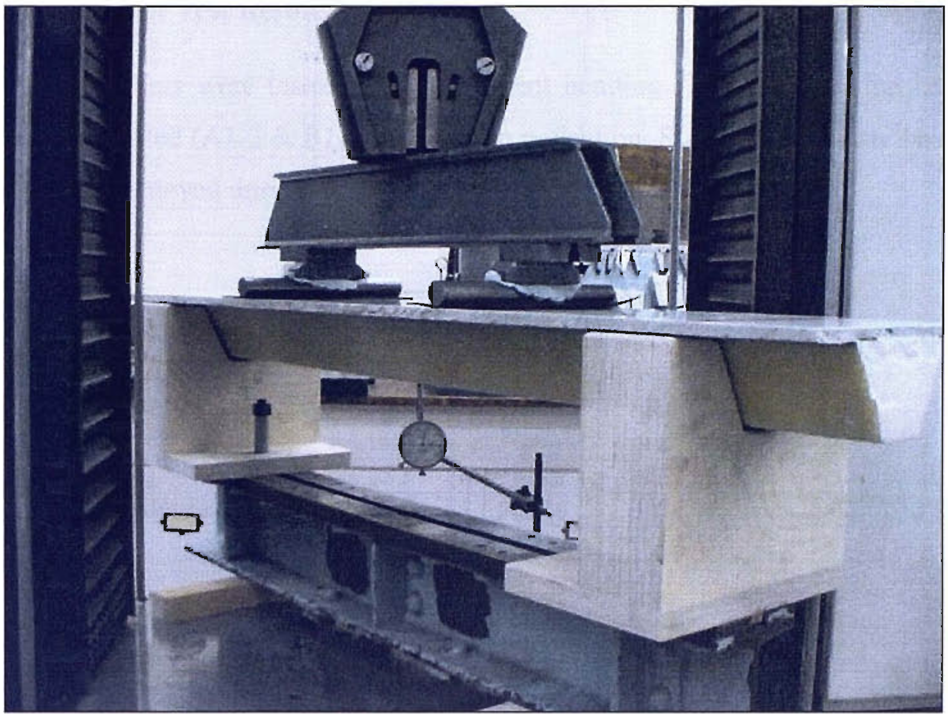

(a)

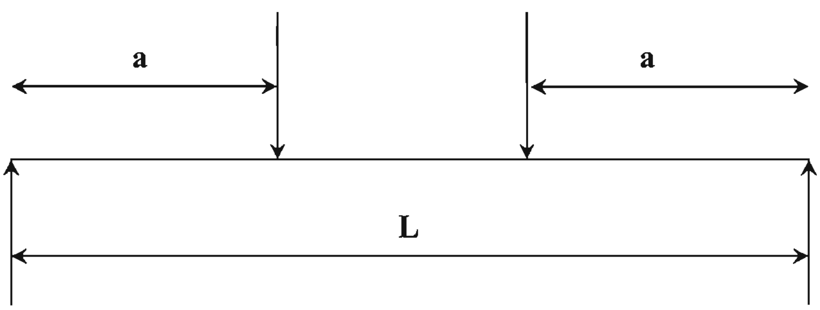

(b)

Figure 4.2 (a) Test rig and equipment (b) Four point bending set-up

Table 4.2 Separation of applied loads and supports for stiffeners A and B

Stiffeners	Distance	
	L (mm)	a (mm)
A	890	245
B	890	245

4.3 Summary of Test Results

A total six stiffeners were tested under four-point bending. Table 4.3 list the key results. Stiffness is presented (A1-3 & B1-3) as kN/mm deflection. Strength values are based on the maximum load achieved during the test.

Table 4.3 Test results summary

Test Specimens		Load at Failure (kN)	Deflection at Failure (mm)	Bending Stiffness (kN/mm)	Audible Cracking (kN)
Stiffener A	A1	23.5	13.75	1.86	12
	A2	59.5	28.59	2.04	10
	A3	64.5	31.67	2.02	10
Stiffener B	B1	54.5	29.33	1.957	12
	B2	55.5	28.19	1.838	8
	B3	52	28.9	1.84	9

Testing led to the determination of the flexural stiffness and strength when the specimens subjected to 4-point bending. The test procedure was the same for each top hat stiffener. All the specimens were tested first to assess the stiffness response of the stiffener sections and not to induce any failure. Specimens were exposed to less than 15kN. As would be expected stiffeners behaved linearly up to 15kN. The derived stiffness for all the stiffeners is given in Table 4.3. When the tests produced cracking sound which was characterised by noise emitted during the loading, the tests were stopped and the specimens unloaded. Table 4.3 also gives the load when the cracking sound was detected by ear. Then all the specimens were reloaded to failure. The failure tests indicate increased stiffener stiffness in some cases when compared to the stiffness observed in the first test. These are shown in Figures 4.2 and 4.3. The load/deflection curves of the failure test have been integrated to determine the energy absorption and hence allow comparison with work done to failure The result of this calculation is given Table 4.4 and details are given in Appendix A.

Table 4.4 Energy absorption of stiffeners

		WORK (J)
STIFFENER-A	A1	156.987
	A2	891.877
	A3	986.575
STIFFENER-B	B1	758.22
	B2	789.835
	B3	725.4

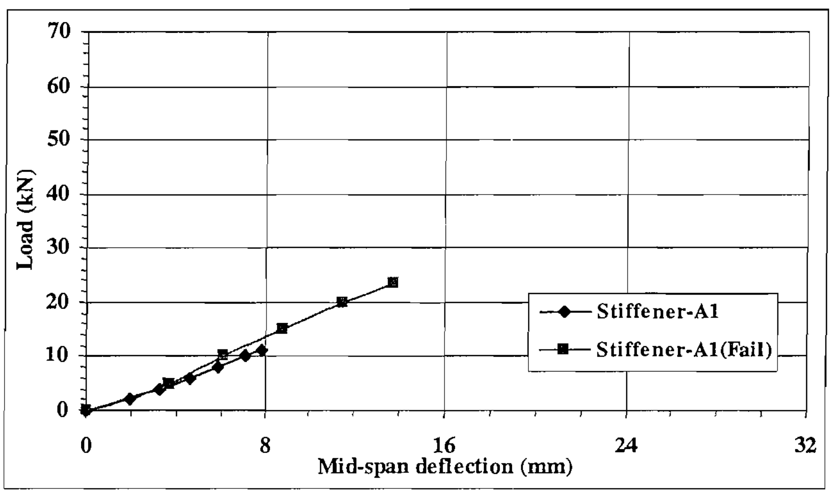

a) Stiffener-A1

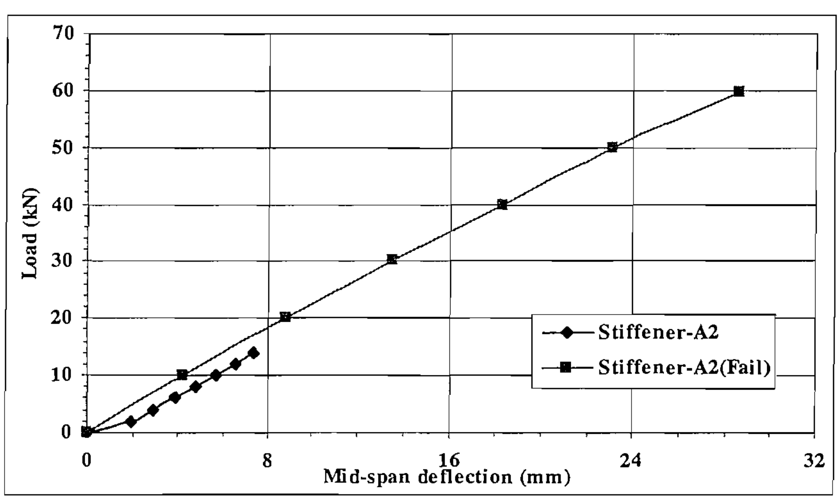

b) Stiffener-A2

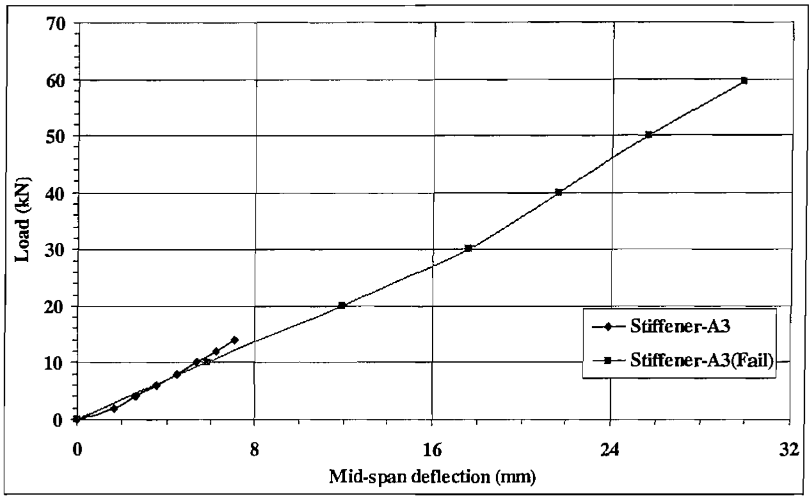

c) Stiffener-A3

Figure 4.3 Load/deflection plots for group Stiffener A

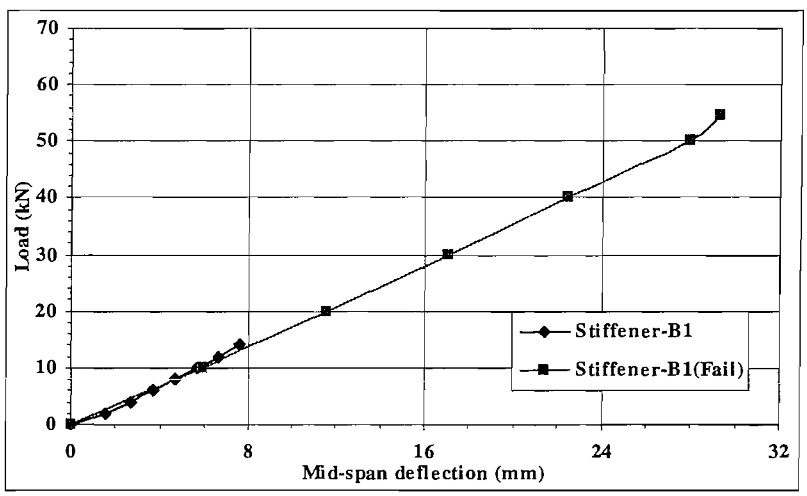

a) Stiffener-B1

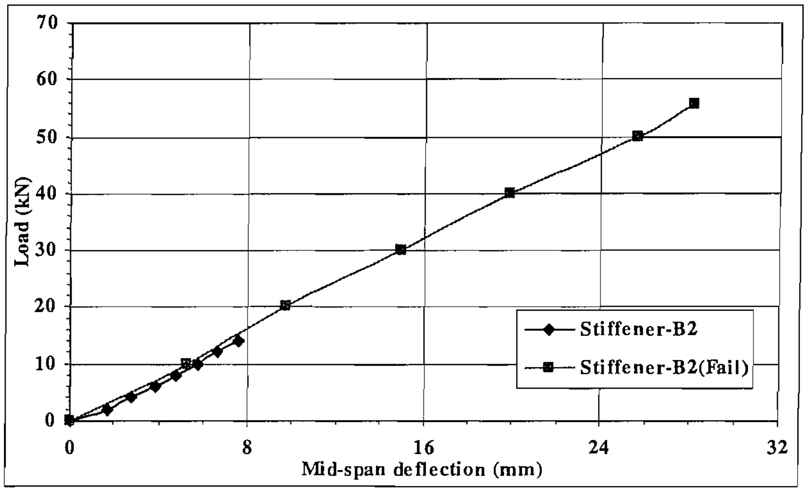

b) Stiffener-B2

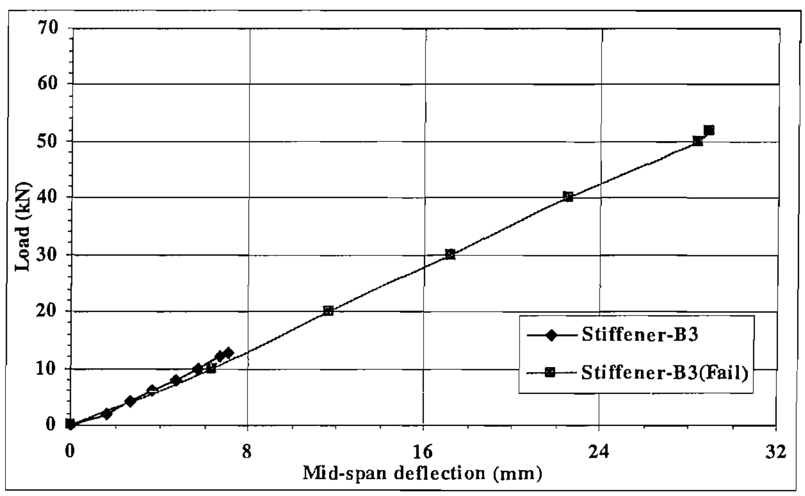

c) Stiffener-B3

Figure 4.4 Load/deflection plots for group Stiffener B

The burning tests on coupons (Appendix B) show that over foam lamination of group stiffener B (2 layers 225 g/m^2 CSM and 2 layers 600 g/m^2 Bias) have higher fibre content by volume than group stiffener A's over foam lamination (3 layers 600 g/m^2 CSM). Examination of the Table 4.3 shows that although group stiffener A had lowest fibre content, they were the strongest and stiffest in some cases. This is because group stiffener A has bigger cross-sectional area than group B which results in bigger second moment of area for the former. Table 4.3 also illustrates that first specimen of group stiffener A (stiffener A-1) had the minimum collapse strength. This is because the unidirectional layer (UD layer), which was laid over the crown is eccentric (see Figure 4.5). This caused stress concentration at the intersection between crown and web, which resulted in the fibre matrix breakage at a small load step. Substantial loading caused propagation of cracking through the web.

Initial damage was invariably matrix cracking for all stiffeners. This was characterised by noise emitted during loading. Table 4.3 gives the initial failure load when the noise was detected by ear. In addition failure was so explosive and destructive that it was difficult to record the damage progression. Failure modes for stiffeners were different based on the different construction type. After initial damage, subsequent loading caused root whitening which is caused by the presence of delamination at curved part of the overlaminate (web/flange corner) close to the support region. At ultimate collapse load, it was observed that a small amount of delamination of the stiffener flange from the base stiffener occurred near the support region in some cases. Final failure for the group stiffeners A took the form of fibre-matrix breakage on the web and flange area. On the other hand, for the group stiffeners B catastrophic shear failure occurs on the web near the support region (see Figure 4.7). From the Table 4.3, it can be seen that the failure load for Stiffener- A3 is 8.4 % more than Stiffener-A2. This caused further failure, i.e. fibre-matrix breakage failure mode near the mid-span and complete separation of stiffener from the base plate at the stiffener's end (see Figure 4.6 (b)). Based on the experimental observation a failure sequence for the top hat stiffener can be summarised as follows:

- Initial matrix cracking
- Root whitening and delamination at the region of the web/flange corner and flange area.
- Final failure mode: fibre matrix breakage for group A and catastrophic shear failure for B.

An optical photograph was used to investigate the detailed failure surfaces, which are illustrated in Figure 4.8.

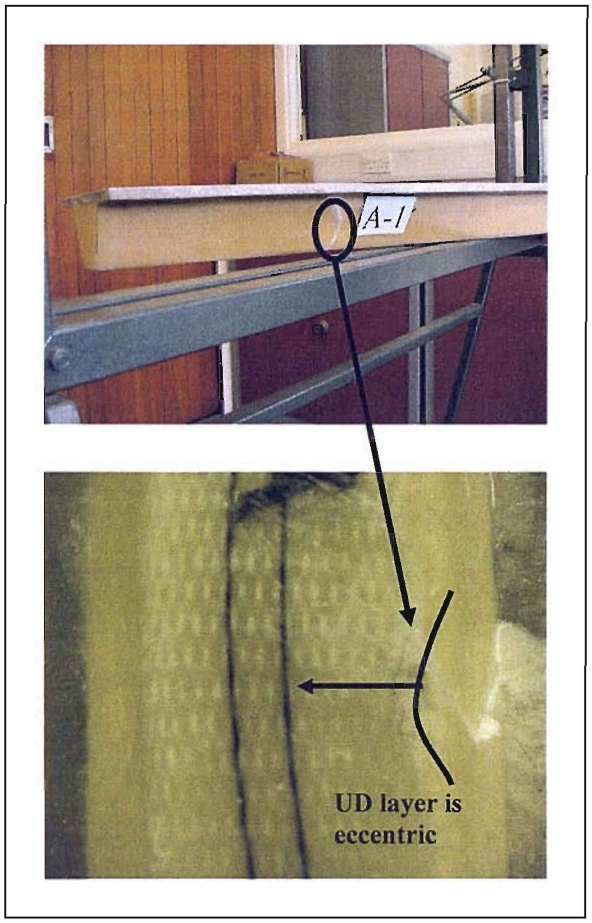

Figure 4.5 Unidirectional layer is eccentric at crown for Stiffener-A1

4.4 Discussion

4.4.1 Effect of Material Choice for Lamination

The material choice appears to have an effect on the performance of top hat stiffeners. Previous works [39, 40, 42] had focused on overlaminate reinforced with woven roving layers with polyester resin. In this study overlaminate constructed by two types of lay-up; Type A and Type B. The Type A lay-up was made up of 3 layers of 600 g/m^2 CSM which was used for the group stiffener A. On the other hand Type B lay-up was made up of 2 layers of relatively lighter 225 g/m^2 CSM stitched to 600 g/m^2 Bias used for group stiffener B. As can be seen from the Figure 4.1 Type A lay-up increased the overlaminate thickness by 66.6% compared to Type B lay-up. Bending stiffness calculations of both types of top hat stiffener also showed that overlaminate reinforced with Type A lay-up increased the EI value by 5% (Appendix C), but Type A lay-up also increased the stiffener weight by14%.

Despite the similarities in failure mechanisms there are differences in failure load and displacement of the both type of stiffeners (see Figures 4.3 and 4.4). These differences seen between the same specimen group highlights the difficulties in producing uniform quality for top hat stiffeners. Table 4.4 shows the energy absorption of both types of stiffeners. From this table it is clear that the energy absorption of the specimens also vary even in the same specimens group which might be the reason just explained above. Generally energy absorptions of the stiffeners' overlaminate made up with Type A lay-up are higher compared to stiffeners' overlaminate made up with Type B lay-up. This is due to fact the Type B lay-up is more brittle compared to Type A lay-up which was also observed during the experimentation regarding failure mode and maximum deflection. As mentioned earlier production quality has an effect on stiffeners performance. Although Stiffener-A1 overlaminate made up with Type A lay-up, it collapsed at the minimum failure load amongst the other stiffeners, due to UD layer laid on the crown eccentrically (see Figure 4.5)

4.4.2 Failure Mechanisms

The experimental programs previously conducted on a top hat slice [45,54,75,76,77] have been based on three-point bending, reverse bending and pull off tests. An interesting comparison can be made between current study and previous work with regard to the failure mechanisms. Interestingly, the initial failure mode is unchanged. The failure started with cracking sound at a small load step which could be interpreted as matrix cracking. Subsequent loading caused the next identified failure which is also unchanged. The nature of this failure delamination in the curved part of the overlamination which is characterised by the whitening. Final failure modes on the other hand vary from sample to sample. In the current study final failure of the group stiffener A whose overlaminate reinforced by 3 layers of 600 g/m^2 CSM took the form of fibre matrix breakage occurring in the web and flange of the stiffeners. The top hat stiffener with overlaminate made up of 2 layers of 225/600 g/m^2 CSM/Bias failed by shear in the web. Final failure of the previous work (see Table 2.2) had shown catastrophic failure which was complete separation of one stiffener flange from the base panel. This comparisons highlight several points.

- The strain that a laminate can reach before micro cracking depends strongly on the toughness and adhesive properties of the resin system. For brittle resin systems, such as most polyesters, this point occurs a long way before laminate failure, and so severely limits the strains to which such laminates can be subjected [78]. As an example under out-of-plane loading top hat stiffeners exhibits firstly matrix cracking. This failure mode will be discussed in chapter 6 experiments on top hat stiffened panel which was mounted with strain gauges.

- The curved part of the overlaminate (web/flange corner or boundary angle) is prone to delamination which is characterised by whitening in this region.
- As it mentioned above group stiffener A whose overlaminate is made up from Type A lay-up exhibit non-catastrophic failure mode compared to failure mode of group stiffener B which was catastrophic shear failure. This indicates that group stiffener A may have advantages from damage tolerance and survivability point of view.

The next chapter will be discussing the mechanics of the top hat stiffener by using FE method to categorise the stress states. These stresses can then be used to assess the likely causes of failure.

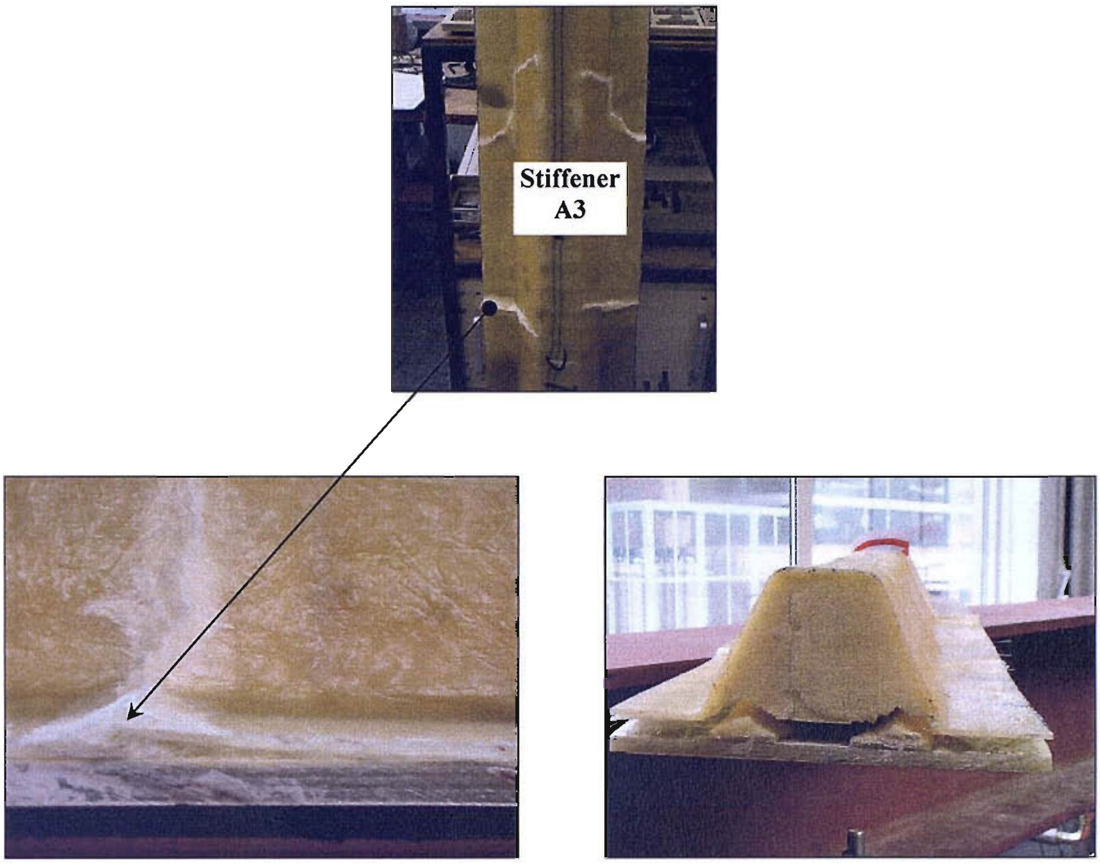

(a) Delamination and fibre-matrix breakage

(b) Complete separation of stiffener from base plate

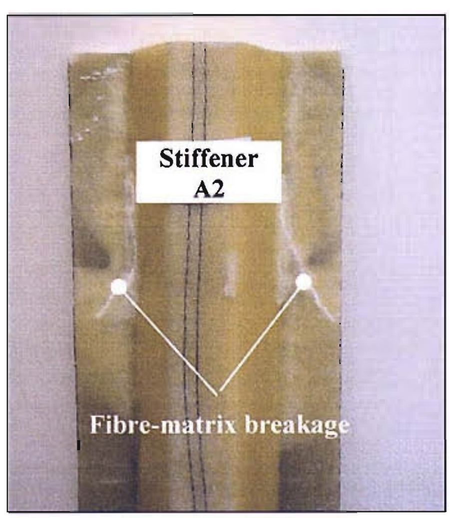

(c) Fibre-matrix breakage on the flange

Figure 4.6 Failure mechanisms of group stiffener A

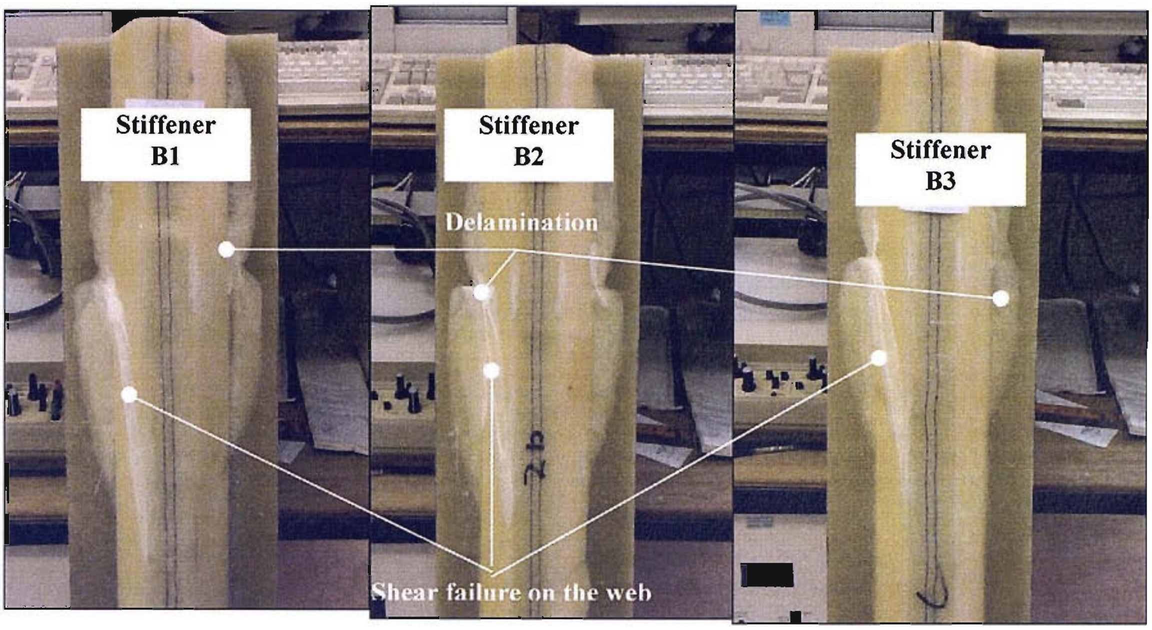

Figure 4.7 Failure mode of group Stiffeners B

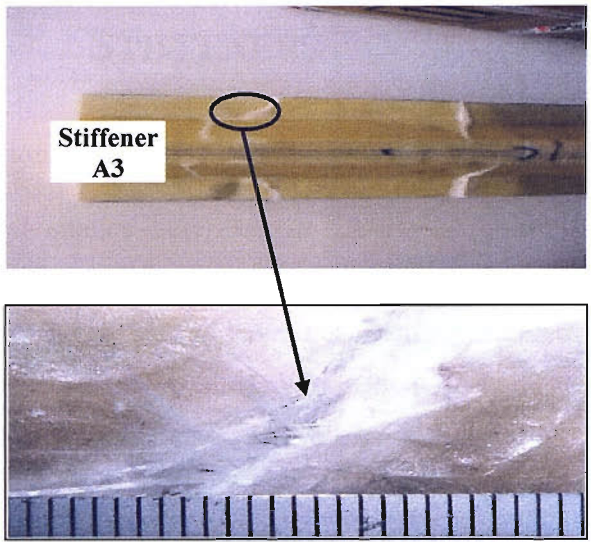

(a): Stiffener-A3
Scale (1mm = 1mm × 3.5)

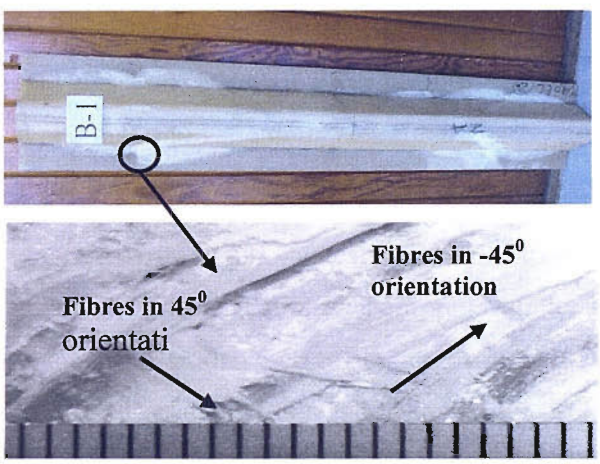

(b): Stiffener-B1
Scale (1mm = 1mm × 5)

Figure 4.8 Macroscopic failure photograph of Stiffeners A3 and B1

Chapter 5 THEORETICAL STUDY OF TOP-HAT STIFFENERS

5.1 Introduction

The experimental studies described in Chapter 4 above have illustrated the overall performance of a wide range of top-hat stiffener. However, the internal load transfer mechanisms, and stress states, have not been considered due to the difficulties in determining this level of detailed information during the experimentation. Previous theoretical analyses (see section 2.2) have been successful in showing this information but have been very limited in the marine field. The work described in this chapter has aimed to redress the shortcomings in the experimental methods by illustrating the load transfer mechanisms within them.

The finite element studies relating the top hat stiffeners were conducted in two stages: 1) detailed 3-D analyses of a wide range of a top hat stiffeners configuration to determine the critical geometrical and material variables 2) Parametric study using 3-D models to illustrate the effect of the critical variables on the performance of top hat stiffeners.

In addition, and prior to stage 1), studies were made to assess the characteristics and ANSYS finite element (FE) packages its element and validity of their application to this problem. Analytical method was also used to predict the global response of top hat stiffeners. Analytical method is based on the 2-D Elastic beam theory. These studies are presented in Appendix C.

5.2 Model Definition

5.2.1 Geometry

The definition of the top hat stiffeners is given in chapter 4. The focus is the behaviour of the stiffener connection to the panel laminate. The top hat stiffener section is symmetric both longitudinally and transversely. Taking advantage of symmetry means that quarter model can be produced with two planes of symmetry being used to define full model (see Figure 5.1). The mesh density can then be refined in the area of complex geometry present at the web/flange corner of the top hat stiffener without overly compromising computational efficiency in ANSYS.

5.2.2 Modelling

The finite element program ANSYS 7.0 Structural U version is used for modelling of the problem. In order to correctly orientate the fibre direction for variation in geometry compared to a global coordinate system, local coordinate systems are set-up. The overlaminate including the web/flange corner, web and web-crown corner have laminate properties associated with defined local coordinate systems, which are shown in Figure 5.2.

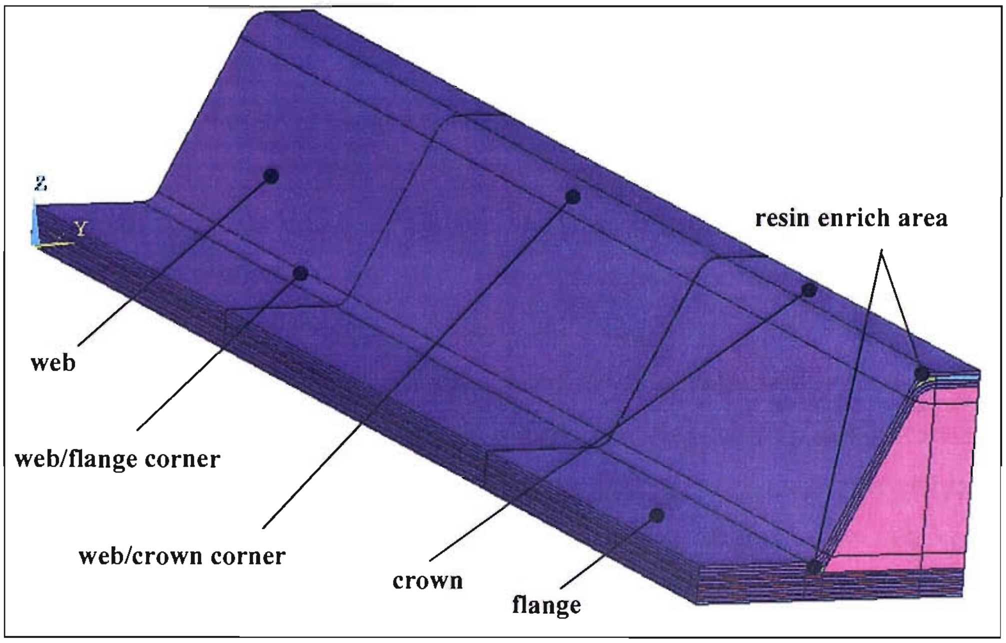

Figure 5.1 Quarter FE model representation of top hat stiffener

5.2.3 Meshing

The mesh of the modelled structure should be generated so to allow a smooth increase in element numbers towards the regions of geometric diversity. The element shape of choice should be hexahedral rather than pyramidal or tetrahedral since this latter element shape is considered to be structurally stiffer. Furthermore hexahedral meshing allows more computationally efficient solution given the reduced number of elements required for meshing. The model is "map" meshed throughout with hexahedra with exception the region of the anticipated high stress is also an area of geometric complexity and is consequently not able to be meshed with hexahedra by ANSYS meshing facility (see Figure 5.3). In this region tetrahedral elements are used and "free" meshed by ANSYS with pyramidal element used at the interface between tetrahedra and hexahedra elements.

In practice 2-D and 3-D models are extensively used to model complex structures. 2-D with shear deformable models are usually preferred to CLPT. However 2-D might not be able to predict the stresses exactly. Since the exact solutions are not available for the top hat stiffened structures and it is very important to calculate the stress state when developing the composite behaviour the 3-D models are employed in the present investigation.

Within the ANSYS 3-D shell elements (labelled Shell91 and Shell99) and 3-D solid elements (labelled Solid46 and Solid45) were considered. Comparison of element formulation as follows

a) Shell elements

There are two eight node shell elements (labelled Shell91 and Shell99). They are basically similar in formulation with Shell99 being an extended version of Shell91 to allow up to 100 layers through thickness instead of 16. The formulation based on the standard isoparametric approach such as given by Yunus [79] . The displacement function is quadratic in the plane of the elements and constant through thickness direction with a correction applied to allow for different surface boundary conditions. Since the formulation allows the curvature there are additional coupling terms between the in-plane and through thickness directions. Strain-displacement relationship is based on the global equations and does not consider the layer arrangement. This is not a particular problem since the displacement continuity requirements between layers limits the amount of variation that can occur. Stresses are computed from strains using local layer properties, thus good layer results are also achieved. The shear strain is adjusted to ensure it is zero at the free surfaces and maximum in the centre of the laminates. The distribution of the shear strain is assumed to be parabolic in nature with a maximum value at mid-plane of one and a half times the average value.

This element formulation incorporates terms to represent curvature and overcomes some of the constant properties through-thickness by incorporating adjustment based on the fact that the shell element is not stacked and therefore certain conditions, such as shear strain at the free surfaces are known. However this type of formulation is not suitable to model the out-of-plane joint problem as some stacking in the through thickness direction is always required [80].

b) Solid Elements

An eight node layered solid element (called Solid46) is available within ANSYS library. It is based on the "non conforming" element of Taylor [29] in the three dimensional form and has a linear displacement function (to which extra quadratic shape function can be added) which is the same in all three orthogonal directions. It is noted in the theory manual this function is attempting to model a multi linear problem in the through-thickness direction. Effective (averaged) material properties are used through thickness and geometric properties are determined from the mid-plane. This last feature leads to inaccuracies in the through-thickness integration when the element has non-parallel faces at the ends of the layers, as required to model curvature. Strains at the points of interest are evaluated from global displacement using the overall strain-displacement relationships and stresses are then determined using the layer properties, within the limitations of the displacement functions stresses are realistic. The exception is through-thickness direction where the nominal stress is calculated from the nodal forces and the effective material properties making it constant through the thickness. The accurate calculation of through- thickness stress is crucial for top hat stiffened structures as the structure sustained damage at the curved part of the overlaminate in the form of delamination well before ultimate in-plane laminate material stress limit is reached. Therefore this type of formulation is not suitable to model top hat stiffened problems

Solid45 element was used for all the modelling of composites in chapters 5 and 7. It is defined by eight nodes having three degrees of freedoms at each node, i.e. translations in the nodal x,y and z direction. Solid45 elements with a quadratic displacement assumption are generally recommended as the best compromise between the relatively low cost but inferior performance of linear elements and the high cost but superior performance of cubic elements (SOLID95). The layers of top hat stiffener have been modelled through thickness with one an element per ply since it is very important to calculate the correct stress state. SOLID45 element is defined by eight nodes having three degrees of freedom at each node: translations in the nodal x, y, and z directions. The theoretical basis of the SOLID45 and its validity to top hat stiffener problem is given in Appendix C.

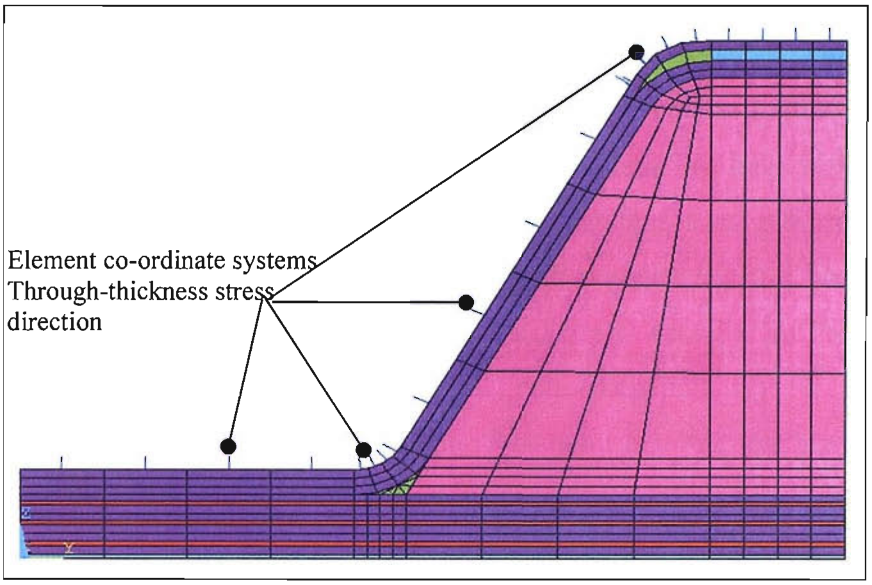

Figure 5.2 Local co-ordinate systems for group stiffener A

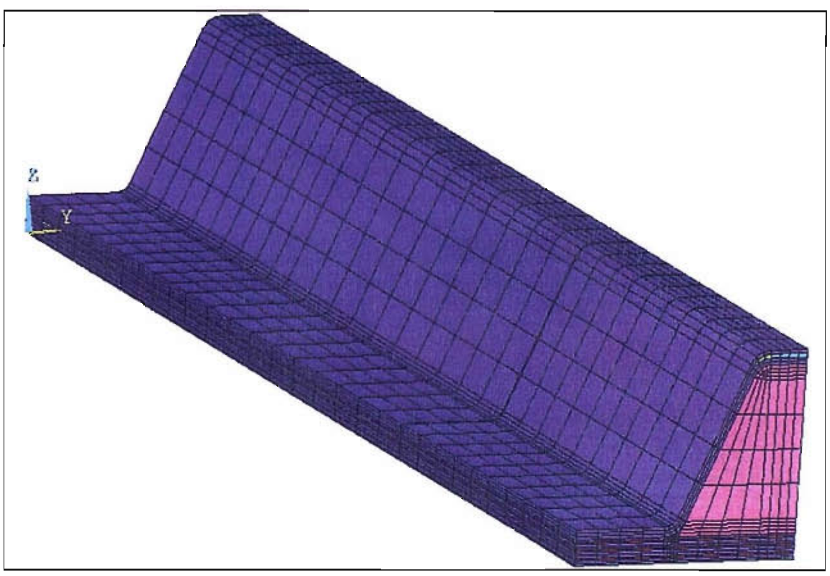

Figure 5.3 Illustration of mesh densities of Stiffener-A2

5.2.4 Material Properties

The laminates of top hat stiffener are made up from chopped strand mat (CSM) in different weight e.g. 600,450 and 225 g/m^2 and glass fabric laid up alternatively 0/90, ±45 and 0 orientation used with isopthalic and polyester resin and exhibiting linear material properties. The material characterization properties are given in Appendix B and listed in Table 5.1.

5.2.5 Loading and Boundary Condition

The test carried out in the experimental program only simply supported boundary conditions are applied to the top hat stiffener section. The loads, which have been applied to the models, have been chosen so as to represent the loads at which damage has been observed in four-point bending experiments. Boundary conditions have been chosen the represent, as close as possible the condition of simply supports. Finite length wooden support has effect on FE model stiffness. A sensitivity analysis has been carried out to account for the difference in the stiffness of the FE model and the test specimen (Appendix C) FE analyses were performed for different three support spans under four-point bending loading and compared to results obtained from 2-D elastic beam theory and experimental finding. As a result of this investigation numerically only lines of nodes in the model are suitably constrained in the direction of the centre of curvature. Figure 5.4 describes the load and boundary conditions applied in the numerical model.

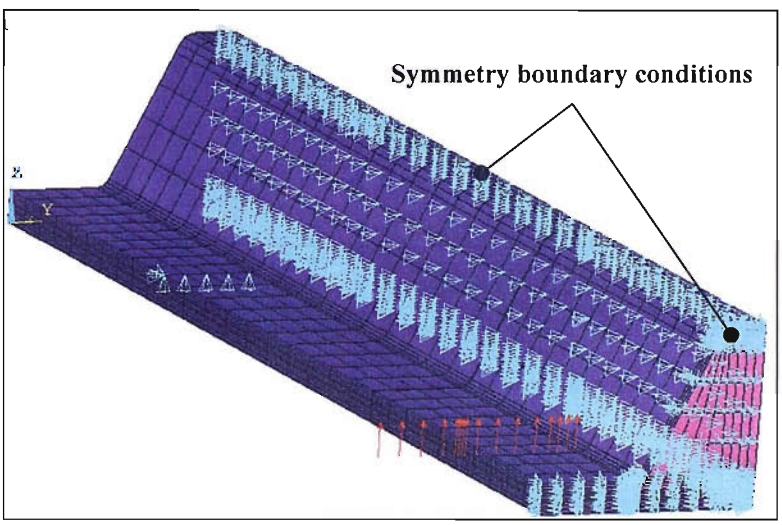

Figure 5.4 FE model representation

5.2.6 Solution

The solution was obtained using the IRIDIS computational facilities at University of Southampton. Iridis contains, 548 processors; consisting of 292 1Ghz Intel Pentium III's; 214 1.8Ghz Intel Xeons, 32 1.5Ghz Intel Pentium IV's and 10 0.8 Ghz Itaniums, Over 300 Gb of memory, 12 Tb of local disk storage and 2.8Tb on RAID5 disk array. Typical solution times for a linear analysis were between 5 and 10 minutes.

Table 5.1 Material Properties

Material	Property	Value
300 g/m^2 CSM with isophthalic polyester resin*	E	8 GPa
	G	3 .1 GPa
	Poissons ratio υ	0.3
	Tensile strength	107.14 MPa
600 g/m^2 CSM with ortophthalic polyester resin	E	6.8 GPa
	G	2.6 GPa
	Poissons ratio υ	0.3
	Tensile Strength$^+$	130 MPa
	Interlaminar tensile strength	11.2 MPa
	Interlaminar shear strength	22 MPa
600 g/m^2 Woven rowing with ortophthalic polyester resin	E_x	14.8 GPa
	E_y	14.8 GPa
	G_{xy}	2.4 GPa
	Poissons ratio υ_{xy}	0.092
	Tensile Strength$^+$	300 MPa
	Interlaminar tensile strength	12.2 MPa
600 g/m^2 Bias layer with ortophthalic polyester resin	E_x	9.9 Gpa
	E_y	9.9 GPa
	G_{xy}	6.6 GPa
	Poissons ratio υ_{xy}	0.49
	Tensile strength	100 MPa
	In-plane shear strength	28.9 MPa
1600/ g/m^2 UD layer with ortophthalic polyester resin	E_x	24.6 GPa
	E_y	7.3 GPa
	G_{xy}	2.3 GPa
	Poissons ratio υ_{xy}	0.39
	Tensile strength$^+$	750 MPa
Polyurethane Foam	E	28 MPa
	G	10.76 MPa
	Poissons ratio υ	0.3

+: Measured values from coupon tests (Appendix B)

The other material properties are derived from the literature [7,40,81] and also derived from manufacturers

5.3 Validation

5.3.1 Introduction

Without a full material characterization available to apply to FE models, it is difficult to ascertain the causes of any disagreement between experimental and predicted data. However it is possible from FEA to determine for assumed material properties the mechanisms behind the experimentally observed stiffener section response. The numerical result analysis is concentrated on the response of Stiffener-A2 and Stiffener-B2.

5.3.2 Load-Deflection Results

For validating the finite element modelling of Stiffener-A2 and Stiffener-B2 the load/deflection characteristics of the models were compared to experimental data, which are shown in Figures 5.5 and 5.6. As detailed in Table 5.2 the difference in stiffness of the predicted response in comparison with experimental data is reasonably good. This provides confidence in the assumptions combined geometry and that the numerical mesh and boundary conditions are sufficiently descriptive of the physical experiment.

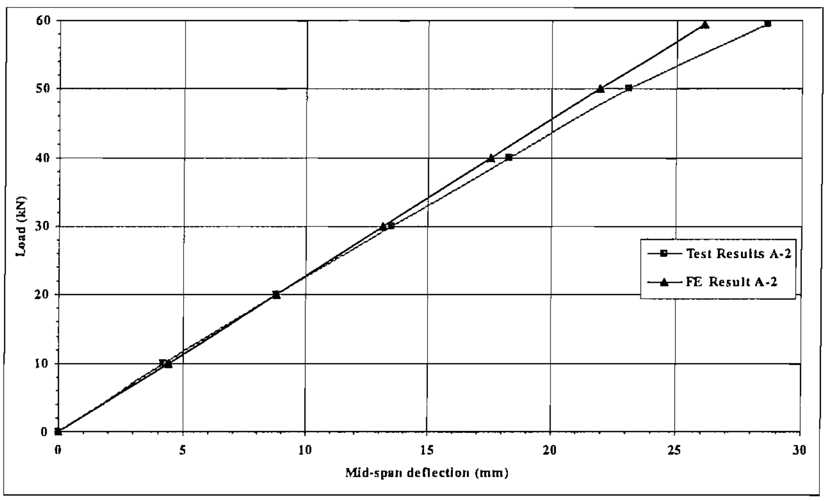

Figure 5.5 Load/deflection plots for Stiffener-A2

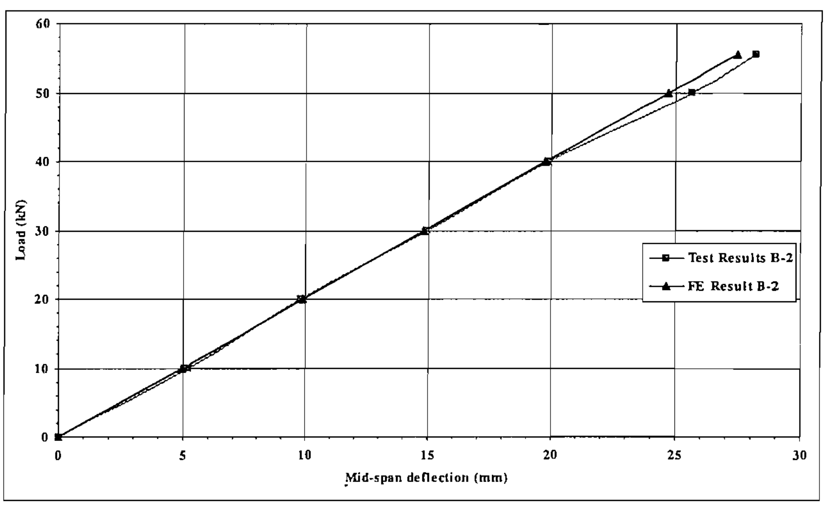

Figure 5.6 Load/deflection plots for Stiffener-B2

Table 5.2 Comparison of predicted stiffness with experimental data

Top Hat Type	Four-Point Bending		
	FE (kN/mm)	Expt. (kN/mm)	Error %
Stiffener-A2	2.28	2.02	8.7
Stiffener-B2	2.02	1.96	2.97

5.3.3 Correlation between Experimental Failure Loads and FE Stress Levels

With the use of laminated plies to transfer loads carried by the base panel into stiffener it is common for the plies to fail within the curved part of the overlaminate specifically fillet radius (web/flange corner) [40]. In this region the developed through-thickness tensile stresses can quickly exceed the strength of laminate due to very low material strength limits. Hence the stress distributions of interest are the overlaminate through-thickness and in-plane stresses, flange plate through-thickness and in-plane stresses. It is also necessary to compare the load transfer mechanisms predicted from the FE models with some experimentally derived failure modes

At experimental initial load of 10kN (4.21mm), audible cracking of the Stiffener-A2 was observed, no apparent damage was visible. At this load level initial stiffness of the test specimen is 2.37kN/mm. The initial stiffness of the FE model is 2.28kN/mm, i.e. FE model 4% flexible than the test specimen. Examination of the stress components in numerical results suggests that no material strength limits were being exceeded at this load which would account for the audible cracking. However it is possible that the presence of voids produced during the manufacturing process results in stress concentrations, which could have caused matrix cracking. In the Stiffener-A2, the overlaminate consists of three layers made of 600g/m^2 chopped strand mat (CSM). Increasing the load to value of 20kN (8.82mm) the maximum through thickness stresses σ_{zz} in Z direction occurring the outer surface of the curved part of the overlaminate is exceeded the material stress limit in Table 5.1 in Figure 5.7. Hence, delamination is likely to form in this location due to high through thickness stresses. This corresponds to position of root whitening which is caused by the presence of delamination observed in the experiment at a load of 20kN.

With increasing the load, the predicted failure within the failure zone will grow and global stiffness will start to reduce with reduce local stiffness in the failure zone.

Considering that the linear-static analysis is unable to describe this reduced stiffness response thereby redistributing the stresses according the future prediction as to sites of failure may be unrealistic.

The next two load steps, the failure happened at a load of 25kN (≅11.5mm) and 40kN (18.3mm). The interlaminar shear stress are exceeded in X-Z and Y-Z plane (σ_{xz}, σ_{yz}) in Table 5.1 in Figures 5.8 and 5.9 in the flange and curved part of the overlaminate respectively. Therefore matrix cracking would be predicted due to high interlaminar shear stress. The curved part of the overlaminate already present delamination at its curved region and being exceeded with an interlaminar shear failure, fibre breakage is expected within this location Damage was visible in this location in the experiments as the top hat stiffener approached final failure.

In case of the Stiffener-B2, the overlaminate consists of four layers, of which two layers are 225g/m^2 CSM and two layers 600g/m^2 Bias [±45^0]. In the experiments, the Stiffener-B2 failed catastrophically. The first identified failure appears to happen at a load of 20kN (9.76 mm). The maximum through thickness stresses in Z direction (σ_{zz}) occurring in the outer surface of the curved part of the overlaminate is exceeded the material stress limit for Bias in Table 5.1 in Figure 5.10. Hence, FE model predicts delamination. This is approximately same location where delamination was seen in the experiment. Increasing the load 25kN (12.22 mm) further leads to next identified failure. The in-plane shear stress occurring in Bias layer in Y-Z plane (σ_{yz}) is higher than the quoted in-plane shear strength of 28.95kN for the Bias material [81] in Figure 5.11. Figures 5.12 and 5.13 show the dominant in-plane stress is 203.5MPa in tension (σ_x) occurring at the web/crown corner and 93.5MPa in-plane shear stresses occurring in the web in X-Y plane (σ_{xy}) for the outer surface of the overlaminate (Bias layer) respectively. Due to the maximum shear stresses is approximately 3.5 times higher than the material stress limits, FE predicts shear failure in the web region before ultimate tensile strength of the material is exceeded. This exactly matches with the experimental findings.

A- Internal Stress Distributions for Stiffener-A2 [Figures 5.7 to 5.9]

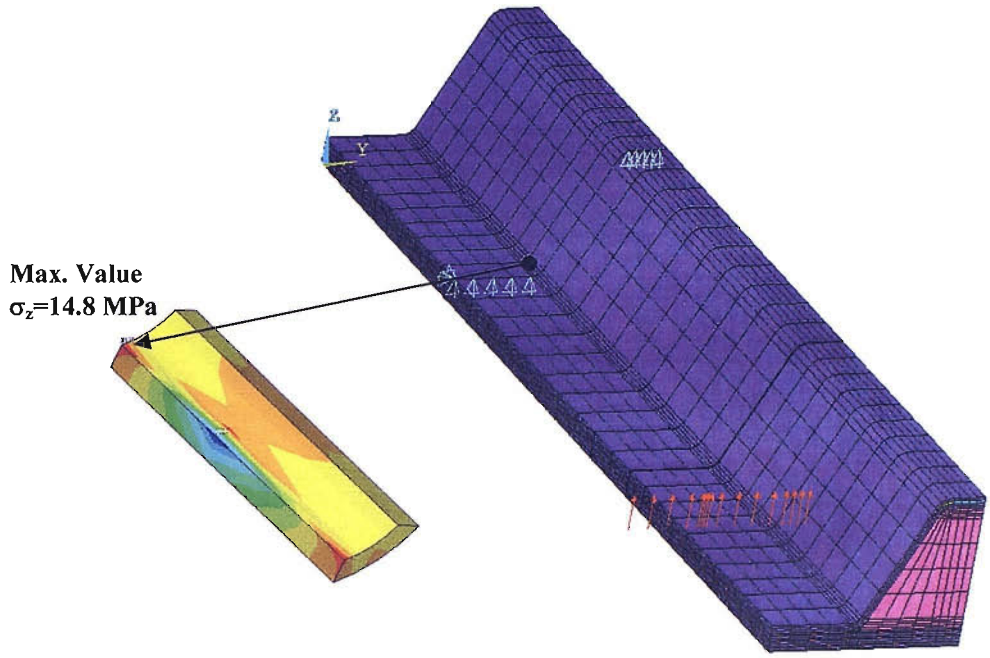

Figure 5.7 Through-thickness stress distributions at a load of 20kN

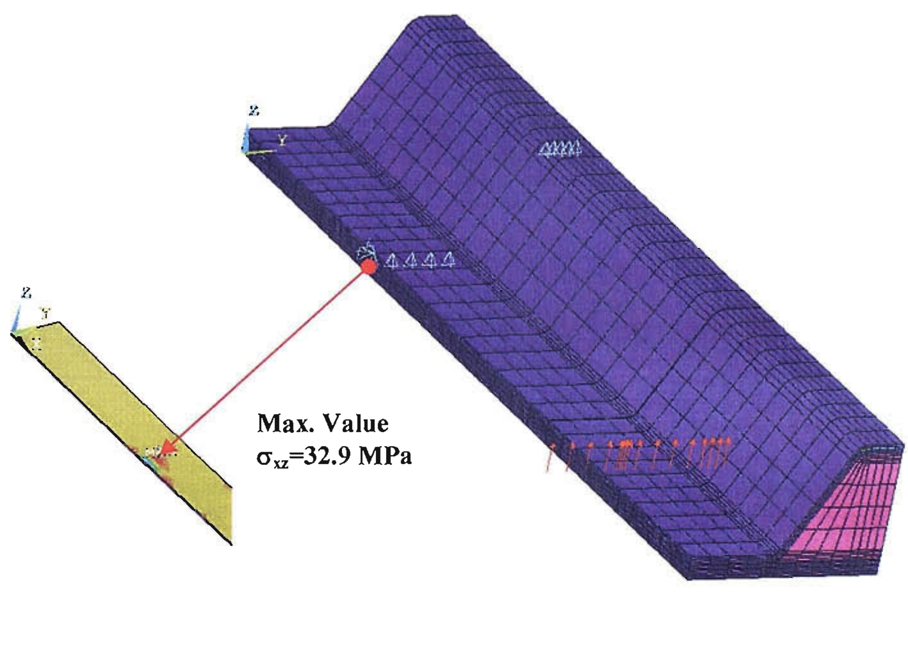

Figure 5.8 Interlaminar Shear stress distribution in X-Z plane at a load of 25kN

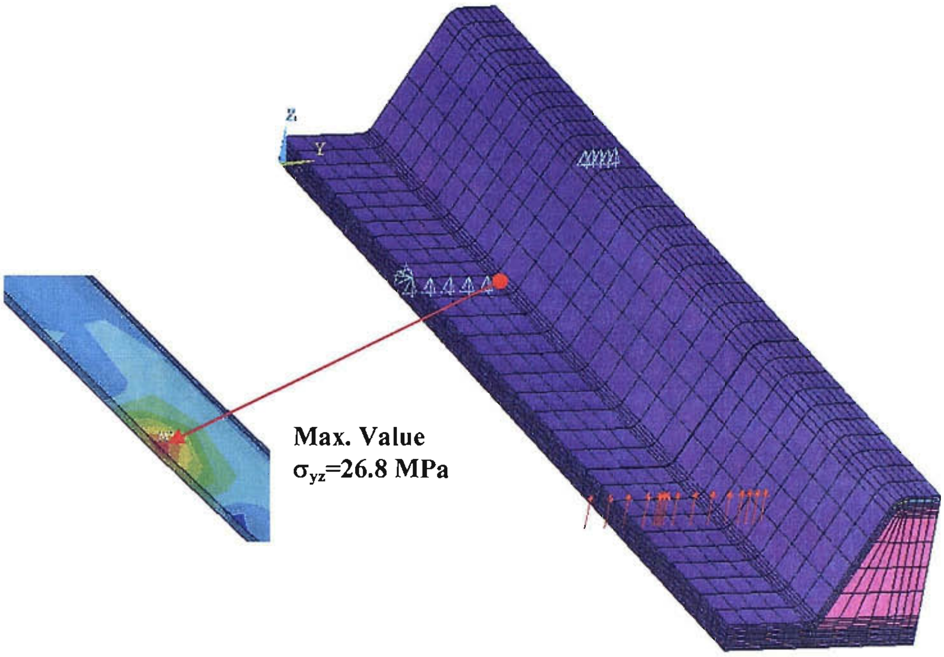

Figure 5.9 Interlaminar Shear stress distribution in Y-Z plane at a load of 40kN

B- Internal Stress Distributions for Stiffener-B2 [Figures 5.10 to 5.13]

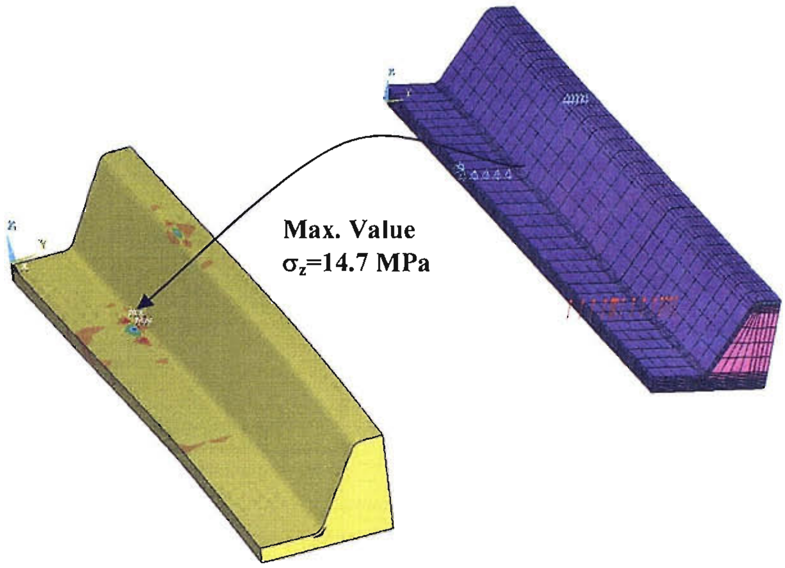

Figure 5.10 Through-thickness stress distribution at a load of 20kN

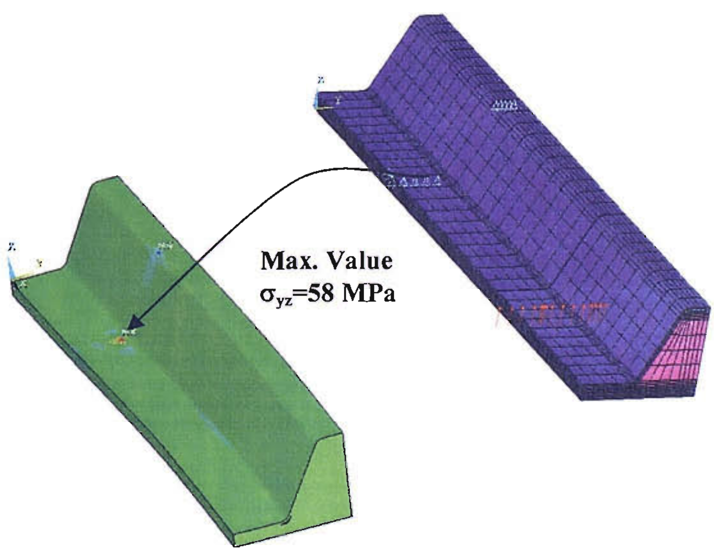

Figure 5.11 Shear stress distribution in Y-Z plane at a load of 25kN

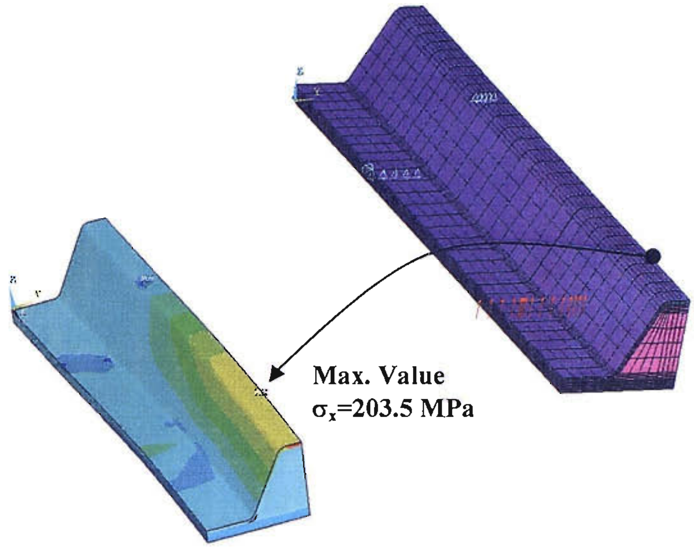

Figure 5.12 Tensile stress distribution at a load of 55.5kN

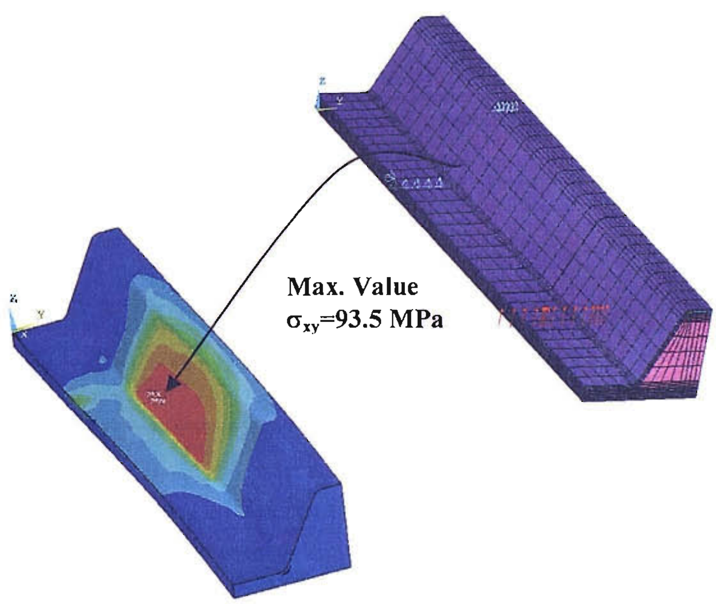

Figure 5.13 Shear stress distribution in X-Y plane at a load of 55.5kN

5.4 Analytical Solution

In the early stage of the design simple method of calculation are needed so that preliminary estimates of the response of the composite top hat stiffeners can be made. 2-D Elastic beam theory was used to predict the maximum deflection, bending stress and shear stress. The results were compared to the finite element results and experimental findings. Good correlation was found on all account. The results were compared to finite element analysis and experimental findings and listed in Table 5.3.

Table 5.3 Comparison between FE, analytical and experimental results from four-point bending test for Stiffener-A2

	FE (SOLID45)	BEAM THEORY	EXPERIMENT
Deflection δ (mm)	27.3	24.3	28.6
Max. Stress σ_x (MPa)	156.2	155.5	NA
Shear Stress τ_{xy} (MPa)	47.2	45.8	NA

The co-ordinate system for FE model is given in Figure 5.15. The location for values of deflection and stresses are given at below

δ_{FE} : (a=625,b=117.5,h=92.85) At the mid-point of the stiffener

$\delta_{ANALYTICAL}$: (a,b,h=92.85) At the mid-point of the stiffener

$\sigma_{x\ FE}$: (a=625,b=117.5,h=92.85) At the mid-point of the stiffener (on the crown)

$\sigma_{x\ ANALYTICAL}$: (a,b,h=92.85) At the mid-point of the stiffener (on the crown)

$\tau_{xy\ FE}$: (a=278,b=54.29,h=19.99) In the web of the stiffener

$\tau_{xy\ ANALYTICAL}$: (a,b,h=21.48) In the web of the stiffener

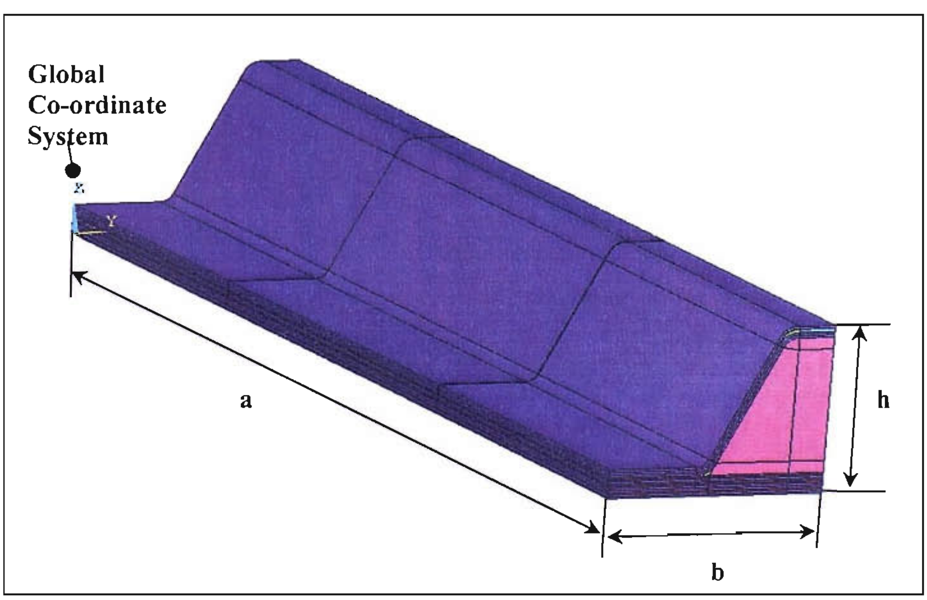

Figure 5.14 Co-ordinate system for top hat stiffener

5.5 Parametric Studies of Top Hat Stiffener to Plate Connections

5.5.1 Basis of the Study

The experimental study in chapter 4 and theoretical study presented here identified the failure mechanisms associated with different top hat stiffener design clearly show the influence of overlaminate lay-up material and thickness on performance of top hat stiffeners. However, to more fully understand the effects of different design variables on the performance of the top hat stiffeners parametric study was completed. The previous work on top hat stiffener to shell plating joints [39, 40] had shown fillet radius and overlaminate thickness were the critical design variables. The effects of those variables on top hat stiffener joint are given in Tables 5.4 and 5.5. Hence the variables considered in this analysis were the lay-up material, overlaminate thickness and the radius of the fillet. Two types of lay-up material were used for the overlamination: (i) 3 layers of 600 g/m^2 CSM (Type A) and (ii) 2 layers of relatively lighter 225 CSM stitched to 600 g/m^2 Bias (Type B). The overlaminate thickness varied between 2 to 5 layers of 600 g/m^2 CSM and 225/600 g/m^2 CSM/Bias for stiffener A and B respectively. The radius of the fillet varied between 12 mm to 60 mm.

Table 5.4 Top hat stiffeners and impact of geometrical variations Centre clamp set-up [39]

Increase in property	Effect on stiffness	Effects on stress in fillet	Effects on stress in overlaminate
Radius	Marginal increase	Minimum at 75 mm	Decrease
Overlaminate thickness	Marginal increase	Increase	Increase

Table 5.5 Top hat stiffeners and impact of geometrical variations Two-clamp set-up [39]

Increase in property	Effect on stiffness	Effects on stress in fillet	Effects on stress in overlaminate
Radius	Increase	Minimum at 75 mm	Decrease
Overlaminate thickness	Increase	Decrease	Increase

5.5.2 Results

The results of this analysis are shown Figures 5.15 to 5.22. This show overall displacement, (predicted at centre of the stiffener), maximum through-thickness stresses (predicted in the web/flange corner), maximum tensile stresses (predicted on the crown) and maximum shear stresses (predicted in the web of the stiffener) for a constant load (in this case 55.5kN chosen as it is the failure load for group stiffener B). Each graph includes a series of curves for different radii. Several features can be seen.

1. Considering the Figures 5.15 and 5.16, the central deflection decreases increasing the overlaminate thickness and fillet radius. This effect is matching with previous work findings [40]. It is also clear from those figures; increase in overlaminate thickness has significant effect on central deflection while this is insignificant by increasing the fillet radius. The figures also show at a same thickness of overlaminate the stiffener with Type A lay-up is more flexible. Similar trend is seen regarding the load/central deflection plots for both types of stiffeners.

2. The maximum tensile stress on the crown decreases with increasing the overlaminate thickness and fillet radius for both types of stiffeners (see Figures 5.17 and 5.18). The range of variation is small when increasing the fillet radius; on the other hand it is much larger when increasing the overlaminate thickness. The figures also indicate that by using stiffener with overlaminate made up Type B reduces the magnitude of tensile stresses by 6.2% with a 4.5 mm overlaminate thickness and a maximum fillet radius.

3. The Figures 5.19 and 5.20 show the maximum shear stress distribution in the web of the stiffener. Similar conclusion as above can be drawn. Overlaminate thickness appears to have significant effect on the shear stress distribution in the web. Shear stress decreasing considerably increasing the overlaminate thickness. Radius of the fillet has small effects on shear stress distribution in the web. For example as the radius of fillet increases from 48mm to 60 mm the shear stress reduces only 3% for both type of stiffeners. Generally shear stress distributions are higher when the Type B lay-up is used for the stiffener overlamination. For example overlamination with a thickness of 2 laminations (2.7 mm) shear stresses increased by 54% by using Type B lay-up.

4. Figures 5.21 and 5.22 show the through-thickness stresses in the web/flange corner. It is found that increase in overlaminate thickness and fillet radius decreases the through-thickness stress distributions. Compared to the tensile and shear stress distributions the effect of the fillet radius considerable. These effects are similar to the previous works [39, 40]. For the both type of stiffeners, the maximum through-thickness stresses in the web/flange corner shows a maximum value with a thickness of two lamination (3mm and 2.7mm for Type A and Type B respectively) and they decrease as the laminations are added. The trend on the other hand varies between two stiffeners. Decrease in through-thickness stresses is considerable when the number of layers increased from 2 to 3 for the stiffener with Type A lay-up. But then the variation is small. For the stiffener with Type B lay-up on the other hand variation is rapidly decreased after overlamination with a thickness of 3 lamination (4.05mm).

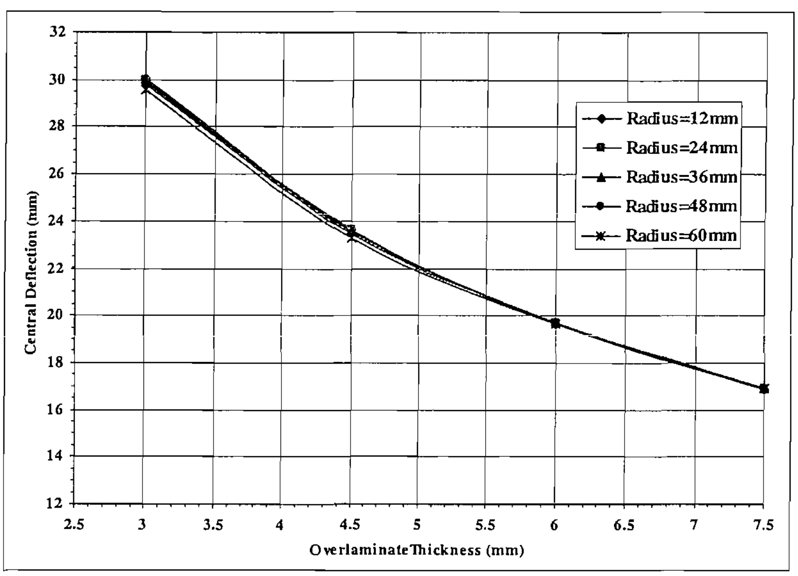

Figure 5.15 Load/Central Deflection plots for stiffeners with a Type-A lay-up

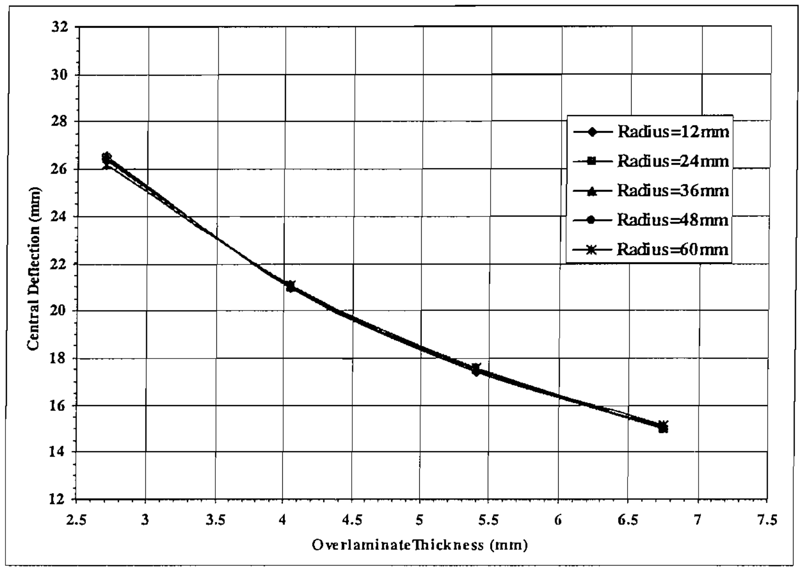

Figure 5.16 Load/Central Deflection plots for stiffeners with a Type-B lay-up

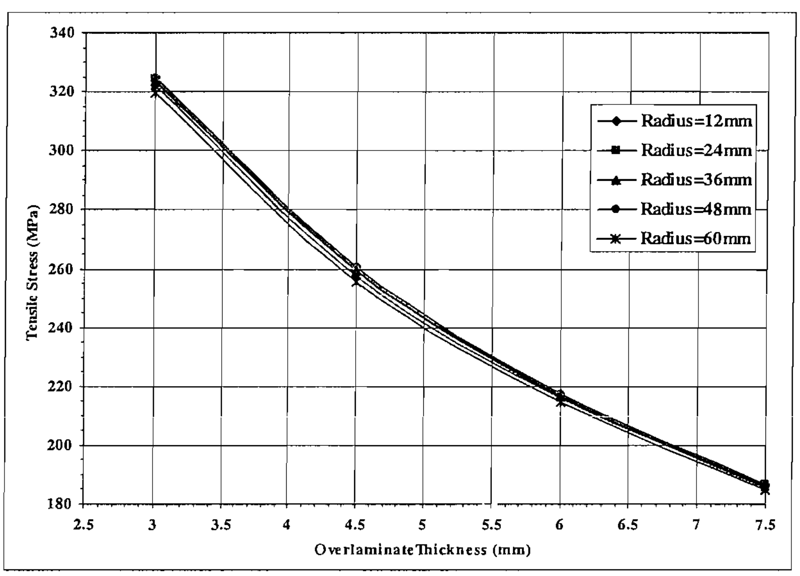

Figure 5.17 Tensile stress distributions for stiffeners with a Type-A lay-up

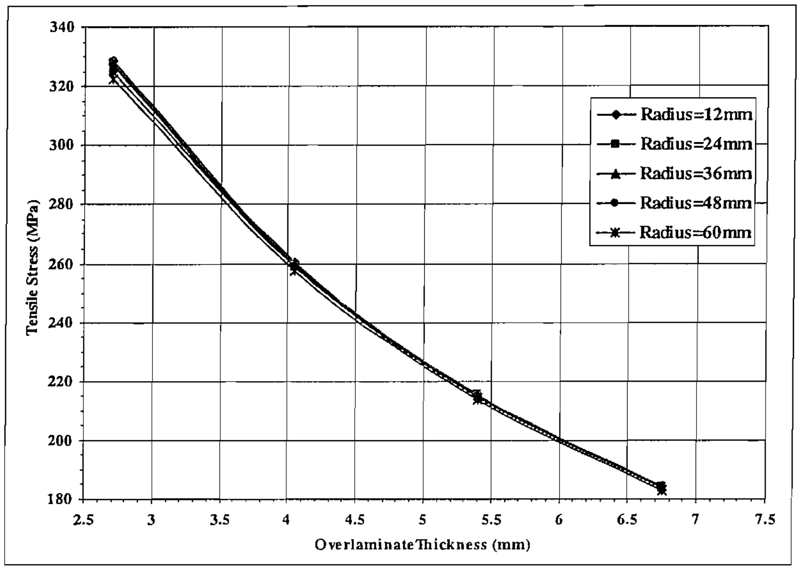

Figure 5.18 Tensile stress distributions for stiffeners with a Type-B lay-up

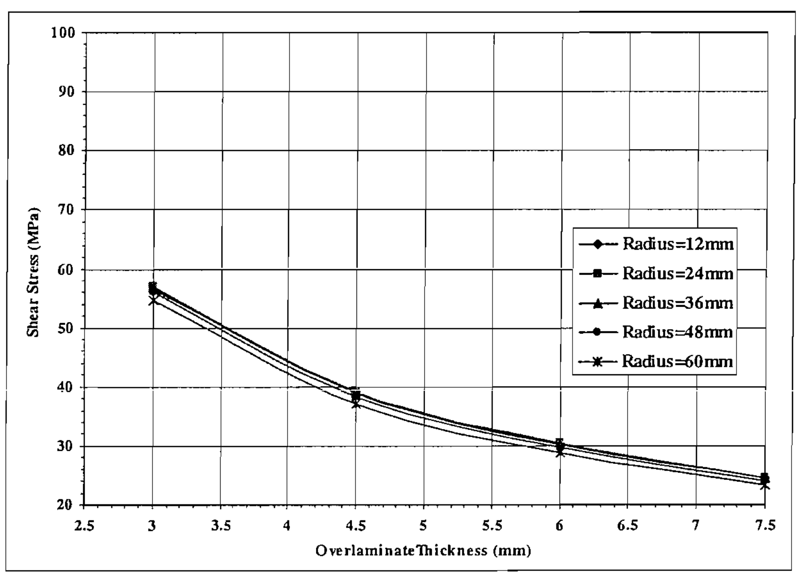

Figure 5.19 Shear stress distributions for stiffeners with a Type-A lay-up

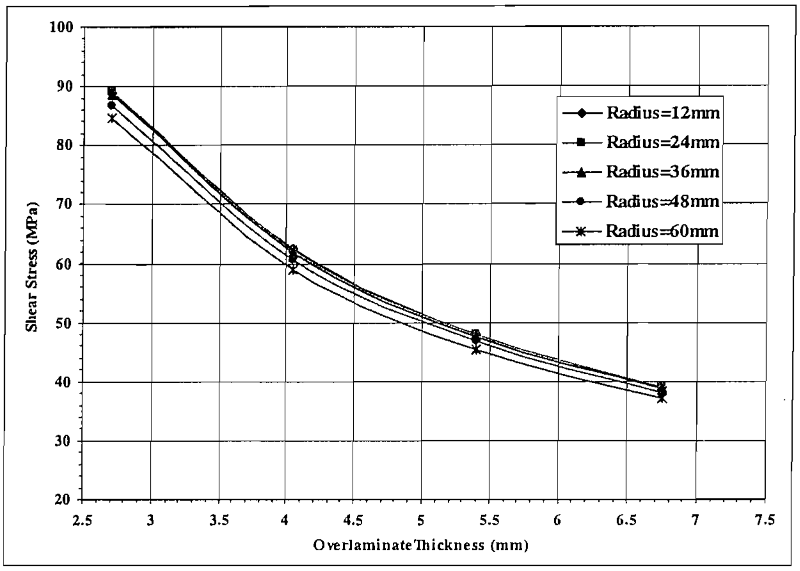

Figure 5.20 Shear stress distributions for stiffeners with a Type-B lay-up

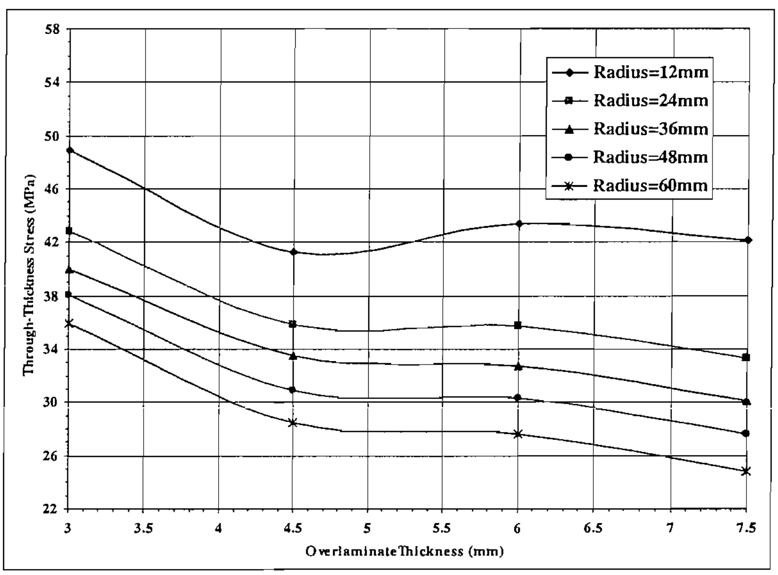

Figure 5.21 Through-thickness stress distributions for stiffeners with a Type-A lay-up

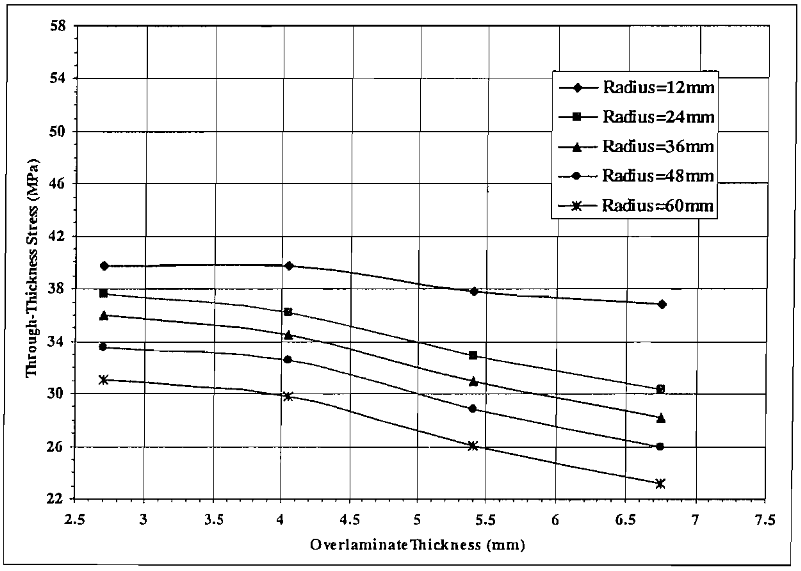

Figure 5.22 Through-thickness stress distributions for stiffeners with a Type-B lay-up

5.6 Discussion

5.6.1 Stiffness Correlation

Table 5.2 describe the comparison between the stiffness predicted by the FE model and experimental results for a failure load. The agreement between experiment and the numerical modelling for the assumed material properties is reasonably good with an error in stiffness 8.7% and 2.97% for Stiffener-A2 and Stiffener-B2 respectively. These results also indicate that the nature of failure for Stiffener-B2 is more brittle than Stiffener-A2. It can be also seen from Figures 5.5 and 5.6 experimental load deflection curves diverging from the FE load deflection curve at higher load step. This is probable because of the FE analyses was conducted in linear region without modelling effects of damage while this effect (reduced stiffness) was apparent in the experiment at higher load step.

5.6.2 Assumed Material Properties and Boundary Condition

As explained above the FE models of both types of top hat stiffeners gave very similar values of stiffness when compared with tested specimens. Therefore assumed material properties were close to those of actual specimen material. In order to represent as closely as possible the simple support conditions, lines of nodes were constrained only in the direction of the centre of the curvature. Sensitivity study on support span is discussed at Appendix C.

5.6.3 Comparison of FE Stress Patterns with Experimental Failure Modes

Initial audible cracking sounds which would account for matrix cracking were detected by ear during the test. These were 10kN and 8kN for stiffeners A-2 and B-2 respectively. Examination of the stress components in numerical results suggests that no material strength limits were being exceeded at this load which would account for the audible cracking. However it is possible that the presence of voids produced during the manufacturing process results in stress concentrations, which could have caused matrix cracking. Figures 4.6 and 4.7 showed relatively large amount of delammination at curved part of the overlaminate and flange of the stiffener. This observation matches with that predicted from FE model (see Figures 5.7 and 5.10), although loads and deflections at which these events are predicted are most likely to erroneous for the reasons previously discussed in section 5.3.3. At ultimate collapse load, it was observed that final failure for the stiffeners-A2 took the form of fibre-matrix breakage and delemination on the flange. On the other hand catastrophic shear failure, which is occurring in the web characterises the final failure of the stiffener-B2. Again FE model successfully predicted the location of through-thickness stress and maximum interlaminar shear stress associated with delamination and fibre-matrix breakage seen in the stiffener-A2 and maximum in-plane shear stress in the web of the stiffener-B2.

5.6.4 Comparison Between the Two Types of Top Hat Stiffeners

The differences between the two types of top hat stiffeners are cross-sectional geometry and overlamination lay-up. From the numerical analyses results, it is clear that the Stiffener-A2 initial and final failure load greater than the equivalent values for the Stiffener-B2. Furthermore the internal stress in all area is reduced for Stiffener-A2 by using CSM lay-up whilst it increased the structural weight up to 14%.

5.6.5 Parametric Studies

The results of this work have illustrated the effects of the variable on top hat stiffeners behaviour. Generally central deflections and stress distributions (through-thickness stress, tensile stress and shear stress) reduce by increasing the overlaminate thickness and fillet radius for the both types of stiffeners. While increase in overlaminate thickness has significant effects on all accounts, increase in fillet radius has only considerable effects on through thickness stress. For example through thickness stress reduced by 15% for stiffener with a Type A lay-up increasing the fillet radius from 12 mm to 24 mm with a thickness of three laminations for overlaminate (4.5mm). At a same overlaminate thickness by using Type B lay-up for the stiffener reduces the central deflection through-thickness stresses and tensile stresses but it increases the shear stresses.

Chapter 6 EXPERIMENTS ON TOP HAT STIFFENED COMPOSITE PANELS

6.1 Introduction

As mentioned in the literature review no systematic test studies of top hat stiffened panels under high transverse pressure have been reported. The situation directly affects the practical use of such composite panels, especially in ship construction. It is important to carry out panel tests to understand the behaviour of panels under high pressure.

The four principal objectives of the experimentation were:

1. Assess the strength of cross stiffened plate panels under uniform pressure load
2. Explore the structural stiffness issues and their dependence on lay up
3. Detail the progressive nature of failure, from matrix cracking through to final collapse
4. Provide validatory data for the theoretical analysis

A total of 11 top hat stiffened panels were tested under uniform pressure. Four different designs were used. These panels were representative of those employed in pleasure boats (see Figure 6.1). The lamination scheme and the cross-sectional geometry of the panels are given in Table 6.1 and Figures 6.2 and 6.3 respectively. There were three specimens of each type (denominated as A, B and C). The panels had dimensions 1m by 1m and the weights of each panel group are listed in Table 6.2. All panels were made up of glass fibre reinforced orthopthalic and isopthalic polyester resin. Isopthalic polyester resin was used for the first ply against the gel coat for environmental protection and also for overlapping patches where the maximum stress concentration occurs. The orthopthalic resin was used for the bulk laminate. The base plate of the panels consisted of 10 layers and the stacking sequence was the same for each type of panel. All panels had trapezoidal polyurethane foam with density 28 kg/m^3. The main difference between the panel groups was the over foam lamination scheme.

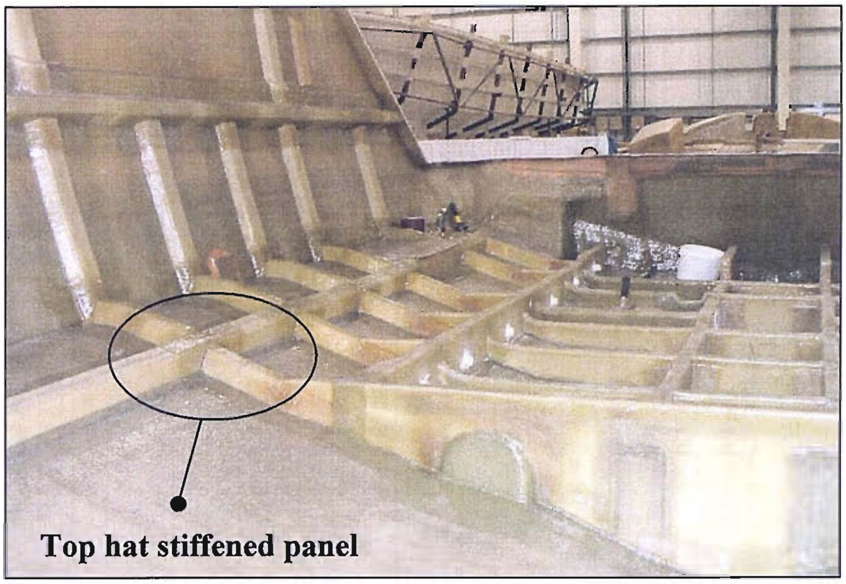

Figure 6.1 Internal structure of the pleasure boat

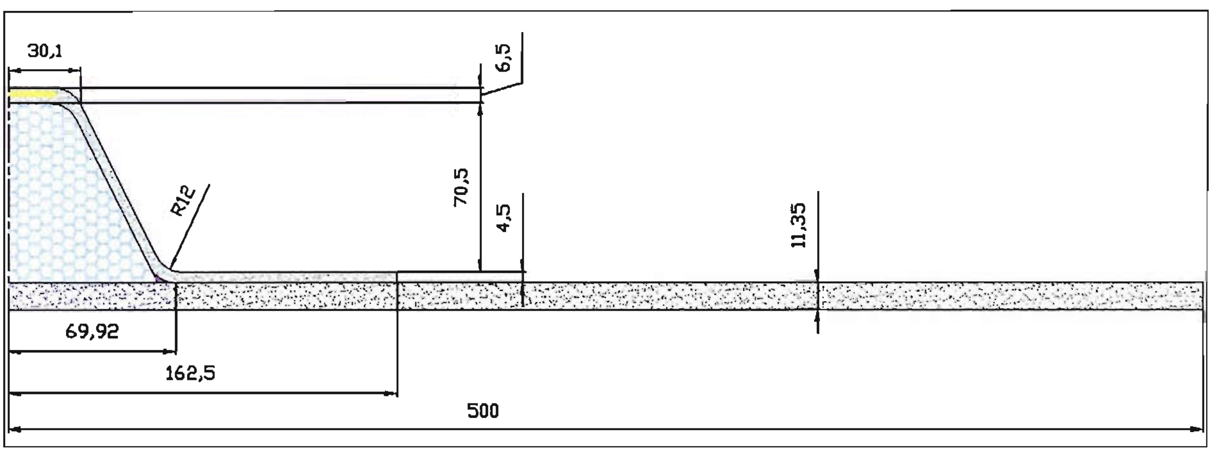

Figure 6.2 Cross-sectional geometry of group panels 1 and 2

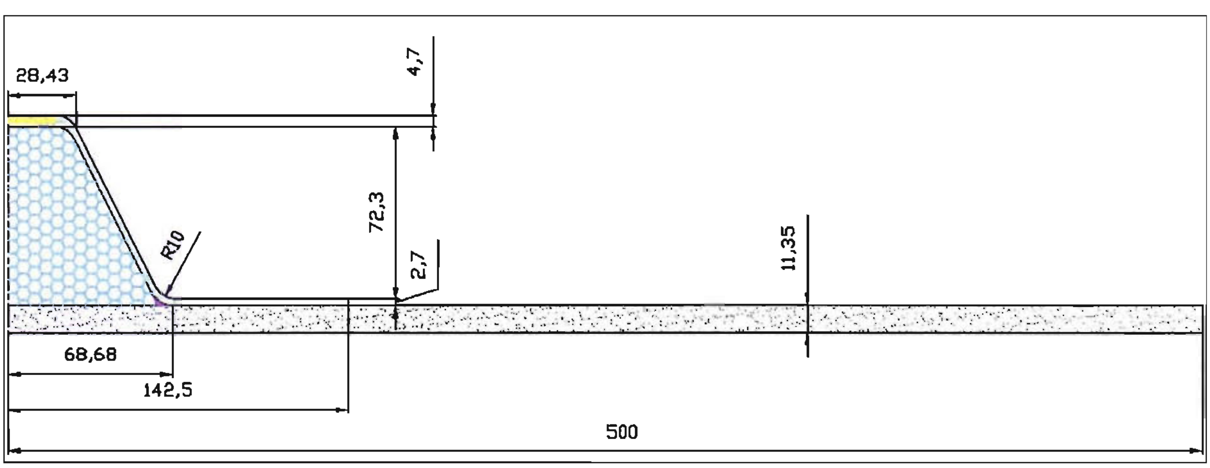

Figure 6.3 Cross-sectional geometry of group panels 3 and 4

Table 6.1 Lamination scheme for group panels 1,2,3 and 4

		Layer No	Panel 1	Panel 2	Panel 3	Panel 4
Base Plate		1	300 g/m^2 CSM	300 g/m^2 CSM	300 g/m^2 CSM	300 g/m^2 CSM
		2	600 g/m^2 CSM	600 g/m^2 CSM	600 g/m^2 CSM	600 g/m^2 CSM
		3	600 g/m^2 WR	600 g/m^2 WR	600 g/m^2 WR	600 g/m^2 WR
		4	600 g/m^2 CSM	600 g/m^2 CSM	600 g/m^2 CSM	600 g/m^2 CSM
		5	600 g/m^2 CSM	600 g/m^2 CSM	600 g/m^2 CSM	600 g/m^2 CSM
		6	600 g/m^2 WR	600 g/m^2 WR	600 g/m^2 WR	600 g/m^2 WR
		7	450 g/m^2 CSM	450 g/m^2 CSM	450 g/m^2 CSM	450 g/m^2 CSM
		8	600 g/m^2 CSM	600 g/m^2 CSM	600 g/m^2 CSM	600 g/m^2 CSM
		9	600 g/m^2 WR	600 g/m^2 WR	600 g/m^2 WR	600 g/m^2 WR
		10	450 g/m^2 CSM	450 g/m^2 CSM	450 g/m^2 CSM	450 g/m^2 CSM
Foam		11	Trapezoidal PU Foam	Trapezoidal PU Foam	Trapezoidal PU Foam	Trapezoidal PU Foam
Over Foam Lamination	Flange	12	600 g/m^2 CSM	600 g/m^2 CSM	225 g/m^2 CSM	225 g/m^2 CSM
		13	600 g/m^2 CSM	600 g/m^2 CSM	600 g/m^2 Bias	600 g/m^2 Bias
		15	600 g/m^2 CSM	600 g/m^2 CSM	225 g/m^2 CSM	225 g/m^2 CSM
		16			600 g/m^2 Bias	600 g/m^2 Bias
	Web	12	600 g/m^2 CSM	600 g/m^2 CSM	225 g/m^2 CSM	225 g/m^2 CSM
		13	600 g/m^2 CSM	600 g/m^2 CSM	600 g/m^2 Bias	600 g/m^2 Bias
		15	600 g/m^2 CSM	600 g/m^2 CSM	225 g/m^2 CSM	225 g/m^2 CSM
		16			600 g/m^2 Bias	600 g/m^2 Bias
	Crown	12	600 g/m^2 CSM	600 g/m^2 CSM	225 g/m^2 CSM	225 g/m^2 CSM
		13	600 g/m^2 CSM	600 g/m^2 CSM	600 g/m^2 Bias	600 g/m^2 Bias
		14	1600 g/m^2 Unidirectional	1600 g/m^2 Unidirectional	1600 g/m^2 Unidirectional	1600 g/m^2 Unidirectional
		15	600 g/m^2 CSM	600 g/m^2 CSM	225 g/m^2 CSM	225 g/m^2 CSM
		16			600 g/m^2 Bias	600 g/m^2 Bias
	Overlapped Patch	17	2 layers 600 g/m^2 CSM 600mm by 600mm		2 layers 600 g/m^2 CSM 400mm by 400mm	2 layers 600 g/m^2 CSM 600mm by 600mm

Table 6.2 Weight of panel

Panel ID	Average Weight (kg)
Panel group 1	24.1
Panel group 2	20.1
Panel group 3	19.5
Panel group 4	20.6

6.2 Test Rig and Equipment

To comply with the requirements of the experimental programme, a test rig constructed to the following specifications was used:

a) The specimens were cross stiffened panels with a loaded area 850mm×800 mm

b) the aspect ratio of the panels was 1:1.0625;

c) uniform pressure over the loaded area of the specimen

d) very stiff edge conditions - as close as practicable to full restraint.

Figure 6.4 shows the test rig that was used for all the panel tests (panels 1, 2, 3 and 4). It consisted of identical upper and lower steel frames. The test panel was sandwiched between the frames which were then bolted tightly together by two lines of bolts all round. The heavy steel frames gave in-plane and rotational restraint to the edges of the panel and were originally intended to simulate fixed boundary condition. The pressure was provided through a synthetic bag placed between the specimen and the lower steel frame. Before a test the bag was filled with water and connected to a large pressure vessel, which created a water reservoir with enough capacity to take up all the panel displacement. Pressure was increased by introducing compressed air through a tap into the top of the pressure vessel and was controlled manually (see Figure 6.5).

6.3 Test Results Summary

A total of 10 individual top hat stiffened panels without strain gauges were tested under uniform pressure. Large amounts of data have been collected. Table 6.3 summarises the test results. The stiffness for each panel was calculated as the slope of the linear portion of the load/deflection plots.

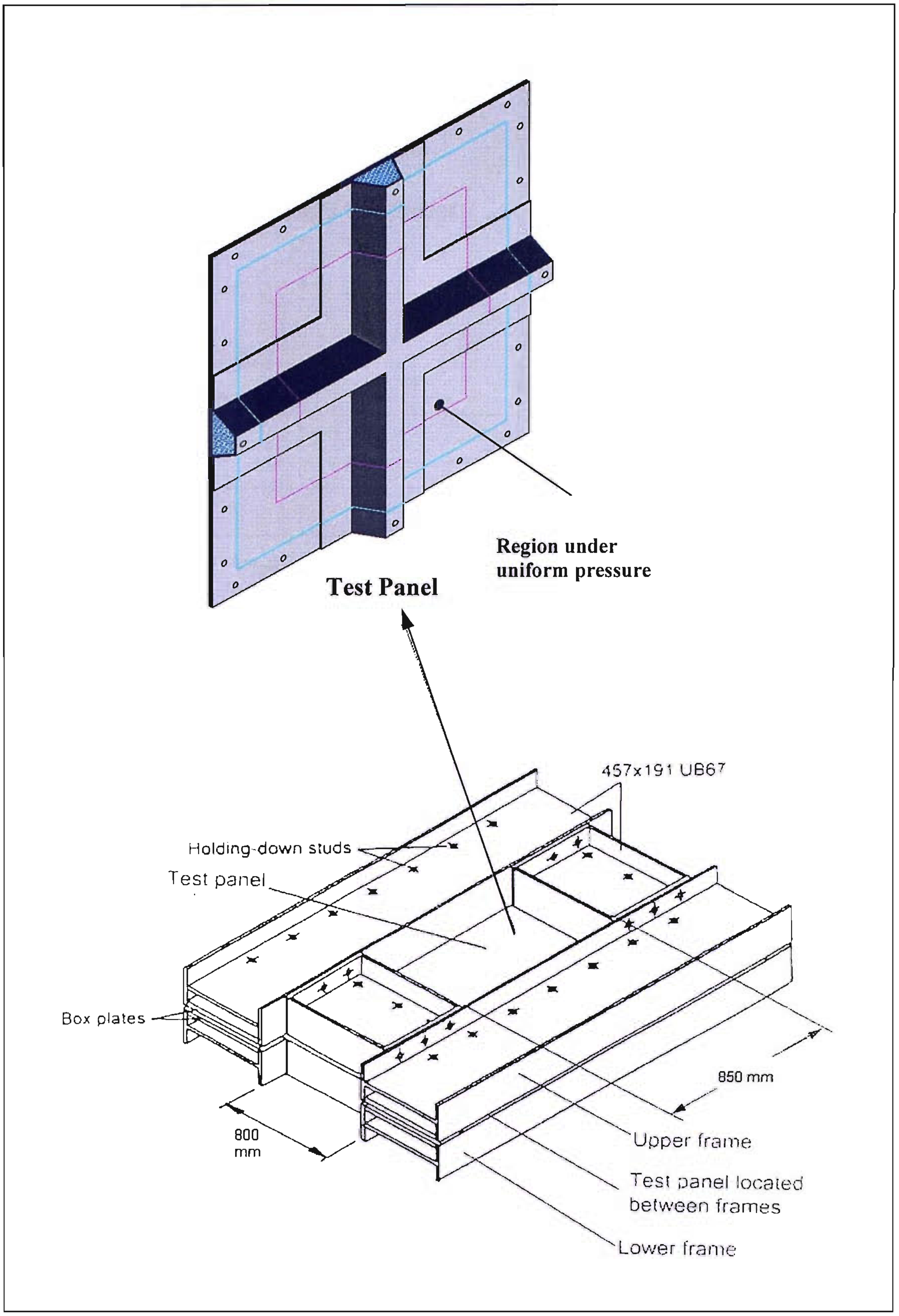

Figure 6.4 Isometric view of test rig

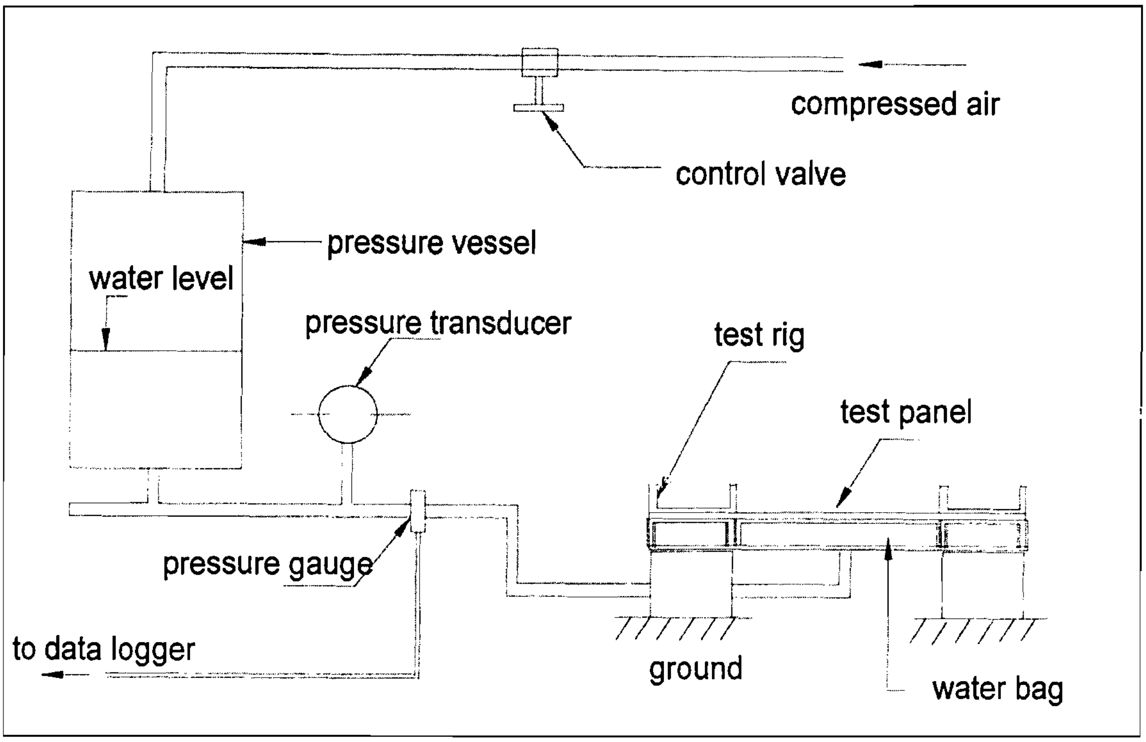

Figure 6.5 Demonstration of the loading system

Strength values are based on the maximum value achieved during the test. As would be expected each panel behaved non-linearly under high uniform transverse pressure. The typical load/deflection plots for the four panel groups are shown in Figure 6.6. The load/deflection curves of the failure panel tests have been integrated to determine the energy absorption of each to allow comparison of work done to failure The result of this calculation is given in Table 6.4 and details are given in Appendix D.

An interesting comparison can be made between panels. Panel groups 1 and 2 had the same overlaminate. The only difference between these panels was, while panel group 1's junction area was strengthened with an overlapped patch made up of 2 layers of 600 g/m^2 CSM, panel group 2 did not have the overlapped patch. The overlapped patch improved the stiffness by 10% and strength by 22.7% but increased the weight of panel group 1 by up to 20%. Panel groups 3 and 4 had the same overlaminate while their overlapped patch geometry and resin material were different (Table 6.1). The overlapped patch geometry for panel group 4 was relatively larger, and was made up with the stronger polyester resin (isopthalic). The larger and stronger overlapped patch increased stiffness by 7.8% and strength by 7.2% with only marginal increases in panel weight. Panel groups 1 and 4 had different overlaminates. Although their overlapped patches were of equal size their resin material was different (see Table 6.1). The burning tests on coupons showed that overlamination of panel groups 3 and 4 had higher fibre content by volume than the overlamination of panel groups 1 and 2 . However Table 6.3 shows that panel group 1 was strongest and stiffest amongst the panels. This is because of this panel group's overlaminate, which was made up of 3 layers 600 g/m^2 CSM and also included 2 layers of 600×600 mm×mm CSM layers. The large cross-sectional area provided improved stiffness and strength but also increased the panel weight by up to 20%.

Table 6.3 Test Results Summary

Panels	Deflection at Failure (mm)	Load at Failure (MPa)	Panel Stiffness (MPa/mm)	Audible Cracking
1-a	17.52	0.325	0.021	0.075
1-b	18.26	0.325	0.0209	0.05
1-c	20.4	0.385	0.0244	0.075
2-a	16.8	0.275	0.0218	0.05
2-c	18.26	0.275	0.0152	0.075
3-a	16.52	0.25	0.0179	0.05
3-c	12.72	0.225	0.0196	0.075
4-a	11.83	0.225	0.0201	0.1
4-b	19.22	0.325	0.0217	0.05
4-c	15.99	0.275	0.0203	0.05

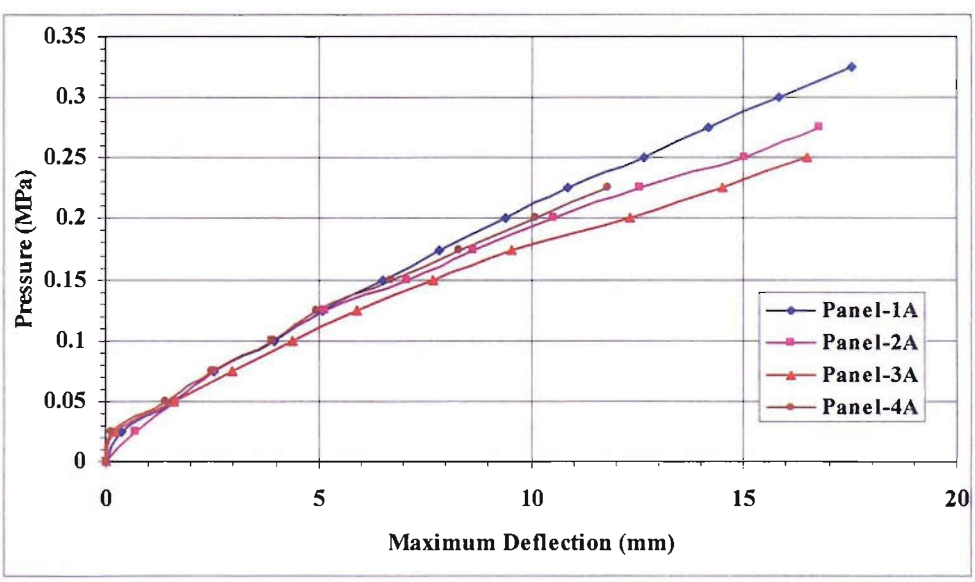

Figure 6.6 Typical load/deflection plots for each group of panels

Table 6.4 Energy absorption of the panels

		Energy (Joule)
Panel group 1	1A	2176600
	1B	2177700
	1C	3191300
Panel group 2	2A	1845010
	2B	2472990
	2C	1771900
Panel group 3	3A	1659880
	3C	1187600
Panel group 4	4A	1062410
	4B	2260830
	4C	1753385

The load-deflection results from panel tests indicate that each of the load deflection curve is outward (convex) while the previous works [82,83] on investigation of flexural behaviour of unstiffened thin laminated composite plates showed that the load deflection curve is inward (concave). The reason for this discrepancy might be due primarily to in the current work panels are stiffened with hat-shaped stiffeners in both x and y direction and the membrane effects are reduced to make the load deflection curve outward.

6.4 Failure Mechanisms

The cross-stiffened GRP panels displayed several distinct failure modes including resin crazing, matrix cracking, and fibre breakage and shear failure. As in the top hat beam panels, the first sign of failure was invariably matrix cracking for all panels at approximately 20% - 25% of the failure load. This was characterised by cracking noise emitted during the loading. Table 6.3 gives the initial failure load when the noise was detected by ear. Final panel failure was so explosive and destructive that it was difficult to record the damage progression.

After matrix cracking, subsequent loading caused visible damage in the form of resin whitening at the junction of the stiffeners and web/flange corner near the support region. The cracking sound did not stop but increased in intensity until specimens failed. The specimens failed dramatically with a loud bang. At ultimate collapse load, it was observed that delamination occurred at the flange/web corner near the support region. There was little warning of the failure in terms of rapid increase in deflection. Final failure of the panel types 1, 2 and 3 took the form of fibre-matrix breakage at the top of the crown of the junction area. In each panel the continuity of the longitudinal stiffener was maintained with appropriate cut-outs in the transverse stiffeners (see Figure 6.7). Hence it has been decided that the final failure occurring in the junction area on the crown took place at this discontinuous region. The panel groups 3 and 4 had the same overlaminate (two layers 225g/m^2 CSM and two layers 600g/m^2 Bias [$\pm 45^0$]). However the failure mode was fibre-matrix breakage for panel group 3 while it was shear failure for panel group 4. This was because panel group 4 had a relatively larger overlapped patch geometry, which was made up of the stronger polyester resin (isopthalic). Based on the experimental observations a failure sequence for the top hat stiffened panel can be summarised as follows:

- Initial matrix cracking
- Resin whitening and delamination at the region of the web/flange corner
- Final failure mode: fibre matrix breakage for panel groups1, 2 and 3 and catastrophic shear failure for panel group 4.

Figures 6.8 and 6.9 show the final locations and failure modes.

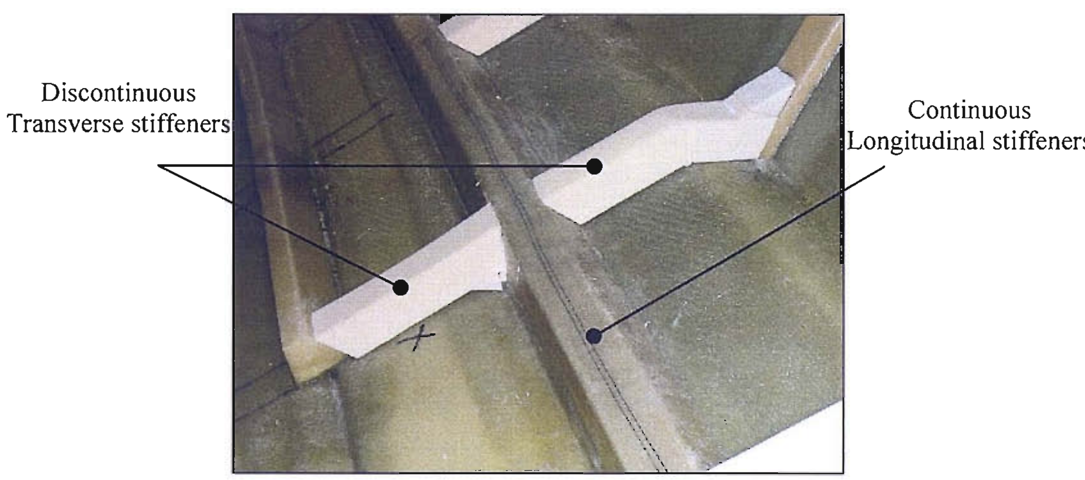

Figure 6.7 Internal structure of the pleasure boat

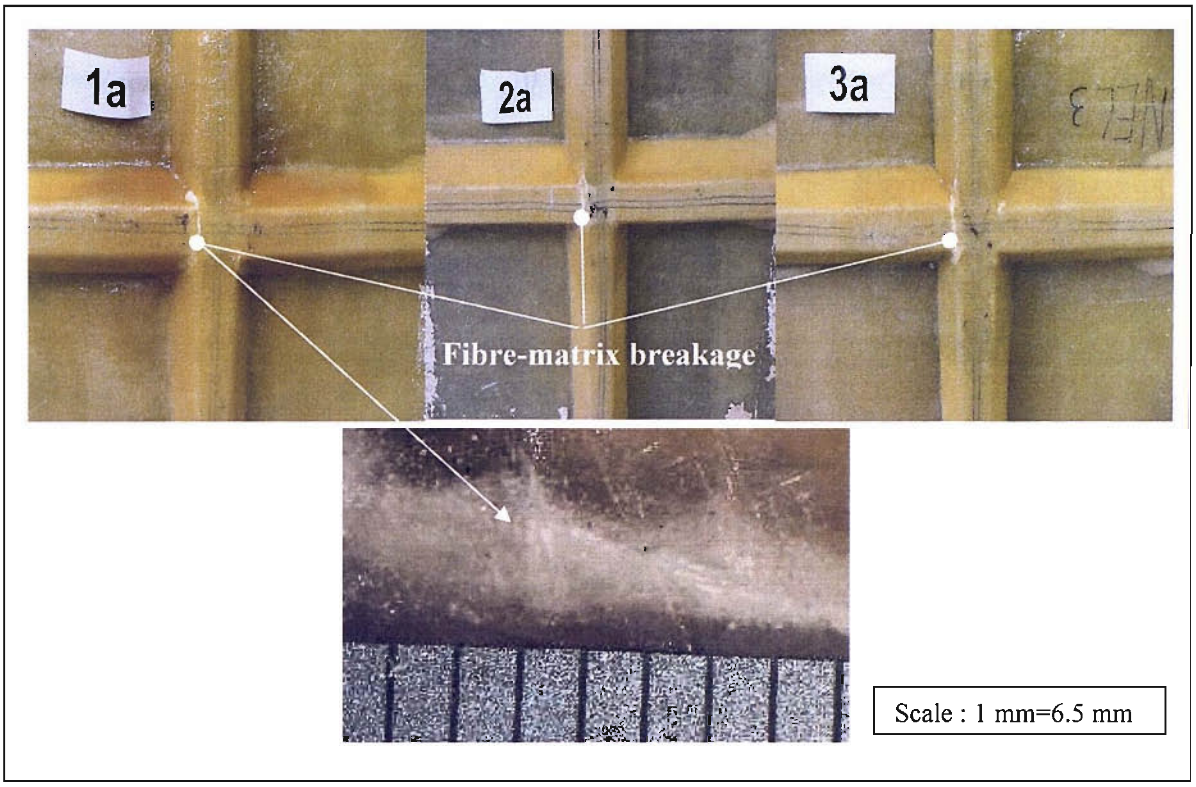

Figure 6.8 Location and description of failure modes and its detailed optical failure photograph

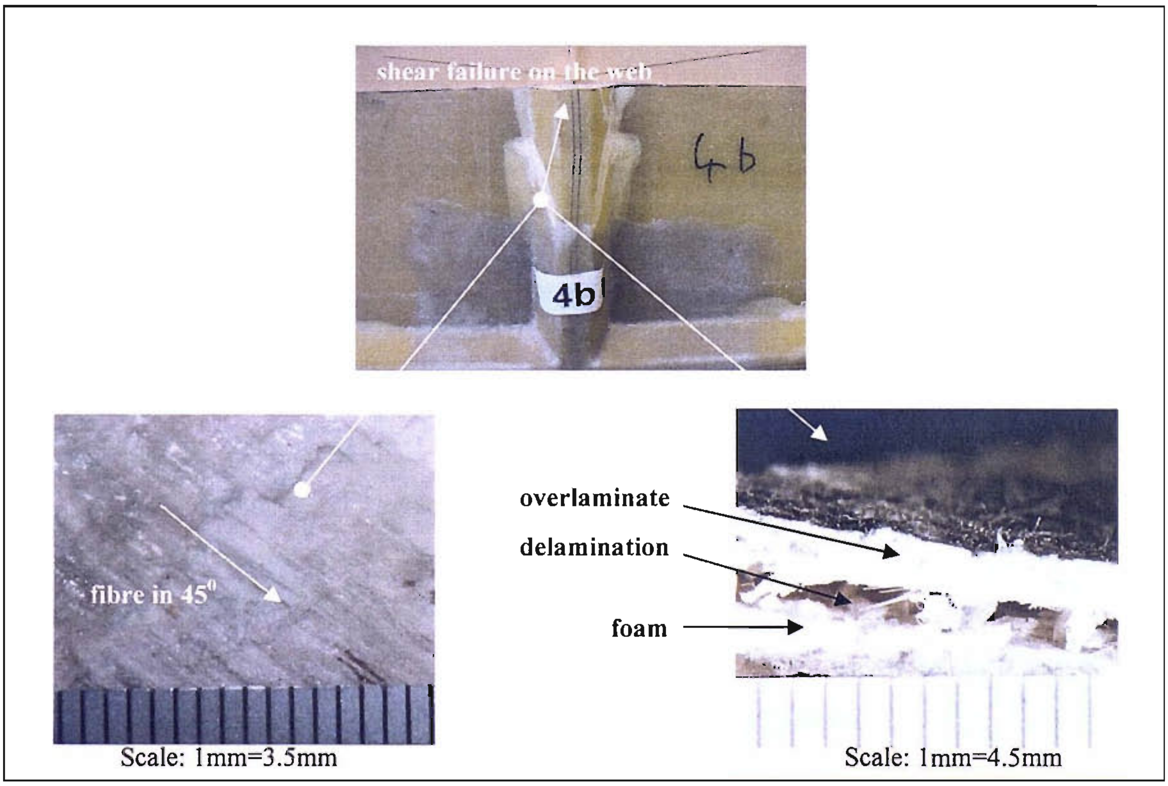

Figure 6.9 Location and description of shear failure mode including close up failure region photograph

6.5 Test Preparation and Strategy for Panel 2B

Previous tests of panel groups 1, 2, 3 and 4 provided precise data for understanding behaviour of the panels. In order to investigate the panel behaviour in more detail, strain-gauges were mounted on both unloaded and loaded surfaces of Panel-2B. The locations of the strain-gauges, which are shown in Figure 6.10, were decided by taking advantage of experience gained in the earlier tests. A digital dial gauge was placed at the centre of the panel on the unloaded surface to measure the central deflection, while two digital gauge were used to monitor the edge displacement at the centre of the long and short edges of the panel.

The Panel 2B was tested in the same test rig as the other panels and its loaded area was 800×850 mm×mm, the same as the other panels. Figure 6.11 shows the overall set-up for the test of Panel 2B. As can be seen a large number of strain-gauges were used to observe strain development in the panel. Before the test all the strain gauges and digital gauges were calibrated carefully. The data from some of the strain gauges was printed directly from a data logger and the remainder were attached to another data logger integrated with a computer acquisition system. Loading procedure was the same as for the other panels. Initial readings were taken on all instruments and pressure was then increased in small increments (0.025 MPa). At each increment pressure and deformations were allowed to settle before readings were taken. This process was continued until the panel failed. The loads at initial and final failure were also noted.

6.5.1 Summary of Test of Panel 2B

The panel 2B was taken to failure and was the only specimen mounted with strain gauges. A nonlinear response was apparent from the load/deflection plots in Figure 6.12.

6.5.2 Strain Distribution and Development

A total of 14 strain-gauges were placed on the loaded and unloaded surfaces of the Panel 2B. It was possible to study strain distribution within the panel. Figures 6.13 and 6.14 illustrate the strain distribution and development along the x direction on the unloaded and loaded surfaces. In Figure 6.13 (unloaded surface) the strain at x=120 mm point (SG9) is bigger than its mirror point x=-120mm (SG7). While in Figure 6.14 (loaded surface) (SG2) and (SG4) look to be symmetrical. Figures 6.15 and 6.16 show the strain distribution and development in the y direction for the loaded and unloaded surfaces.

To study the symmetry of the strain between the x and y directions Figures 6.13, 6.14, 6.15 and 6.16 have been superimposed and plotted in Figures 6.17 and 6.18. The figures show that all the strain gauges on the loaded surface are reading negative in compression, while on the unloaded surface, on the crown and base plate they are positive in tension as expected. The figures also show that the strains in the x direction are bigger than those in y direction at high pressure. As mentioned earlier on the panel continuity of longitudinal stiffener is maintained with appropriate cut-outs in the transverse members (see Figure 6.7). Hence it has been decided that the stiffener in x direction is continuous. The results also indicate that although the panel is considered to be symmetrical in the x-y plane the strain distributions were not symmetrical as expected. Surely it is because the stiffener was continuous in the x direction but not in the y-direction.

The development of strain can also be studied in the web of the stiffeners. A local coordinate system was set-up on the web of the stiffeners (see Figure 6.19). The x axis was set-up along the stiffeners while the y axis was on the web surfaces. Strains in y direction in both stiffeners were initially negative (compression) (SG11 and SG12) at pressure of 0.1MPa. However with increase of pressure up to 0.295MPa the strains in SG12 fluctuated but remained negative. On the other hand after 0.25MPa SG11 increased quickly in positive direction (see Figure 6.20). The same behaviour was observed in the strain distribution of SG11 in x axis. The strain in this case initially was positive in tension and after 0.25MPa it grew in compression (see Figure 6.21). Change in strain from negative to positive or vice versa for SG11 after 0.25MPa is possibly because of the progressive damage accumulation which was apparent after this load step.

6.5.3 Failure Mechanisms of Panel 2B

Panel 2B was taken to failure and exhibited the same failure mechanisms with the panel groups 1, 2 and 3. Examining Figure 6.22 the progression of failure for Panel 2B can be described. The panel started to crack at about 0.05MPa (2.84mm central deflection) as determined by noise emitted. At a pressure of 0.1MPa (4.27mm central deflection) visible whitening, which is caused by presence of delamination occurred at web/flange corner near the support region. Between 0.1MPa and 0.2MPa pressure loading delamination propagated towards to flange. Increasing the pressure to 0.25MPa (14.24mm) lead to fibre matrix breakage at the intersection of the stiffeners' webs and at the flange area where the delamination observed before. At the experimental failure pressure 0.295MPa (20mm), fibre-matrix breakage propagated through the web to crown where the two top hats intersect at the centre of the panel. Examination of Panel-2B after the experiment showed that there was no damage on the loaded surface of the panel while complete separation of the overlaminate from the base plate and foam cracking at the ends of the stiffeners had occurred on the unloaded surface. Figures 6.22 and 6.23 show the final failure modes and locations of Panel-2B.

6.6 Discussions

6.6.1 Panel Behaviour

A total of 11 top hat stiffened panel were tested under uniform pressure. It is clear that from the load deflection plots they behaved non-linearly.

6.6.2 Lay-up Material

Table 6.4 shows the energy absorption of the all panels. The panel group 1 (overlaminate made up 3 layers of 600 g/m^2 CSM and its cross-section strengthened with 2 layers of 600 g/m^2 CSM with a size of 600×600 mm×mm and reinforced with orthopthalic resin) had the highest energy absorption in each panel group , followed by the panel group 2 (overlaminate made up 3 layers of 600 g/m^2 CSM), panel group 3 (overlaminate made up of lighter 225 g/m^2 CSM stitched to 600 g/m^2 Bias material and its cross-section strengthened with 2 layers of 600 g/m^2 CSM with a size of 400×400 mm×mm and reinforced with orthopthalic resin) and panel group 4 (overlaminate made up of lighter 225 g/m^2 CSM stitched to 600 g/m^2 Bias material and its cross-section strengthened with 2 layers of 600 g/m^2 CSM with a size of 600×600 mm×mm and reinforced with isopthalic resin). This indicates the importance of choice of lay-up material for overlamination and overlapped patch. From this table it is also clear that, there are some differences in energy absorption of the panel specimens even they are made of same design. The same observation has been made considering the failing displacement and failure loads for the panel specimens (see Table 6.3). These differences seen between the same design highlights the difficulties in producing quality of the top hat stiffened panels.

The overlapped patch which used for strengthening the cross-sectional area has effect on both strength and failure mechanisms. This was apparent between panel groups 3 and 4. Although they had the same overlaminate, their overlapped patch geometry and resin material were different. The overlapped patch geometry for panel group 4 was relatively larger, and was made up from stronger polyester resin (isopthalic) which resulted in improved stiffness and strength. Panel groups 1 and 4 had different overlaminates. Although their overlapped patches were of equal size, their resin material was different. The burning tests on coupons showed that overlamination of panel groups 3 and 4 had higher fibre content by volume than the overlamination of panel groups 1 and 2. However Table 6.3 shows that panel group 1 was strongest and stiffest amongst the panels. This indicates that the amount of reinforcement in the panel determines the strength and stiffness. However the distribution of that reinforcement is very important. The tests on both structural elements showed that the more even the distribution of reinforcement in every direction the better strength and stiffness.

6.6.3 Strain Distributions

As would be expected measured strains at the loaded surface were compressive and there was tension on the unloaded surfaces (except on the web through the crown measured strain in compression) . This is because plate bending develops tensile stresses on the unloaded surface and compressive stress at the loaded surface.

The strains in the x direction were bigger than those in the y direction at high pressure. The panel continuity of the longitudinal stiffener is maintained with appropriate cut-outs in the transverse members. Hence it has been assumed that the stiffener in the x direction was continuous. The results also indicate that although the panel was considered to be symmetrical in the x-y plane the strain distributions were not symmetrical as expected. Surely it is because the stiffener was continuous in the x direction but not in the y-direction.

Considering the Figures 6.17 and 6.18 the range of variation in strain for the strain gauges SG8 and SG3 are much larger than the others. There are several reasons for this variation. Firstly both strain gauges located at the centre of the panel's loaded and unloaded surface where the bending stresses are higher. Secondly both strain gauges are mounted in x-direction. As mentioned above stiffener in x direction is continuous, which results in higher strain measurement and finally, the final failure occurred at the centre of panel's unloaded surface destroyed the strain gauge (SG8) which caused jump in strain value.

The maximum measured strain values were order of 15.9×10^{-3} for the Panel-2B which was lower than strain capacities measured in the coupon test. There are some reasons for this discrepancy. First the strain gauges had a gauge length of 10 mm and measured local values of surface strain in the resin whereas the strains in the coupon test were average values over the length of the coupon. Second, the coupons were subjected to direct tensile tests whereas there was considerable bending and transverse shear at the centre of the panel.

The measured maximum failure strain (0.0159) was compared to failure strain of the orthopthalic polyester resin (0.02) and it was found that measured maximum strain was smaller than the failure strain of the orthopthalic resin.

6.6.4 Failure Mechanisms

The first sign of failure was invariably matrix cracking for all panels Subsequent loading caused resin whitening at the curved part of the overlaminate near the support region. The final failure mode of the group panels 1, 2 and 3 was the same. As mentioned above the panel continuity of longitudinal stiffener was maintained with appropriate cut-outs in the transverse stiffeners. While the bending stresses were taken by the continuous stiffeners' web and crown due to the discontinuity of the transverse stiffeners these stresses were only taken by the crown at the intersection region. Hence final failure of the panel groups 1, 2 and 3 took the form of fibre-matrix breakage at this discontinuous region. On the other hand the final failure mode of the group 4 panels took the form of shear failure in the web. This was because the larger overlapped patch made of the strongest polyester resin (isopthalic) prevented the failure mode seen in the other panel groups.

6.7 Conclusion

The tests described above have demonstrated the bending behavior of GRP top hat stiffened panels. Several conclusions can be drawn

- Damage of the panels started with matrix cracking followed by delamination at the curved part of the overlaminate near the support region. The panels failed by fiber-matrix breakage at the cross-sectional region except in group panel 4 which failed in the web of the stiffener due to the shear induced failure.
- The use of larger overlapped patch reinforced with strongest isopthalic resin caused catastrophic shear failure for panel group 4. This highlights the importance of choosing lay-up material and its geometry for overlapped patch.
- On the panel continuity of the longitudinal stiffener was maintained with appropriate cut-outs in the transverse members. The fact that the strains in the x direction were bigger than the strains in the y direction demonstrated this. Hence it has been decided

that the final failure in the junction area on the crown took place at the discontinuous region.

- Panel group 1's, overlaminate, which is made up from 3 layers 600 g/m^2 CSM and also including 2 layers 600×600 mm×mm overlapped patch made up 600 g/m^2 CSM layers provide big cross-sectional area improves stiffness and strength of the panels amongst the others while increase the panel weight up to 20 %.
- As expected all the strain-gauge values at the loaded surface were negative (in compression) while they were positive (in tension) on the unloaded surface except strain values through the web were still negative (in compression).
- The strain distributions lacked symmetry in the warp and weft directions although the panel was considered to be symmetrical in the x-y plane. Surely it is because the stiffener was continuous in the x-direction but not in the y-direction.

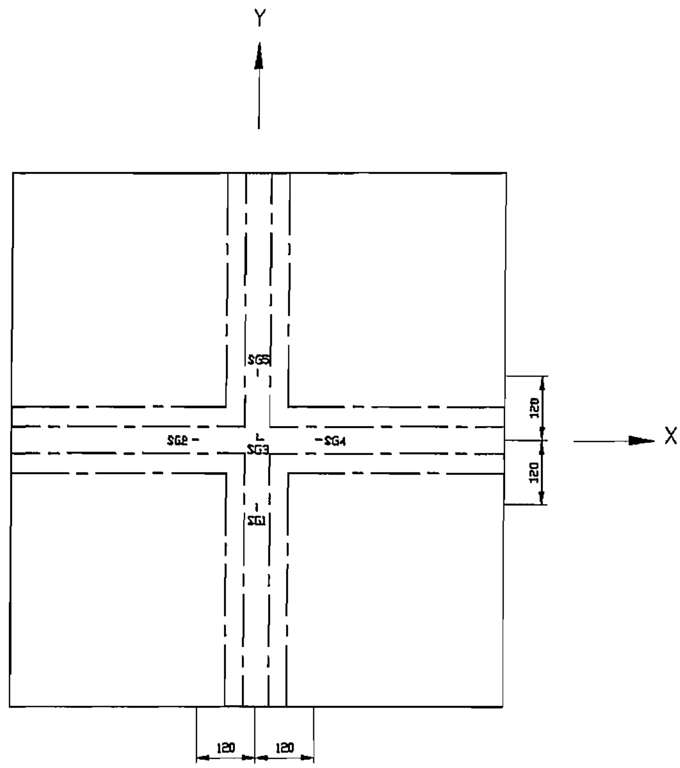

(a) on loaded face

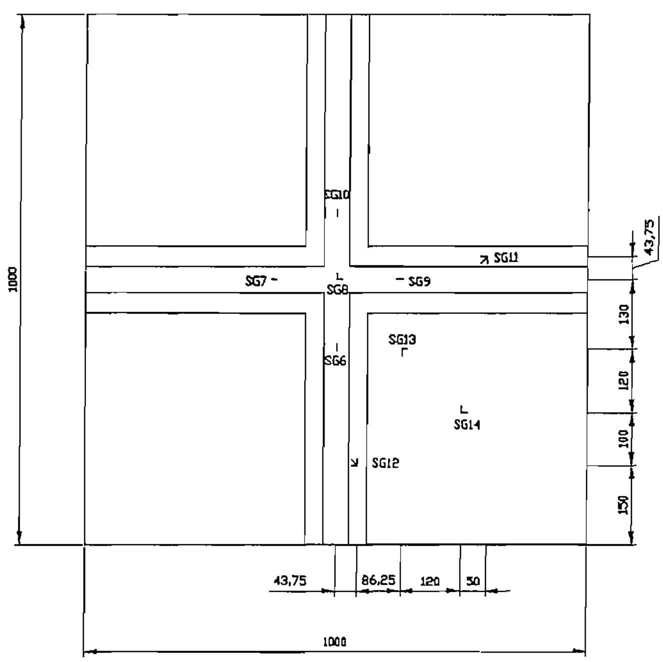

(b) On unloaded face

Figure 6.10 The locations and numbering of strain gauges (a) loaded surface (b) unloaded surface

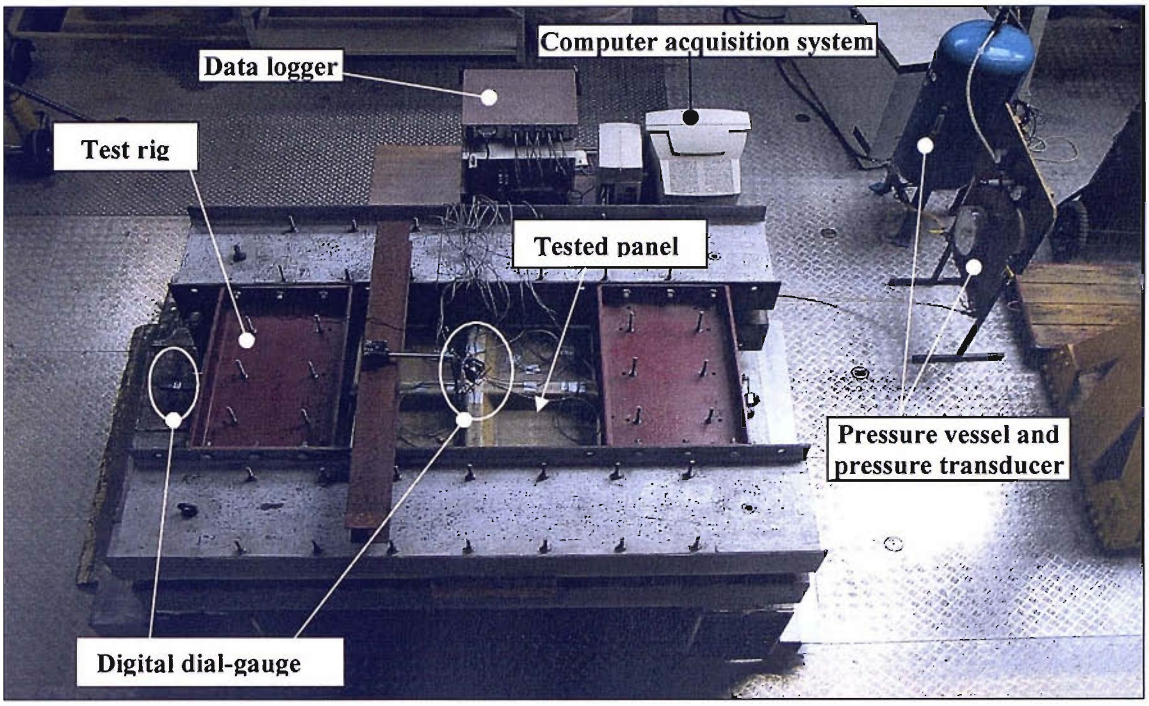

Figure 6.11 The set-up for test on Panel-2B

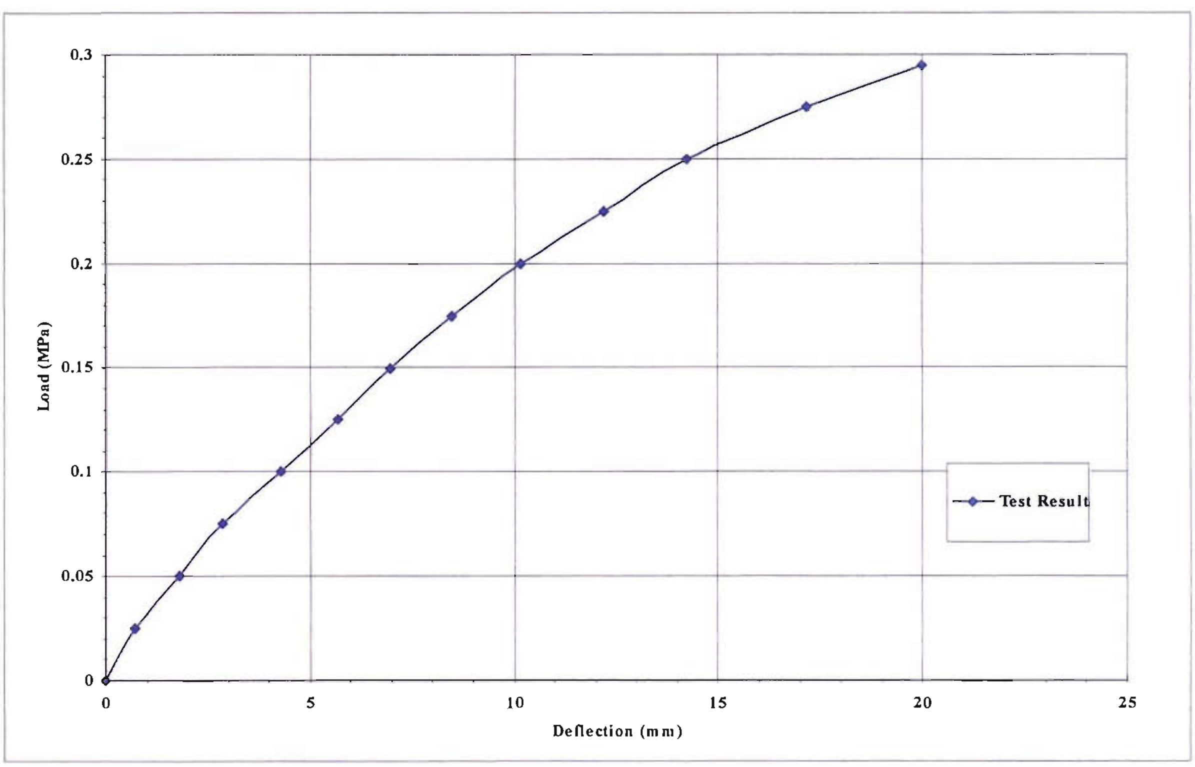

Figure 6.12 Load-Deflection Plots of Panel-2B

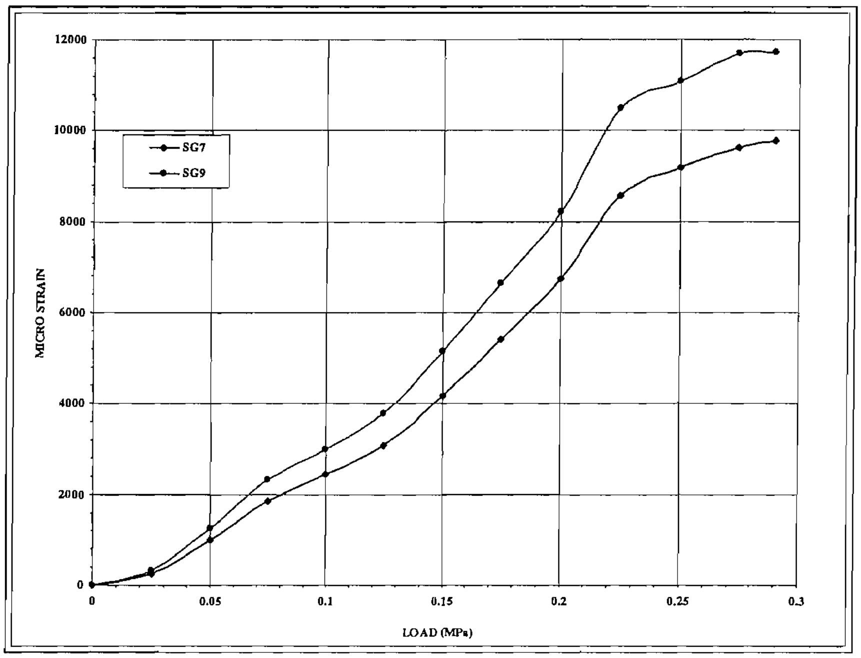

Figure 6.13 Strain distributions along the x-axis at unloaded surface

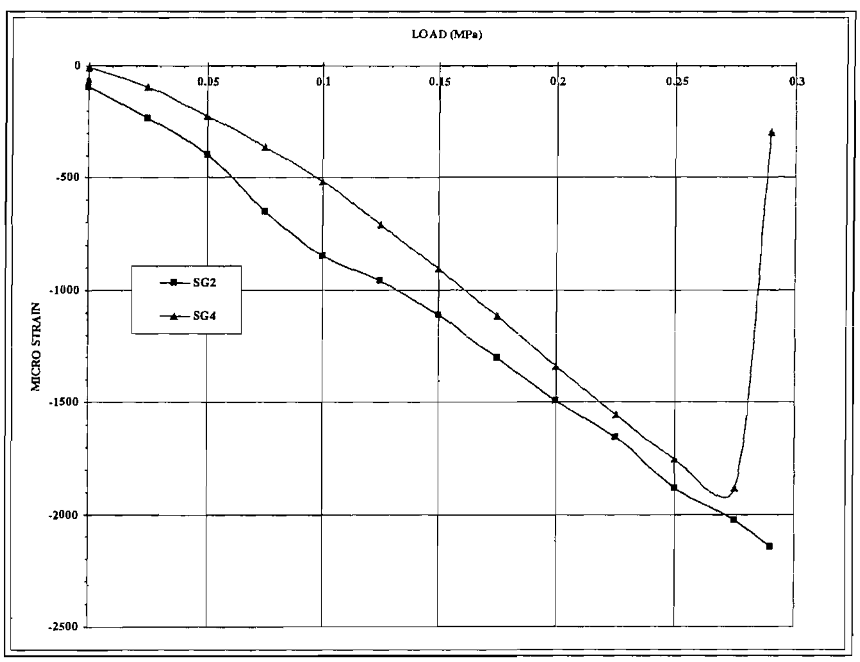

Figure 6.14 Strain distribution along the x axis at loaded surface

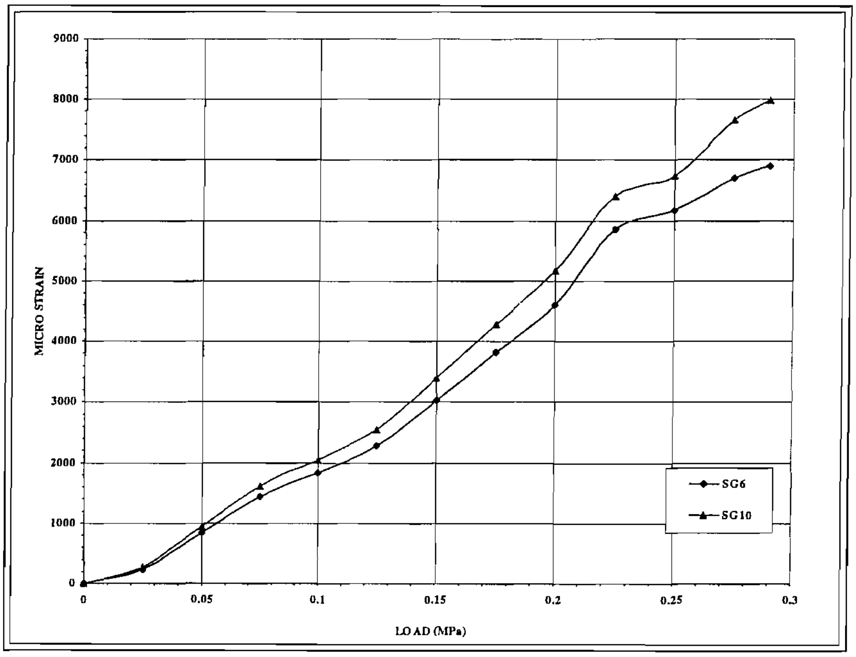

Figure 6.15 Strain distribution along the y-axis at unloaded surface

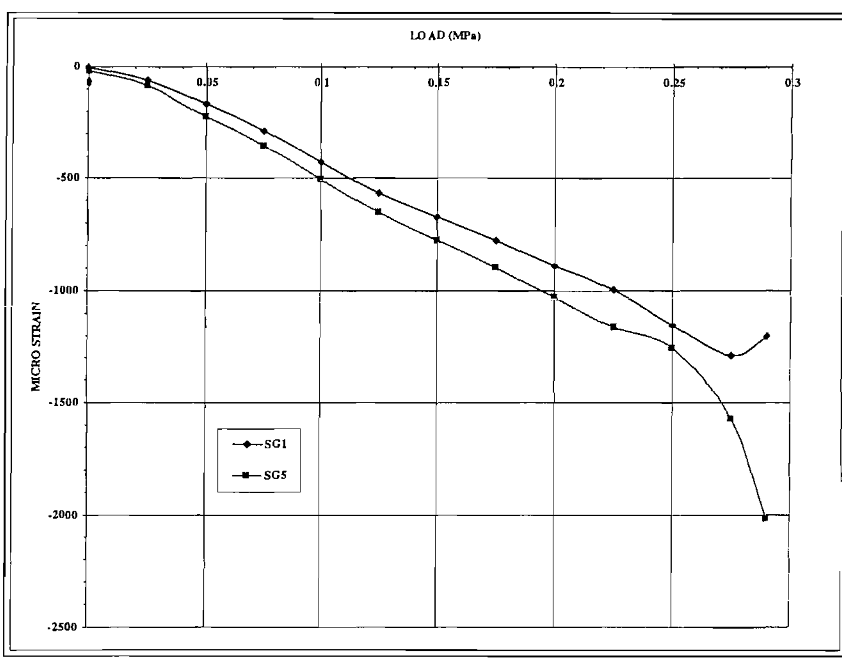

Figure 6.16 Strain distribution along the y-axis at loaded surface

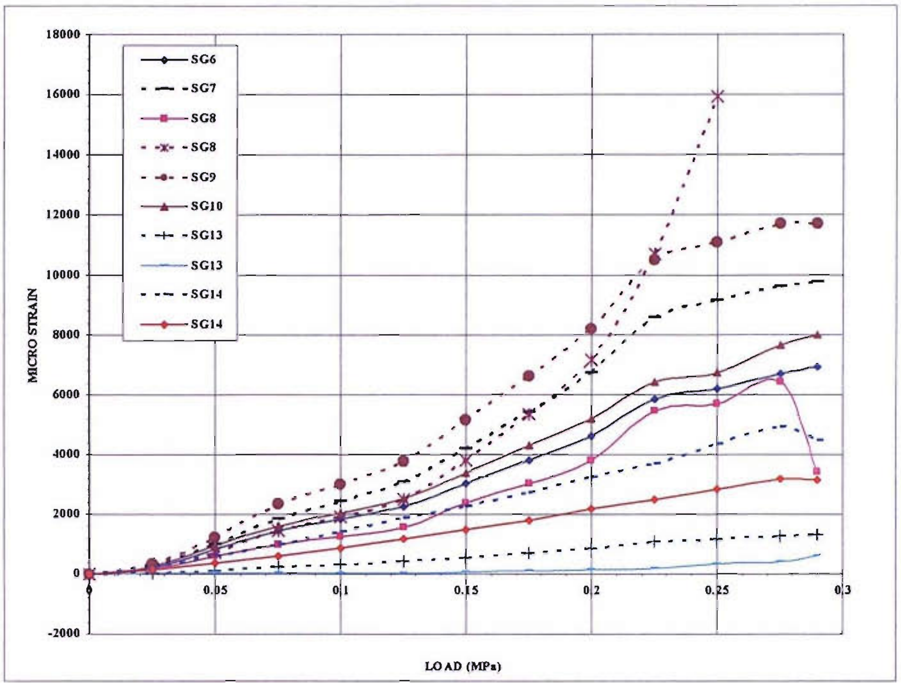

Figure 6.17 Strain distribution along the x and y axes at unloaded surface

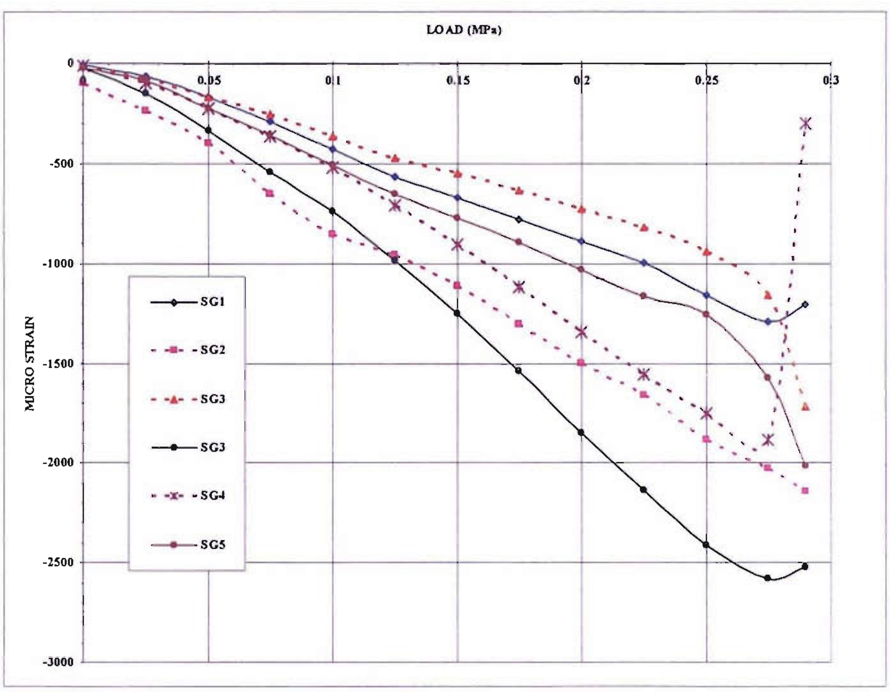

Figure 6.18 Strain distribution along the x and y axes at loaded surface

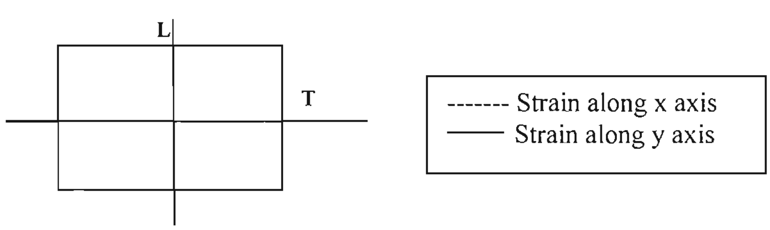

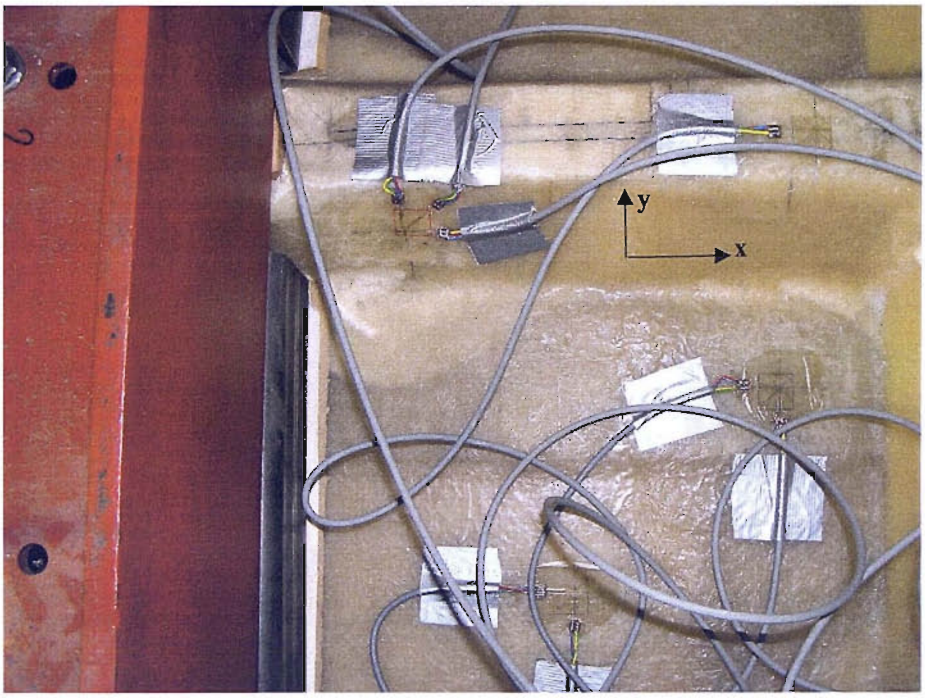

Figure 6.19 Local co-ordinate system on stiffeners' web

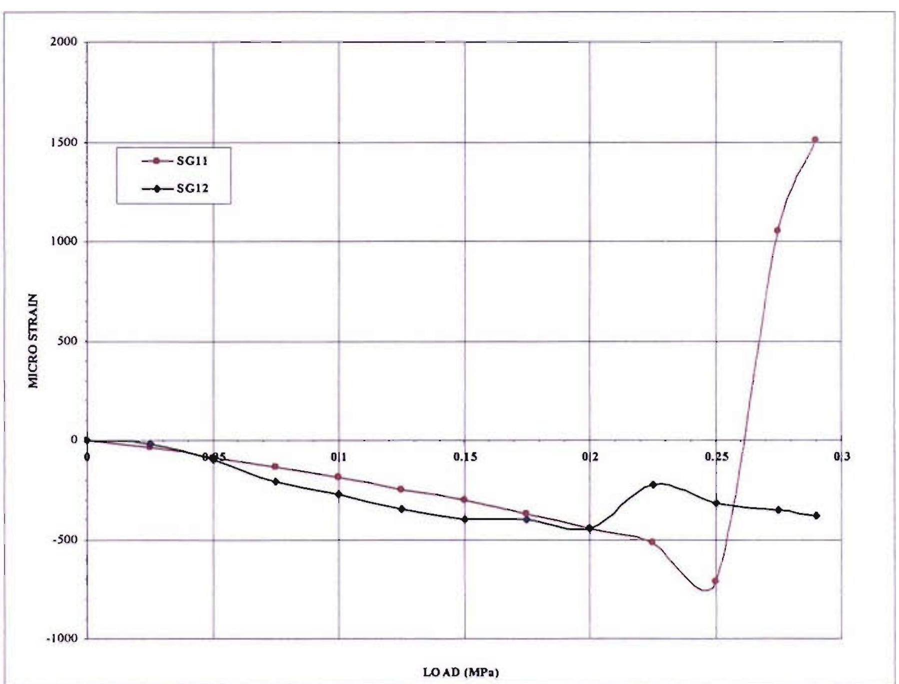

Figure 6.20 Strain distribution along the y-axis (local co-ordinate system) for both stiffeners (SG11 and SG12)

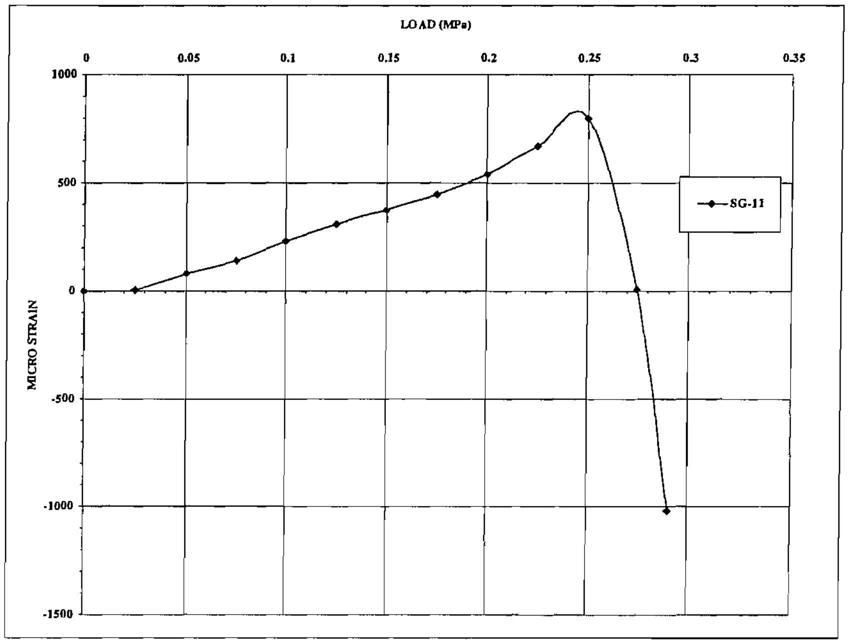

Figure 6.21 Strain distribution along the x -axis for SG11

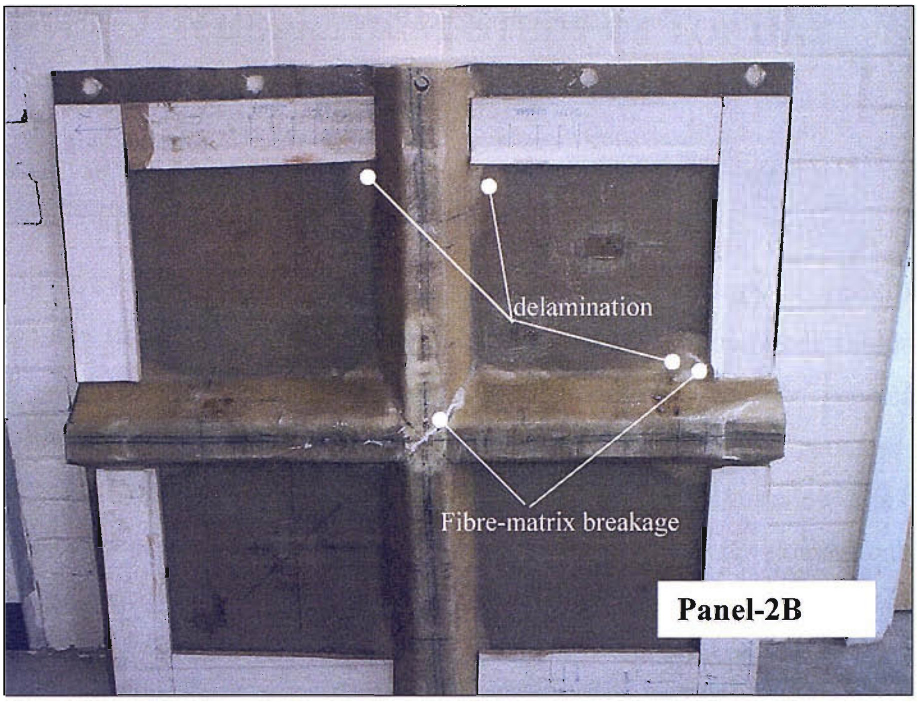

Figure 6.22 Final Failure of Panel-2B

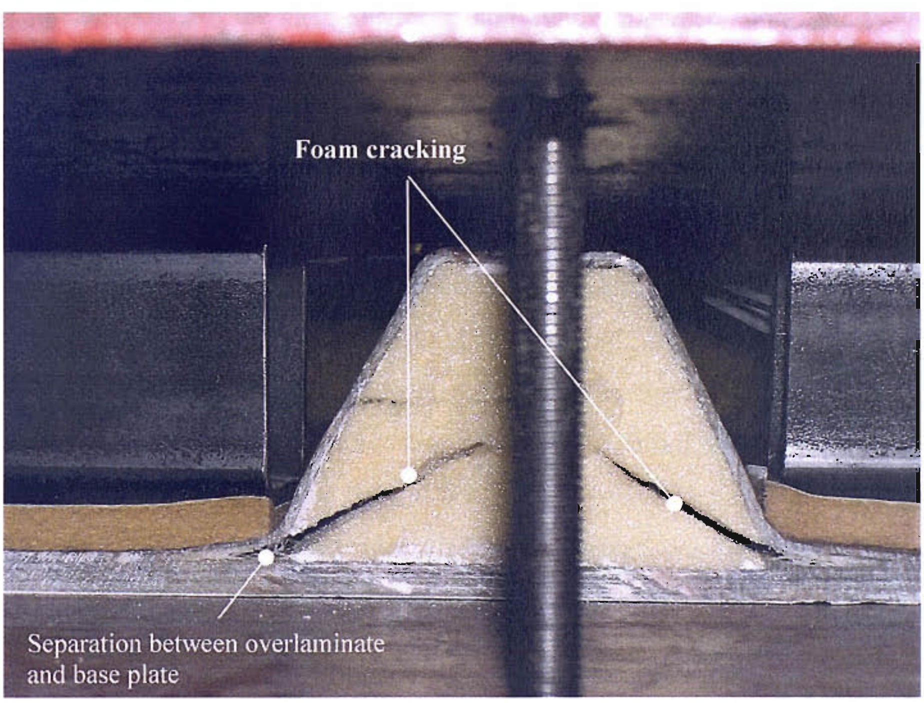

Figure 6.23 Final Failure of Panel-2B

Chapter 7 THEORETICAL STUDY OF TOP HAT STIFFENED PANELS

7.1 Introduction

Structural integrity of large ship hulls or decks made from GRP requires the quantification of deformation and stress state in the structures under various load conditions caused by ship sag, wave slap and equipment load. These structures have complex geometries and composite material is anisotropic and heterogeneous. FE studies of ship structures such as stiffened panels provide valuable design guidance. From the literature review it is clear that few examples of correlations between measured behaviour and finite element calculations are currently available [57, 82, 83]. After definition of representative type of structure (a top hat stiffened single skin hull) and construction of a test set up (chapter 6) allowing the loading such panels (uniform pressure loading of 1m by 1m panels) numerical modelling was performed using ANSYS finite element codes. Systematic calculations were performed for deflection, strains and stress using three-dimensional solid element. The results of the modelling will be compared to the experimental findings to validate the numerical model and further understanding of the internal stress pattern within the different constituents of the panels, which can then be used to assess the likely causes of panel failure.

7.2 Modelling

A CAD drawing described in Chapter 6 provided the definition of the top hat stiffened panels' structures. The concern was the connection between top hat stiffener and base plate and cross-section region of the two hat type stiffeners. As far as the numerical model is concerned top hat stiffened panels problem is very similar to the top hat stiffener problem. The main differences being the loading and boundary conditions. Hence the modelling criteria determined for top hat beam panels have been applied to the cross-stiffened hat-shaped composite panels, and all observations made in chapter 5 can be equally well applied here. Numerical models were constructed for Panel-2B using commercial ANSYS FE codes. A numerical analysis was made of the static pressure loading case on a partially simply supported (clamped boundary conditions are given at the corner of the panels) panel to make a positive correlation between measured and calculated values of central panel displacement and strain under distributed static pressure loading. The model was three-dimensional and was meshed with SOLID45 elements. The constituents of the stiffened panel (quarter model) and its meshed geometry are given in Figures 7.1 and 7.2 respectively.

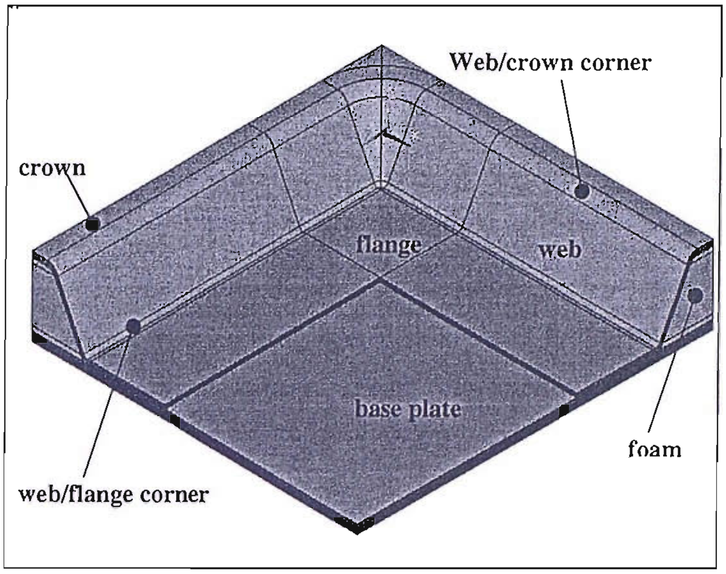

Figure 7.1 Constituents of the stiffened panels

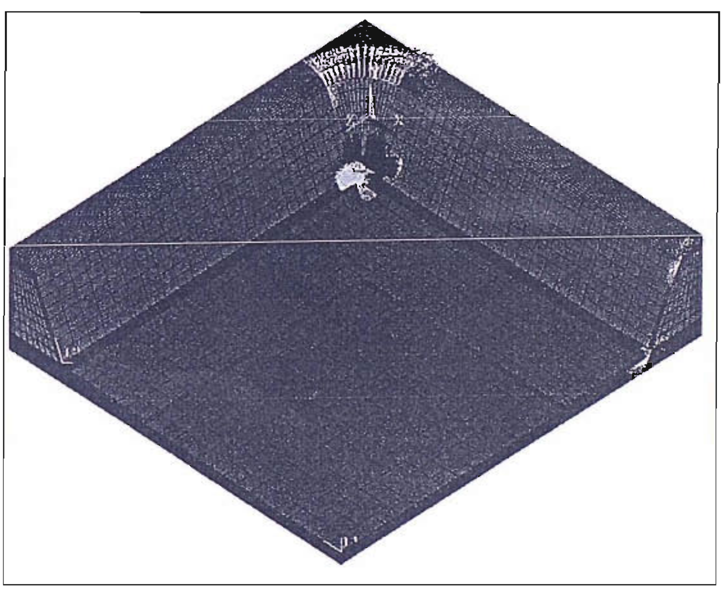

Figure 7.2 Illustration of the mesh densities Panel-2B

7.3 Load and Boundary Conditions

A top-hat cross-stiffened panel is typically subjected to hydrostatic pressure. This load scenario can be represented experimentally by a uniform pressure test. All test panels have been tested under uniform pressure, which was provided by water bag placed between specimen and lower steel frame (see Figure 7.3:(a)). Although the test panels were sandwiched between the two heavy steel frames and tightly bolted together by two lines of bolts all around, it was found that there were small in-plane inward displacements. These were measured from dial gauges placed at the middle of the short and long edges of the panel during the test. At first there were no in-plane edge displacements, but, as the pressure increased the membrane tensions became big enough to overcome the friction between panel and test rig and eventually pull the panel inwards. Hence it has been decided that the model is partially clamped, which means clamped boundary conditions were given at the each corner of the panels while simply supported edge conditions were given along the panel edges (see Figure 7.3(b)). The materials properties given in chapter 5 were used for the numerical analysis.

7.4 Validation of Results

7.4.1 Load- Deflection Results

In order to verify the validity of the numerical models of Panel-2B a comparison has been made between experimental and numerical results. Figure 7.4 shows experimental and numerical deflection values at the centre of the cross-stiffened panel. Because the numerical analysis was conducted in the linear range without including the effects of both geometrical and material non-linearities an expected deviation from the experimental load is noticed in this plot. Experimental finding resulted in relatively stiffer behaviour as compared to numerical results. This might be due to possible effect of membrane action of the panel which resulted in increase in stiffness.

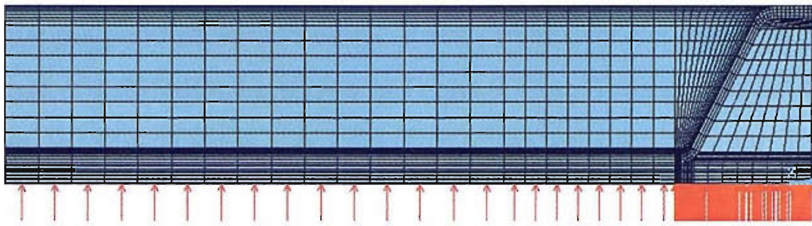

(a)

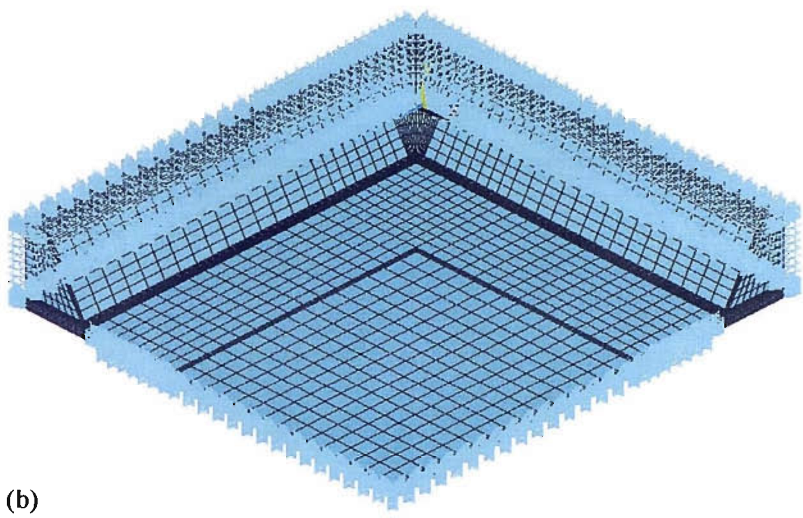

(b)

Figure 7.3 Loading and boundary condition (a) uniform pressure (b) simply supported boundary condition

7.4.2 Correlation between Experimental Failure Loads and FE Stress Levels

Examination of the stress components in the numerical results suggests that transverse tensile stress limit of the UD layer in Table 5.1 has been exceeded in Figure 7.5. This is approximately seven times higher than the ultimate transverse tensile strength of UD layer, which means the matrix cracking starts at load of 0.04 MPa. Interestingly the audible cracking was observed at a load of 0.05MPa. Increasing the load to value of 0.1MPa the maximum through thickness stresses σ_{zz} in Z direction occurring at the web/flange corner (curved part of the overlaminate) exceeded the material stress limit in Table 5.1 in Figure 7.6. Hence, delamination is likely to form in this location due to high through thickness stresses. This corresponds to position of root whitening which is caused by the presence of delamination observed in the experiment at a load of 0.1MPa.

As mentioned in chapter 5, it has been assumed that any damage experienced in the real structure will offset the load path and stress distribution compromising the validity of the FE model past the point of initial failure. Stress patterns for the Panel-2B at the experimental failure load of 0.295MPa are shown in Figure 7.7 (a): Tensile stress at the outer surface of the crown, (b) Tensile stress at outer surface of the web/crown corner. The magnitude of the tensile stresses occurring both at the web/crown corner and the crown region (see Figures 7.7(a) and Figures 7.7(b)) are higher than the ultimate tensile strength of the CSM layer (130MPa) which is obtained from the coupon tests. Fibre matrix breakage therefore would be predicted through the web to the crown in the intersection area. This is exactly match as the experimental findings.

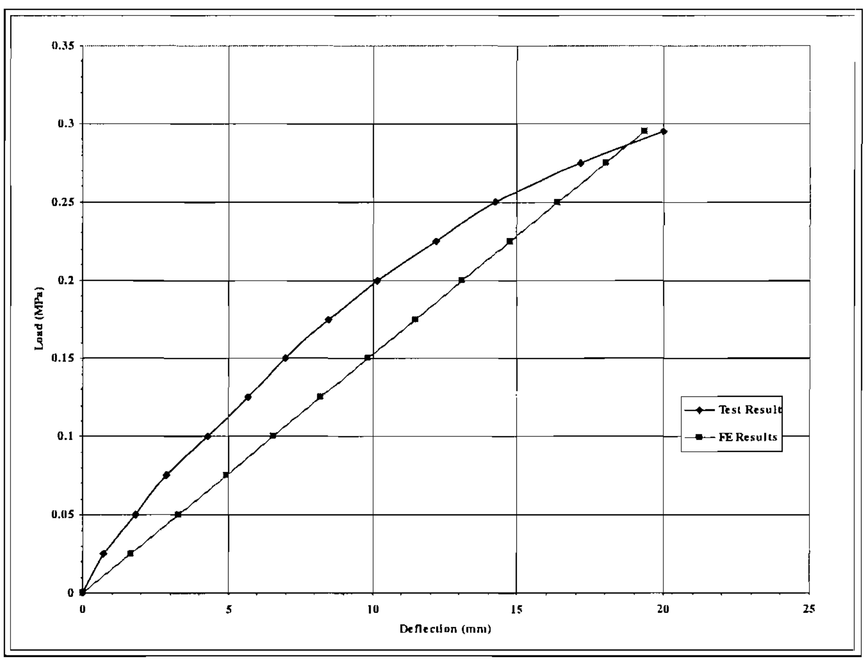

Figure 7.4 Central deflection vs. to pressure of Panel-2B

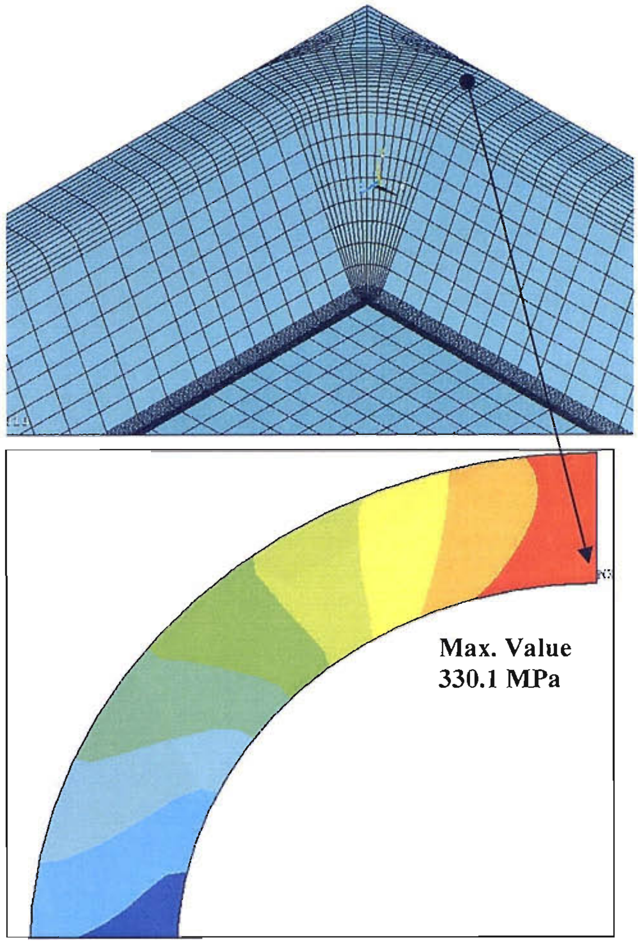

Figure 7.5 Transverse tensile stress distribution at UD layer at a failure load

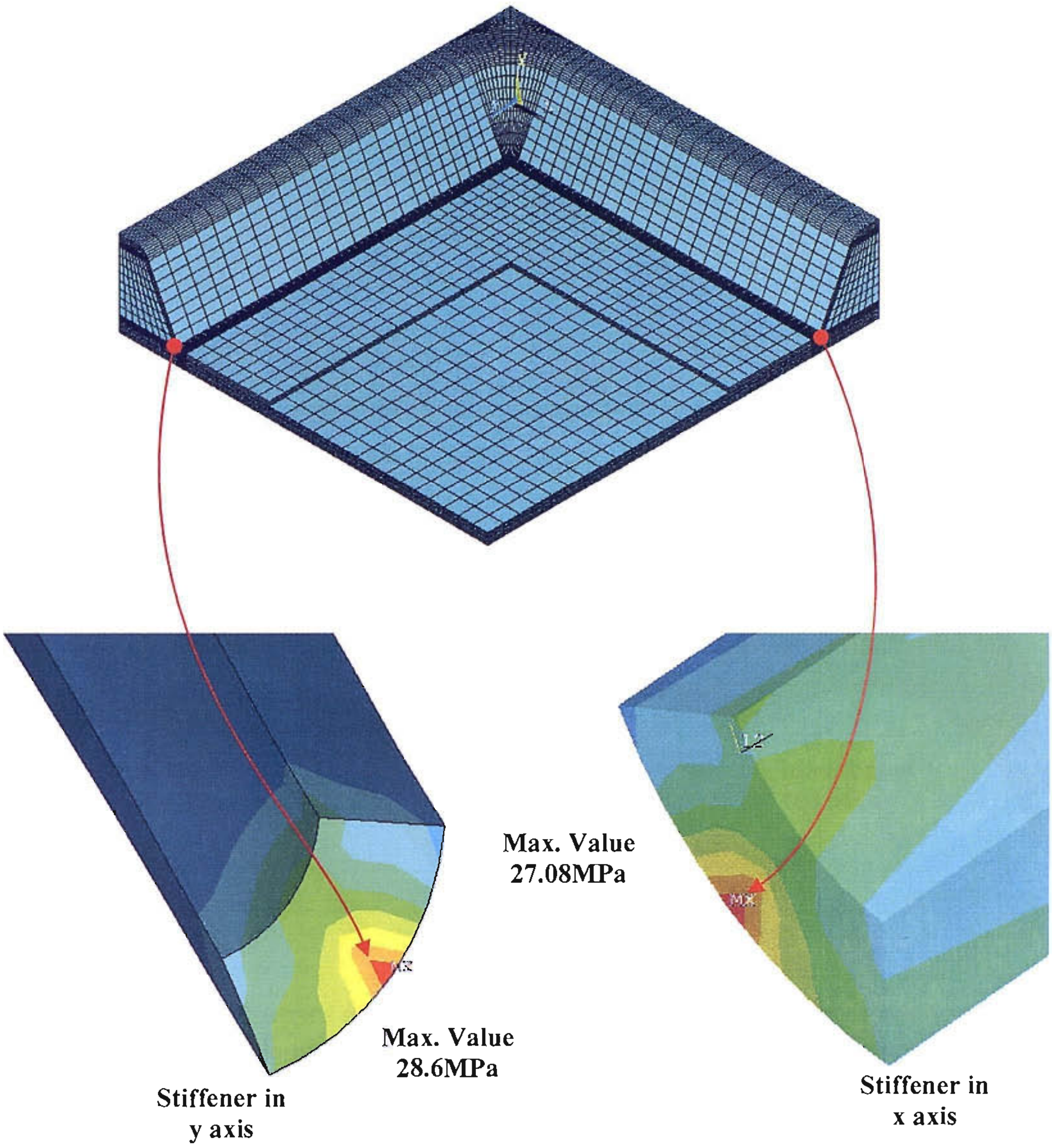

Figure 7.6 Through thickness stress at web flange corner in X and Y direction at the end of stiffener at a load of 0.1MPa

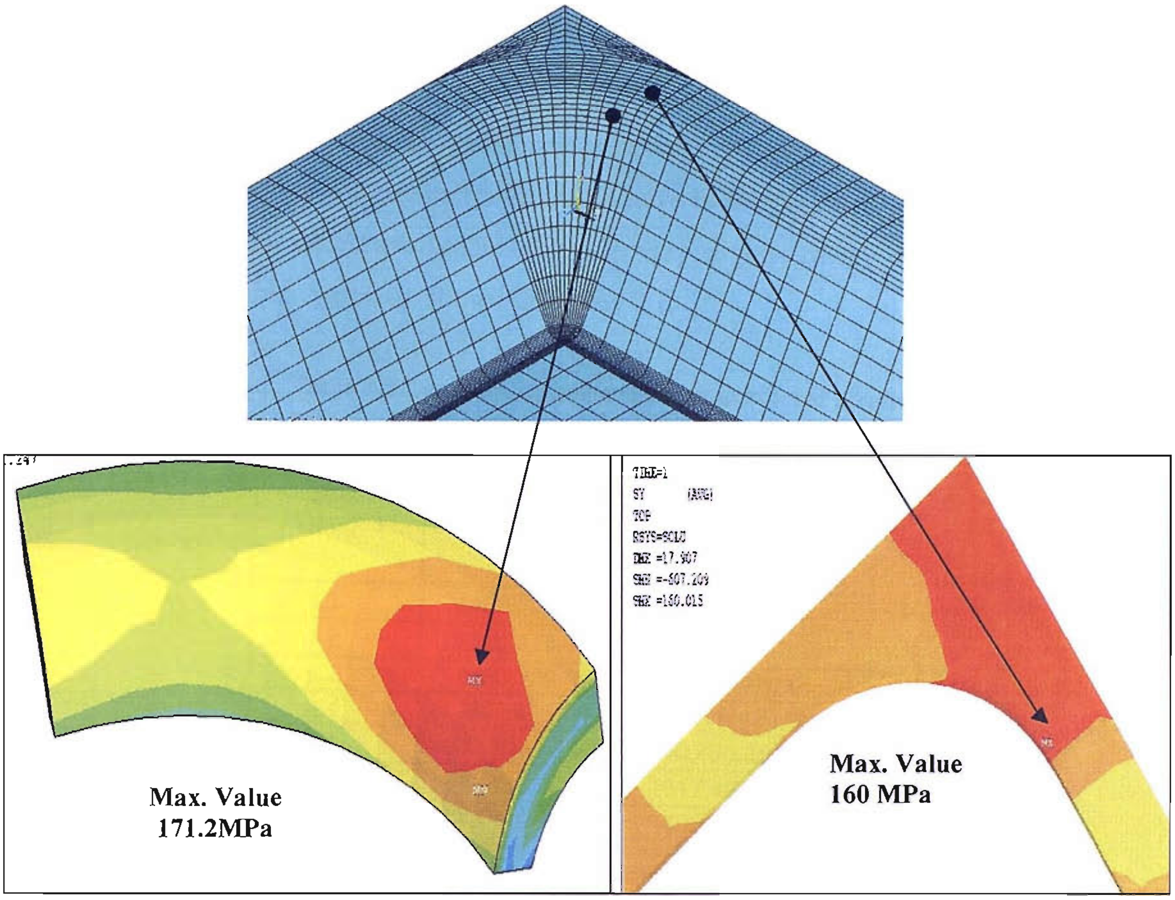

(a) (b)

Figure 7.7 Tensile stress distributions in outer surface of the overlaminate at a failure load (a Tensile stress at outer surface of te web/crown corner (b) Tensile stress at outer surface of the crown

7.4.3 Correlation between Experimental and FE Strain Results

Strain reflects the local behaviour of the panel. Strain gauges used in the test were 10 mm long and were mounted on both loaded and unloaded surfaces of the Panel-2B. With respect to strains the experimental results for Panel 2B have been compared with numerical results. The locations of measured and predicted strains vary slightly owing to the mesh geometry; however comparable values are shown in Tables 7.1.

Table 7.1 Location of measured and predicted strain

Strain Gauges	Location of measured and predicted strain	
	Experiment (mm)	FE (mm)
1*	(400,305,0)	(400,307,0)
2*	(520,425,0)	(517.5,425,0)
3	(400,425,0)	(400,425,0)
4	(400,425,0)	(400,425,0)
7*	(400,305,92.85)	(400,296.25,92.85)
8*	(280,425,92.85)	(517,425,92.85)
9	(400,425,92.85)	(400,425,92.85)
10	(400,305,92.85)	(400,425,92.85)
13	(468.5,150,50)	(447.7,139.8,50.8)
14	(468.5,150,50)	(447.7,139.8,50.8)
15	(468.5,150,50)	(447.7,139.8,50.8)
19	(530,295,15.85)	(528.7,296.2,15.85)
20	(530,295,15.85)	(528.7,296.2,15.85)
21	(650,175,11.35)	(641,174.8,11.35)
22	(650,175,11.35)	(641,174.8,11.35)

***: Due to quarter model of FE, it has been assumed that strain gauges 1 and 6, 2 and 5, 8 and 11 and 7 and 12 have the same strain values**

Figures 7.8: (iii) and (iv) show that the central strain versus pressure curves in x and y direction at loaded surface of the Panel-2B. As mentioned in the chapter 6 no damage was observed on the loaded surface of the panel after the experimentation. Hence it can be seen very good predictions for central strains on the loaded surface are achieved in the numerical model.

However Figure 7.9: (c) and (d) which show the central strains versus pressure curves on the unloaded surface, good agreement between the FE model and experiment can only be seen below pressure 0.25MPa. After that jump in the strain occurs in the x-direction for the experiment. At 0.25MPa experimental analysis showed that the panel sustained damage in the form of fibre-matrix breakage at the intersection of the stiffeners' web. At failure pressure (0.295MPa) fibre-matrix breakage propagated to the crown at the centre of the panel and destroyed the central strain gauge which leads to jump in strain.

It is also noticed that the strain predicted by numerical model in undamaged area match well with the measured strain. Figures 7.8: (i) and (ii) show the strain distributions on the loaded surface while Figures 7.9: (a), (e), (g), (h), (j), (k) and (l) show the strain distribution on the loaded surface in the both x and y directions. Good agreement between numerical model and test can be seen.

Figures 7.9: (b) demonstrate the strain distributions in y-axis (SG6 and SG10) at unloaded surface of the Panel-2B. The strains predicted from the numerical model have large difference from the tested ones although the strain gauges were located in undamaged area. On the other hand this probable because of the top hat stiffener assumed to have continuity in both x and y direction in the model while top hat stiffener has a discontinuity on the y direction as mentioned in chapter 6. Similar trend is seen in Figure 7.9:(f)

The comparison between predictions and test above show that the numerical model can provide good prediction of overall behaviour of the panel under high transverse pressure and provide reasonable prediction of local behaviour of the panel

Figure 7.8 Strain development at loaded surface of the Panel-2B

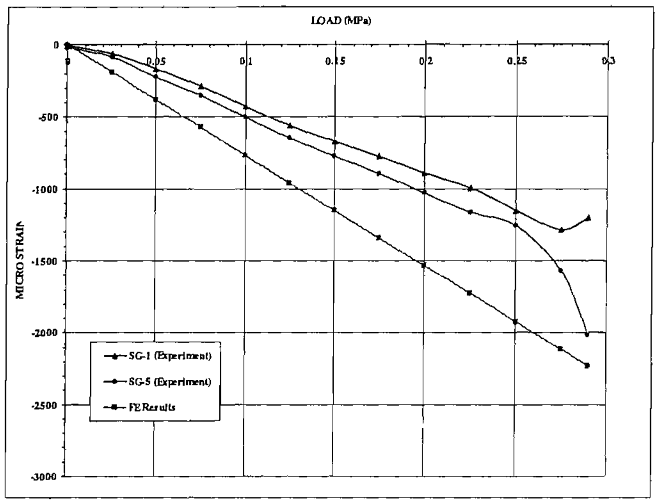

(i) Strain distributions in the y direction (SG1 and SG5) at loaded surface

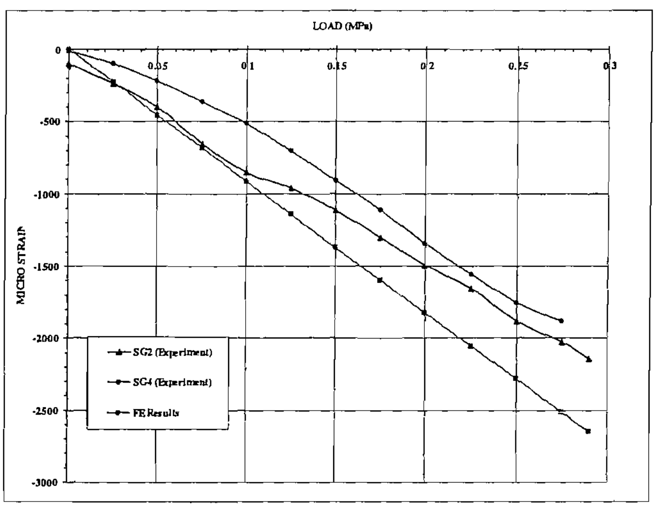

(ii) Strain distributions in the x direction (SG2 and SG4) at loaded surface

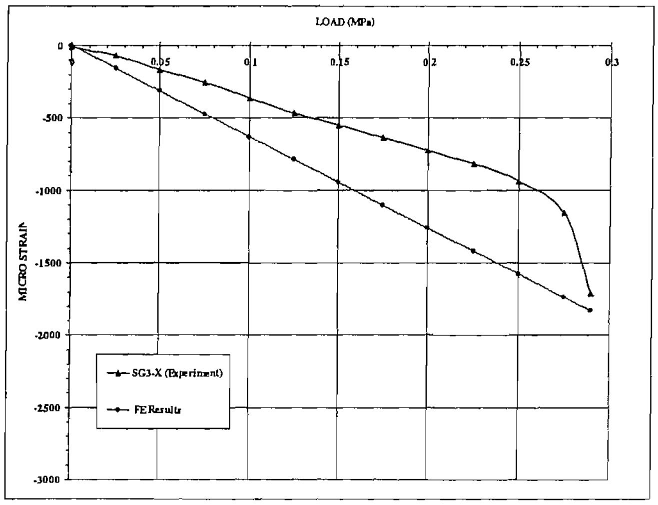

(iii) Central strain distributions in the x direction (SG3) at loaded surface

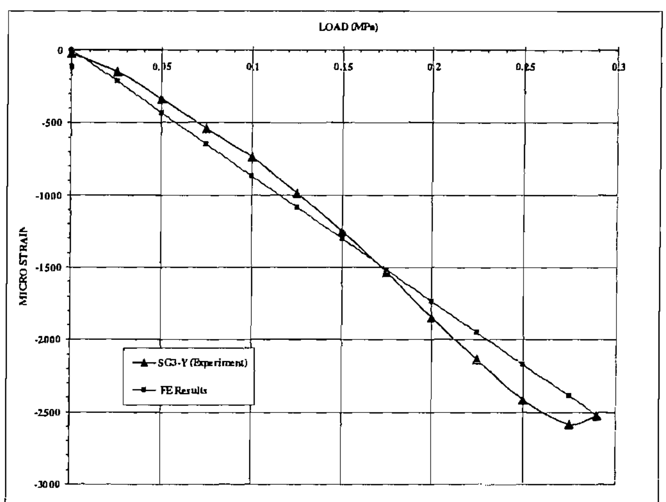

(iv) Central strain distributions in the y direction (SG3) at loaded surface

Figure 7.8 Strain development at loaded surface of the Panel-2B

Figure7.9 Strain development at unloaded surface of the Panel-2B

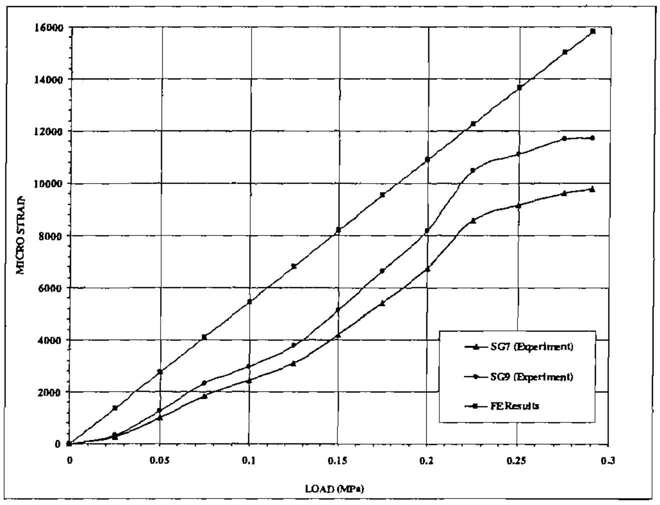

(a) Strain distributions in the x direction (SG7 and SG9) at unloaded surface

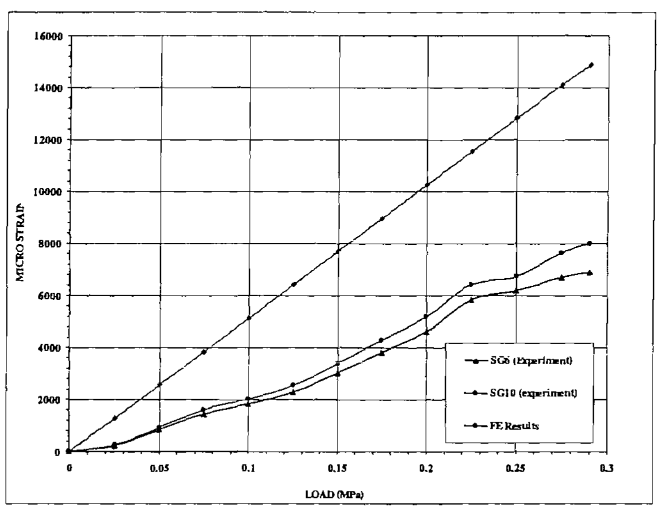

(b) Strain distributions in the y direction (SG6 and SG10) at unloaded surface

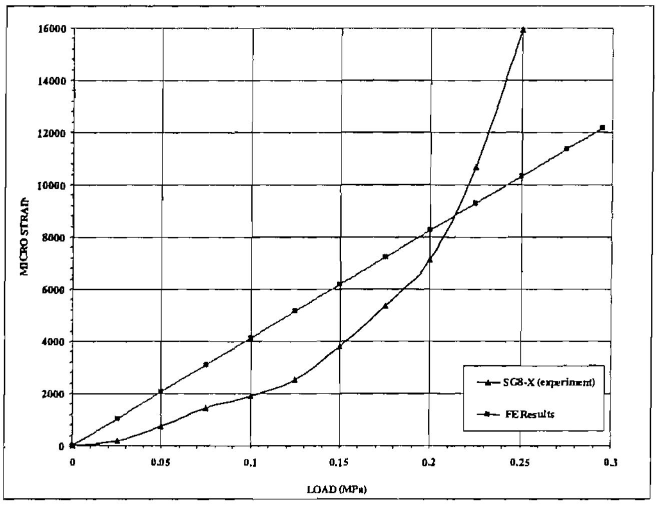

(c) Central strain distributions in the x direction (SG8) at unloaded surface

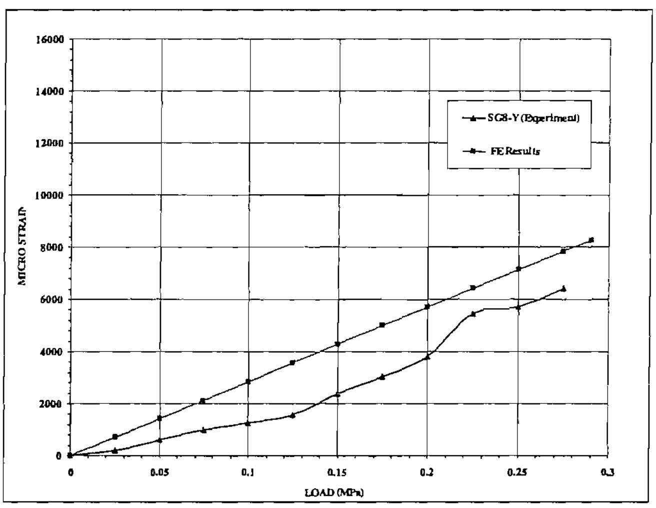

(d) Central strain distributions in the y direction (SG8) at unloaded surface

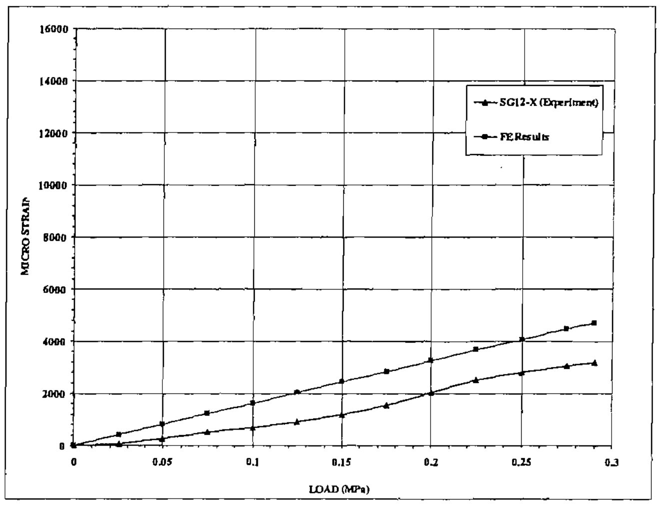

(e) Strain distributions in the web in the x direction (SG12) at unloaded surface

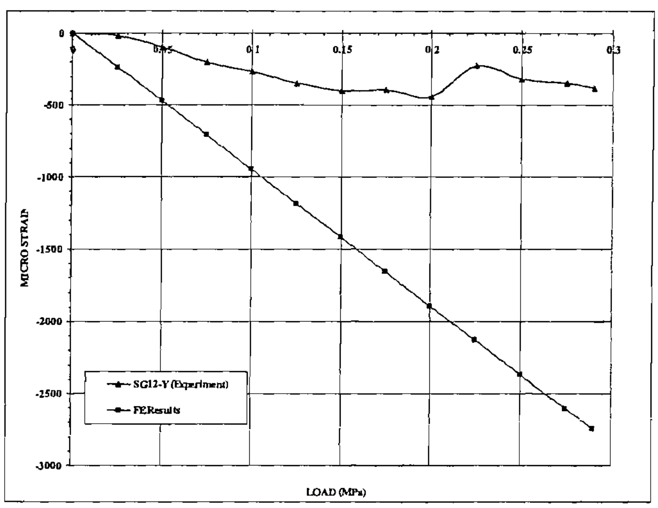

(f) Strain distributions in the web in the y direction (SG12) at unloaded surface

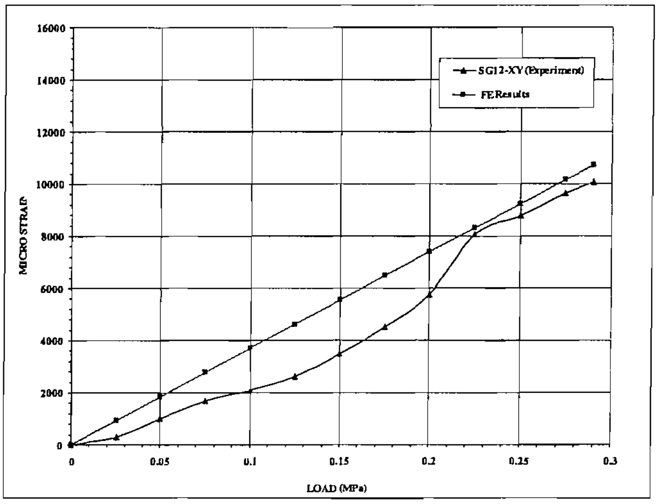

(g) Strain distributions in the web in the xy direction (SG12) at unloaded surface

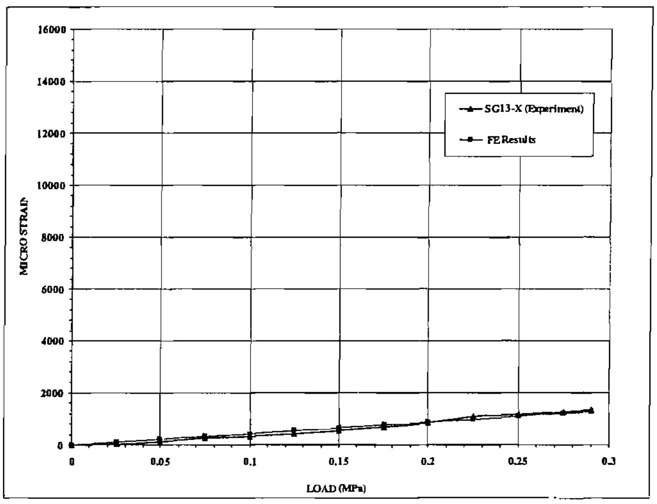

(h) Strain distributions in the x direction (SG13) at unloaded surface

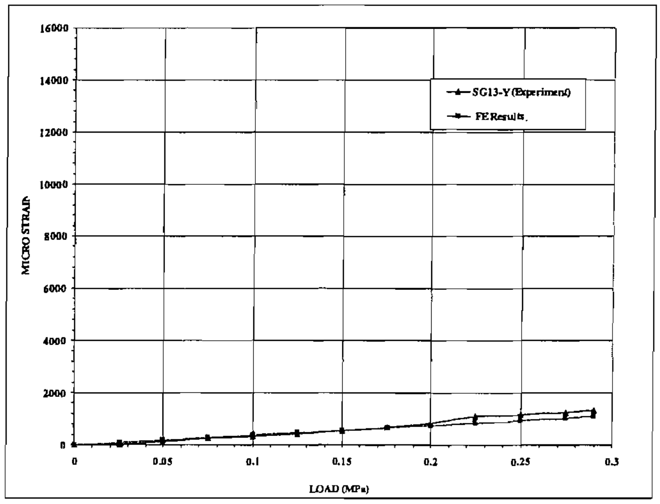

(j) Strain distributions in the y direction (SG13) at unloaded surface

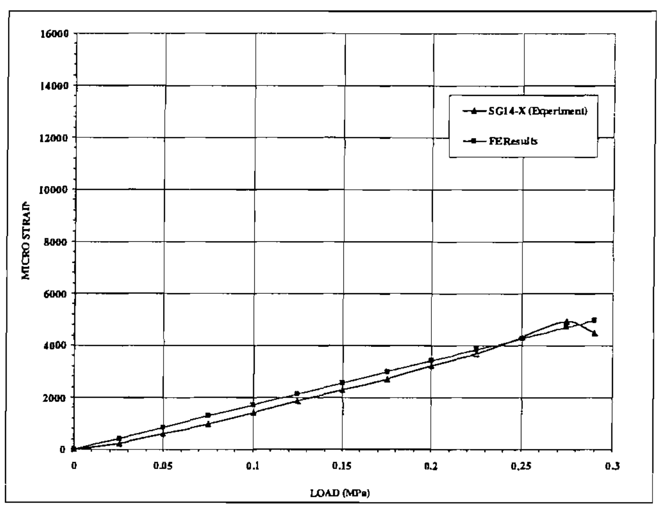

(k) Strain distributions in the x direction (SG14) at unloaded surface

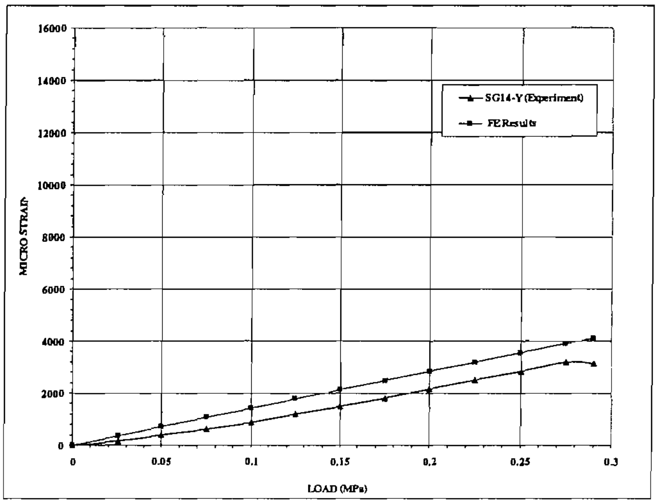

(l) Strain distributions in the y direction (SG14) at unloaded surface

Figure 7.9 Strain development at unloaded surface of the Panel-2B

7.5 Discussion

7.5.1 Comparison of deflection between model and test

Deflection reflects the overall behaviour of the panel. It can be seen from the Figure 7.4 there is deviation between experimental and numerical results. This probable because of the numerical analysis was conducted in the linear range without including the effects of both geometrical and material non-linearities while these effects were apparent in the experimental results. Predicted maximum deflection on the other hand agrees well with the experimental results.

7.5.2 Comparison of FE Stress Patterns with Experimental Failure Modes

There is currently limited numerical modelling information available about behaviour of composite panels subjected to uniform pressure [57, 82, 83] while significant body of work related to buckling analysis of the top hat stiffened panels [44,49,62-66]. The previous work [82, 83] clearly showed that damage tolerance of thin flat composite plates under uniform pressure. Choqueuse [57] investigated the top hat stiffened sandwich plate under uniform pressure. The numerical results was compared the over all panel behaviour and measured strain data. Satisfactory result was obtained in the case of global load deflection; less satisfactory results were obtained comparison between predicted and measured strains. There was no attempt made correlation between finite element derived failure stresses and material failure data at experimental failure loads which was considered at present work.

Detailed finite element model have been generated to represent the top hat stiffened panel. Internal stress pattern have been yielded for the top hat stiffened panel under uniform pressure which are representative of typical in service loads. The finite element results compare well with the experimental findings. The most notable are that under uniform pressure load, the delamination which occurred at curved part of the overlaminate (web/flange corner) close to support region are due to excessive through-thickness stresses and damage in the crown at the centre of the panel is due to excessive in plane tensile stresses. The failure of the top hat stiffened panel under uniform pressure is that of fibre-matrix breakage at the centre of the panel and complete separation of the overlaminate from the base panel at the free edge of the stiffener. The analysis also showed that the curved region of the overlaminate (top hat stiffener's web/flange corner) is delamination prone areas as in the top hat stiffener case in the chapter 5. These finding are exactly matching with the previous work on out of plane joint problems [38, 42].

7.5.3 Comparison of Predicted Strains with Measured Strains

The strains predicted from the numerical model match well with the measured strains in the undamaged area. This was apparent when the compare the central strain on the both loaded and unloaded surfaces of the panel. While the predicted central strains are in a good agreement with the measured strain at loaded surface (undamaged area), jump in strain was observed at the centre on the loaded surface of the panel due to final failure, fibre-matrix breakage occurred at this region. The numerical model over predicted the strain values where the strain gauges were located on the stiffener in the y direction at unloaded surface. This is probable because of the stiffener has discontinuity in the y direction while top hat stiffeners assumed to have continuity in both x and y direction in the model.

Chapter 8 CONCLUSIONS

8.1 Introduction

This chapter presents a summary of the research undertaken in the last three years. All of the relevant conclusions from the previous chapters are brought together.

8.2 Summary

8.2.1 Research Motivation

The main aim of the work has been to understand more fully the behaviour of typical ship type FRP single skin composite structures, namely: top hat stiffeners and top hat stiffened panels, under representative static loading conditions. A review of the available literature showed that most codes for design of these structures particularly within the marine industry have been largely based on the empirical evidence. Limited work has been directed to calculate the structural capabilities of these structures. It followed that lack of data take account of load transfer and failure mechanisms exhibited by these structures. This gives an opportunity to carry out fundamental research aimed at further investigating the problem experimentally and theoretically. It was hoped that any findings could thus be used for structural optimisation and weight minimisation of large stiffened plate structures.

8.2.2 Experiments on Top Hat Stiffeners

The four point bending loading was adopted for the top hat stiffener test. The primary aims of the experimental programmes were to determine the critical design variables that affect the structural performance of top hat stiffeners, to study the failure mechanisms associated with different design and provide validatory data for theoretical analyses. This was achieved in all three areas. The lay-up materials and overlaminate thickness were shown to be critical design variables while fillet radius being considerably less significant. Both types of stiffener design prone to premature failure by delamination at the curved region of the overlaminate (web/flange corner) near the support region. The final failure for the group stiffener A took the form of fibre-matrix breakage on the web and flange area. On the other hand catastrophic shear failure is occurring in the web characterises the final failure of the group B design near the support region. Load deflection curves were taken from all samples as validatory data for the theoretical analysis.

The experimental programme also illustrated several other points. Principle amongst these was the relationship between quality of construction and design of the stiffeners. For example first specimen of the group stiffener A (stiffener A1) had minimum failure load due to UD layer is set up on the crown eccentrically. The group stiffeners B were found to be more consistent in their performance. The large deflection achieved with the group stiffener A reflected the high energy absorption available with overlaminate made up of three layers of 600 g/m^2 CSM. It would be particularly important the behaviour of the top hat stiffened structures within a ship structure that is continuously subjected to hydrostatic and other loads. Further work required in this area to determine the significance of these structures long term performance. The results of the experimental programme also showed benefits of using relatively lighter CSM (225 g/m^2) with stitched Bias lay-up in overlaminate reduce structure weight by up to 14 % with only marginal decreases in ultimate strength. The concept of thin overlaminate is positive feature is contrary to current design guidelines, which promote the use of excessively thick and hence stiff overlaminate. This is particularly surprising when one consider the inherent flexibility of GRP structures due to the relatively low modulus.

8.2.3 Theoretical Model of Top Hat Stiffeners

Validating the FE models in chapter 5 with the experimental load deflection results showed the degree of care required to achieve consistent results with the FE method. Most importantly the accurate representation of the structural geometry and the use of representative material properties were shown to be critical. This last feature is particularly important with composite materials since more obscure properties are not necessarily available but may play a significant role in the behaviour of these structures, particularly governing its failure mechanisms. The derivation of composite material properties including failure properties, is an essential prerequisite to accurate analysis, and is an area most worthy of further consideration.

By showing the internal stress distribution within the both types of stiffeners described in chapter 5 were able to illustrate load transfer mechanisms seen during the experimental programme. It has been shown that the delamination prone areas for both types of top hat stiffeners are located in the web/flange corner (curve region of the overlaminate) close to the outer surface near the support region. The delaminations are likely to be due to excessive through thickness stresses. Final failure of group stiffeners A, which took the form of fibre-matrix breakage in the web and flange is likely to be due to the excessive in-plane tensile and shear stresses. In the case of group stiffener B, final failure occurs in the web due to the excessive shear stresses

The results of the parametric studies have illustrated the effects of the variables on the top hat stiffener behaviour. Material choice and overlaminate thickness have significant effects on the top hat stiffener behaviour and can be optimized for a given application. Generally central deflections and stress distributions (through-thickness stress, tensile stress and shear stress) reduce by increasing the overlaminate thickness and fillet radius for the both types of stiffeners. While increase in overlaminate thickness has significant effects on all accounts, increase in fillet radius has only considerable effects on through thickness stress. For example through thickness stress reduced by 15% for stiffener with a Type A lay-up increasing the fillet radius from 12 mm to 24 mm with a thickness of three laminations for overlaminate (4.5mm) which could overcome the delamination problem. At a same overlaminate thickness by using Type B lay-up for the stiffener reduces the central deflection through-thickness stresses and tensile stresses but it increases the shear stresses.

Analytical method was used to predict the maximum deflection, bending stress and shear stress. The results were directly compared the finite element and experimental findings (maximum deflection) and indirectly compared with the FE results (bending stress and shear stress). Good correlation was found on all account.

8.2.4 Experiment on Top Hat Stiffened Panels

A total of 11 individual top hat stiffened panel have been tested to failure to investigate the effects of material composition, panel geometry on strength and stiffness under transverse pressure. This appears to be the first time this has been done so comprehensively. The strain gauges were mounted on one of the panel on both loaded and unloaded surface in many places to investigate the strain development. Digital gauges were also used to measure lateral deflection and in-plane edge displacement. Load deflection curves were taken from all samples as validatory data for the theoretical analysis. The experimental programme illustrated several other points.

Experimental investigation has exposed the areas of weakness within the structure and the failure mechanisms, which occurs when these structures are subjected to typical in-service loads. As in the top hat stiffener test, the lay-up materials and overlaminate thickness were shown to be critical design variables. Damage started in all panels with matrix cracking followed by delamination at the curved part of the ovelamination near the support region. Except group panels 4, all the panels failed by fibre matrix breakage at the intersection region while group panels 4 failed by shear induced failure at the web. This is because of the group panels 4's larger overlapped patch, which is made up stronger isopthalic polyester resin result in different failure mechanisms amongst the panels. This highlights the importance of choosing lay-up material and geometry for the overlapped patch.

The panel group 1 whose overlaminate made up of 3 layers of 600 g/m^2 CSM and overlapped patch made up of 2 layers of 600 g/m^2 CSM with a size of 600×600 mm×mm had maximum strength and stiffness. This indicate that the amount of reinforcement in the panel determine the strength and stiffness. However the distribution of that reinforcement is very important. The more even the distribution of reinforcement in every direction the better strength and stiffness.

As would be expected measured strain at the loaded surface in compression and it is in tension in unloaded surfaces (except on the web through the crown measured strain in compression). This is because of plate bending develops tensile stresses on the unloaded surface and compressive stress at the loaded surface which are known as membrane stresses.

It is clear that from the strain development, the strains in the x direction are bigger than those in y direction at high pressure. The panel continuity of longitudinal stiffener is maintained with appropriate cut-outs in the transverse stiffeners. Hence it has been decided that the stiffener in x direction is continuous. The results also indicate that although the panel is considered to be symmetrical in the x-y plane the strain distributions were not symmetrical as expected. Surely it is because the stiffener was continuous in the x direction but not in the y-direction.

8.2.5 Theoretical Model of Top Hat Stiffened Panels

FE model was generated for the Panel-2B and it has been validated directly, in the case of global load/deflection and strain results, and indirectly by comparing finite element derived failure stresses with material failure data at experimental failure loads. Reasonable correlation was found on all counts.

Assessments of internal stress distributions within the Panel-2B indicate that the curved region of the overlaminate (stiffener's web/flange corner) near the support region is a delamination prone area due to high through-thickness stress as in the top hat stiffener case (see Figure 7.6). This match with the experimental observation (see Figure 6.22). At ultimate failure pressure it was observed that final failure of the panel-2B took the form of fibre-matrix breakage on the crown where the two top hat stiffeners intersect. Again FE model successfully predicted the location of maximum bending stresses (see Figure 7.5 and 7.7) associated with fibre-matrix breakage.

The strains predicted from the numerical model match well with the measured strains in the undamaged area. Figures 7.8: (iii) and (iv) show that the central strain versus pressure curves. As can be seen very good prediction for central strains for loaded surface in the x-direction and y-direction are achieved in the FE model compared to experimental results. However Figure 7.9: (c) and (d) which show the central strains versus pressure curves at unloaded surface, good agreement between the FE model and experiment can only be seen below pressure 0.25MPa. After that jump in the strain occurs in the x-direction for the experiment. This is because of the strains are very sensitive to local damage. This is a shortcoming of the numerical model which needs to be developed further. Figures 7.9: (b) demonstrate the strain distributions in y-axis (SG6 and SG10) at unloaded surface of the Panel-2B. The strains predicted from the numerical model have large difference from the tested ones although the strain gauges were located in undamaged area. On the other hand this probable because of the top hat stiffener assumed to have continuity in both x and y direction in the model while top hat stiffener has a discontinuity on the y direction as mentioned in chapter 6.

8.2.6 Coupon Tests

Experimental studies were conducted to investigate the material properties of the constituents of the test specimens. A large numbers of coupons were tested in tension and bending to obtain the stiffness and strength of the materials in different direction.

8.3 Conclusions

From the experiments and theoretical analyses that were carried out to investigate the structural performance of typical ship structural elements under representative static load condition, the following can be concluded.

- The experimental and theoretical studies presented here identified the failure mechanisms associated with different top hat stiffener designs and clearly showed that importance of the lay-up material and overlaminate thickness on the top hat stiffener performance. The influence of these design variables was further illustrated by the results from parametric studies of top hat stiffened structures. Increased overlaminate thickness and fillet radius were shown to reduce central deflection and stresses in all areas, whilst increasing the overlaminate thickness has significant effects on all accounts, there is only considerable effect on through-thickness stresses were seen increasing the fillet radius. This work also shows at a same overlaminate thickness by using Type B lay-up for the stiffener reduces the central deflection through-thickness stresses and tensile stresses but it increases the shear stresses.

- The Structural performance of top hat stiffened panel was similar that of top hat stiffeners in that lay-up materials and overlaminate thickness was the critical design variables. Both experiments on top hat stiffener and top hat stiffened panels show that by using the Type A lay-up for the stiffener's overlaminate improve the strength, stiffness and energy absorption for both type of structures which means that the amount of reinforcement in the panel determine the strength and stiffness. However the distribution of that reinforcement is very important. The tests on both structural element show that more even the distribution of reinforcement in every direction the better strength and stiffness.

- Material properties have also influence on failure mechanisms. While by using Type A lay-up for the stiffener's overlamination caused a fibre-matrix breakage final failure mode for the top hat stiffeners (group stiffener A) and top hat stiffened panels (group panels 1,2 and 3) the final failure mode took the form of catastrophic shear failure by using the Type B lay-up for top hat stiffeners (group stiffener B) and top hat stiffened panels (group panels 4). The use of relatively small size of overlapped patch made of orthopthalic polyester resin prevents catastrophic shear failure for group panel 3, although its stiffener made of similar lay-up with group panel 4. This highlights the importance of choosing lay-up material and its geometry for overlapped patch.

- Numerical works clearly showed the load paths associated with the two loading method were likely produce the failure mechanisms seen in real ship structures that is premature failure by delamination. Delamination prone areas are located the curved region of the overlamination (web/flange corner) close to support region. Delaminations are likely to be due to excessive through-thickness stresses

- The strains predicted from the FE model agree reasonably well with the test results. The FE method provides a useful tool to investigate the behaviour of the composite panels under high transverse pressure.

- Despite the similarities in failure mechanisms for both top hat stiffeners (Stiffener group A and B) and top hat stiffened panels (Panel groups 1,2,3 and 4), the same group specimens failed at different load and exhibited different stiffness, failing deflections and giving a range of energy absorption. These highlights the difficulties in producing quality of those specimens.

8.4 Recommendations for Further Work

The current work highlighted some areas which require further investigations.

1. During the experimental work it was not possible to determine the internal stress states that were developed within the stiffener for correlation with theoretical studies. Techniques needs to be developed that allow this level of information to be determined from within complex shapes such as top hat stiffened composite structures.

2. The behaviour of ship's components under static loading configuration have been successfully represented using strength based approaches. In order to represent typical in-service dynamic loads, however an assumed static load situation has been adopted. Since typical in-service loading conditions are largely dynamic, these existing models must be adapted so as to able to represent dynamic loads such as impact and fatigue load scenarios.

3. The development of dynamic test programme (impact and fatigue tests) highlights another problem encountered during the course of this work that of the limited amount of material property data available for these materials. It is necessary to determine the salient properties of the all combinations of material used their strain rate and temperature dependencies and their fatigue behaviour. All these necessary if a thorough theoretical analysis to be completed experimental programme.

4. A full non-linear progressive damage model would improve the FE analysis with its regard to for iteration between stress components and stiffness reduction.

REFERENCES

1. Shenoi, R.A. and Wellicome, J.F., Eds. "Composite Materials in Maritime Structures", Vol. 1. 1993, Cambridge University Press.
2. Shenoi, R.A. and Wellicome, J.F., Eds. "Composite Materials in Maritime Structures", Vol. 2. 1994, Cambridge University Press.
3. Dixon, R.H., Ramsey, B.W. and Usher. P.J., "Design and Build of GRP Hull of HMS WILTON. in Proceedings of the Symposium on GRP Ship Construction", 1972. London: RINA.
4. Hellbratt, S.E., "Experiences from Design and Production of the 72m CFRP-Sandwich Corvette Visby", in 6th International Conference on Sandwich Structures. 2003. Florida, USA.
5. Halmatic, "Largest Mast Uses Specialised Materials and Processes, in Ship & Boat International", 2002. p. 26-27.
6. Henton, D., "Glass Reinforced Plastics in the Royal Navy", Trans RINA. 1967. London: RINA.
7. Smith, C.S., "Design of Marine Structures in Composite Materials", published by Elsevier Applied Science,1990.
8. Gibbs and Cox, "Marine Design Manual for GRP", McGraw Hill Book Company, New York, 1960.
9. Tsouvalis, N. and Spanopoulos. G.,"Design Curves for Selecting Hat-Type Stiffeners in FRP Boats", in FAST 2003. Ischia (Gulf of Naples), Italy.
10. "Rules for Yachts and Small Craft", Lloyd's Register of Shipping, London, 1983.
11. "Rules for Building and Classing Reinforced Plastic Vessels", American Bureau of Shipping, New York, 1978.
12. "Guide for Building and Classing High Speed Craft", American Bureau of Shipping, New York, 1997.
13. "Rules for Classification of High Speed and Light Craft", Det Norske Veritas, Hovik, 1991.
14. NES 140, "GRP Ship Design", Naval Engineering Standards, Issue 2, Undated.
15. Noor, A.K. and Burton, W.S., "Assessment of Shear Deformation Theories for Multilayered Composite Plates", Appl. Mech. Rev., 1989. **42**(1).

16. Whitney, J.M., " Structural Analysis of Laminated Anisotropic Plate", published by Technomic, Lancaster, Pa.: 1987.

17. Reissner, E., "The Effect of Transverse Shear Deformation on the Bending of Elastic Plates", Journal of Applied Mechanics, 1945. **12**: p. 69-77.

18. Mindlin, R.D., "Influence of Rotary Inertia and Shear on Flexural Motion of Isotropic Elastic Plates", Journal of Applied Mechanics, 1950. **18**: p. 31-38.

19. Yang, P.C., Norris, C.H. and Stavsky, Y., "Elastic Wave Propagation in Heterogeneous Plates", International Journal of Solids and Structures, 1966. **2**: p. 665-684.

20. Whitney, J.M. and Sun, C.T., "A Higher Order Theory for Extensional Motion of Laminated Composites" Journal of Sound and Vibration, 1973. **30**(1): p. 85-97.

21. Whitney, J.M., "Shear correction factors for orthotropic laminates", Journal of Applied Mechanics, 1973. **40**: p. 302-304.

22. Knight, N.F. and QI, Y., "Restatement of First-Order Shear Deformation Theory for Laminated Plates", International Journal of Solids Structures, 1997. **34**(4): p. 481-492.

23. Lo, K.H., Christensen, R.M. and Wu, E.M., "A Higher Order Theory of Plate Deformation: Part 2 Laminated Plates", Journal of Applied Mechanics, 1977: p. 669-676.

24. Reddy, J.N., "A Simple Higher-Order Theory for Laminated Composite Plate", Journal of Applied Mechanics, 1984. **51**: p. 481-492.

25. Liu, D. and Xiaoyu, L.I., "An Overall View of Laminate Theories Based on Displacement Hypothesis", Journal of Composite Materials, 1996. **30**(14).

26. Reddy, J.N.,"A Generalization of Two-Dimensional Theories of Laminated Composite Plates", Commun. Applied Numerical Methods, 1987. **3**: p. 113-180.

27. Paepegem, W.V. and Degrieck, J., "Modelling Strategies for Fatigue Damage Behaviour of Fibre-reinforced Polymer Composites", European Journal of Mechanical and Environmental Engineering, 2001. **46**(4): p. 217-227.

28. Chang, F.K. and Springer, G.S., "The Strength of Fibre Reinforced Composite Bends", Journal of Composite Materials, 1986. **20**: p. 30-45.

29. Taylor, R.L., Beresford, P.J. and Wilson, E.L., "A Non Conforming Element For Stress Analysis", International Journal for Numerical Methods in Engineering, 1976. **10**: p. 1211-1219.

30. Chang, F.K., "The Strength Analysis of Wooden Bends", Journal of Reinforced Plastics and Composites, 1986. **5**: p. 239-252.

31. Botello, S., Onate, E. and Miquel. J., "A Layer wise Finite Element Model for analysis of Composite Plates and Shells", in ICCM9. 1993. University of Zaragosa: Woodhead Publishing Ltd.

32. Reddy, Y.S.N. and Reddy, J.N., "An Accurate Prediction of Failures in Composite Laminates Using a Layerwise Model", in ICCM9. 1993. University of Zaragosa: Woodhead Publishing Ltd.

33. Reddy, J.N., "A Refined Nonlinear Theory of Plates with Transverse Shear Deformation", International Journal of Solid and Structures, 1987. **20**: p. 881-896.

34. Reddy, J.N., "On Refined Computational Models of Composite Laminates" International Journal on Numerical Methods in Engineering, 1989. **27**: p. 361-382.

35. Robbins, J.D.H. and Reddy, J.N., "Modelling of Thick Composites Using a Layer-Wise Laminated Theory", International Journal for Numerical Methods in Engineering, 1993. **36**(4): p. 655-678.

36. Flanagan, G., "A Sublaminate Analysis Method for Predicting Disbonds and Delamination Loads in Composite Structures", Journal of Reinforced Plastics and Composites, 1993. **12**: p. 876-887.

37. Pagano, N.J., "On the Calculation of Interlaminar Normal Stress in Composite Laminate", Journal of Composite Materials, 1974: p. 65-81.

38. Hawkins, G.L., "Assessment of Damage Tolerance Levels in FRP Ship Structures", in Lightweight and Composite Structures Research Group, 1995, University of Southampton: Southampton. p. 1-80.

39. Dodkins, A.R., Shenoi, R.A. and Hawkins, G.L., "Design of joints and attachments in FRP ships' structures. Marine Structures", 1994. **7**(2-5): p. 365-398.

40. Shenoi, R.A. and Hawkins, G.L., "An investigation into the performance characteristics of top-hat stiffener to shell plating joints", Composite Structures, 1995. **30**(1): p. 109-121.

41. Junhou, P. and Shenoi, R.A., "Examination of key aspects defining the performance characteristics of out-of-plane joints in FRP marine structures", Composites Part A: Applied Science and Manufacturing, 1996. **27**(2): p. 89-103.

42. Phillips, H.J., Shenoi, R.A. and Moss, C.E., "Damage mechanics of top-hat stiffeners used in FRP ship construction", Marine Structures, 1999. **12**(1): p. 1-19.

43. Blake, J.I.R., Shenoi, R.A., House, J. and Turton, T., "Strength Modelling in Stiffened FRP Structures with Viscoelastic Inserts for Ocean Structures", Journal of Ocean Engineering, 2001. **29**: p. 849-869.

44. Smith, C.S., "Compressive Strength of Transversely Stiffened FRP Panels' in Aspects of the Analysis of Plate Structures", (Eds. D.J. Daw et al) Clarendon Press: Oxford, 1985,

45. Ray, C. and Satsangi, S.K., "Finite Element Analysis of Laminated Hat-Stiffened Plates", Journal of Reinforced Plastics and Composites, 1996. **15**: p. 1174-1193.

46. Prusty, B.G., "Linear static analysis of composite hat-stiffened laminated shells using finite elements", Finite Elements in Analysis and Design, 2003. **39**(12): p. 1125-1138.

47. Paul, T.K. and Sinha, P.K., "Design of hat-stiffened composite panels loaded in axial compression" Composite Structures, 1992. **21**(4): p. 205-209.

48. Agarwal, B. and Davis, R.C., "Minimum Weight Designs for Hat-Stiffened Composite Panel under Uniaxial Compression", 1974, Langley Research Centre: Washington D.C. p. 1-11.

49. Ko, W.L. and Jackson, R.H., "Compressive Buckling Analysis of a Hat-Stiffened Panel" 1991, Dryden Flight Research Centre: California.

50. Ko, W.L. and Jackson, R.H., "Shear Buckling Analysis of a Hat-Stiffened Panel", 1994, Dryden Flight Centre: California.

51. Vitali, R., Park, O., Haftka, R.T., Sankar, B.V., Rose, C.A., "Structural Optimization of Hat-Stiffened Panel Using Response Surfaces. Journal of Aircraft, 2002. **39**(1): p. 158-166.

52. Lamberti, L., Venkataraman, S., Haftka, R.T., and Johnson, T.F., "Preliminary Design Optimization of Stiffened Panels using Approximate Analysis Models", International Journal for Numerical Methods in Engineering, 2003. **57**(10): p. 1351-1380.

53. Collier, C.S., "Thermoelastic Formulation of Stiffened, Unsymmetric Composite Panels for Finite Element Analysis of High Speed Aircraft", 1994, NASA and Lockhead Engineering, Virginia.

54. Elliott, D.M., "Mechanical Testing of Composite Joints", in Interim Report. 1994, DRA/AV AWS TR94212.

55. Funatogawa, O., Kimpara, L., and Takehana, M., "On the stiffening Effect of Hat-Shaped Stiffeners on a Plate, Bending of Single Stiffener Model", J.S.N.A, 1978. **144**.

56. Funatogawa, O., Kimpara, L., and Takehana, M., "On the stiffening Effect of Hat-Shaped Stiffeners on a Plate, Buckling of a Hat Stiffened Panel", J.S.N.A, 1979. **145**.

57. Choqueuse, D., Davies, P., and Bigourdan. B."Correlation Between Tests and Calculations for Composite Materials in Marine Applications. in Nautical Construction with Composite Materials", 1992. Paris (France): Service de la Documentation et des Publications (S.D.P.).

58. Reichard, R. "Composite Preform Frames for GRP Structures. in Technology and Material Needs for the Year 2000", 1997. Paris (France): SAMPE Europe.

59. Lewit, S.M. and Reichard, R., "The Use of Composite Preform Frame Technology for GRP Marine Structures", in Proceedings of MACM'96. 1996.

60. Mouring, S.E. "Structural Behaviour of Composite Panels Stiffened with Perform Frames", in Seventh International Conference on Marine Applications of Composite Materials. 1998. Melbourne, Florida: Composite Education Association.

61. Mouring, S.E., "Buckling and Postbuckling of Composite Ship Panels Stiffened with Preform Frames", Ocean Engineering, 1999. **26**(8): p. 793-803.

62. Lee, S., Xiong, Y., Benak, T.J. and Heat, J., "Design Analysis Manufacture and Experimental Performance of Hat-Stiffened Composite Panel". 1997, Centre for Advance Engineering Materials, The Hon Kong University of Science and Technology.

63. Jiang, W., Bao, G. and Roberts, J.C., "Finite Element Modelling of Stiffened and Unstiffened Orthotropic Plates", Computers & Structures,, 1997. **63**(1): p. 105-117.

64. Roberts, J.C., Bao, G. and White, G.J., "Experimental, Numerical and Analytical Results for Bending and Buckling of Rectangular Orthotropic Plates", Composite Structures, 1998. **43**(4): p. 289-299.

65. Falzon, B.G. and Steven, G.P., "Buckling Mode Transition in Hat-Stiffened Composite Panels Loaded in Uniaxial Compression", Composite Structures, 1997. **37**(2): p. 253-267.

66. Falzon, B.G., "The Behaviour of Damage Tolerant Hat-Stiffened Composite Panels Loaded in Uniaxial Compression", Composites Part A: Applied Science and Manufacturing, 2001. **32**(9): p. 1255-1262.

67. Baker, D.J. and Rousseau, C.Q., "Design and Evaluation of a Bolted Joint for a Discrete Carbon-Epoxy Rod-Reinforced Hat Section. 1996, National Aeronautics and Space Administration: Virginia.
68. Lyson, D.J., J. Naval Science, 1979. **5**: p. 182.
69. Hall, D.J. and Robson, B.L. Composites, 1984. **15**: p. 266.
70. Smith, C.S., "Structural Problems in the Design of GRP Ships. in Proceedings of the Symposium on GRP Ship Construction", 1972. London: RINA.
71. Harrhy, J. "Structural Design of Single Skin Glass Reinforced Plastic Ships", in Proceedings of the Symposium on GRP Ship Construction. 1972. London: Rina.
72. Harris, A.J., "The Hunt Class Mine Countermeasures Vessels", Trans RINA, 1980. **122**: p. 485.
73. Pitts, E.C., "Experience with the Design of GRP MCM Vessels", in RINA Symposium on Mine Warfare Vessels and Systems. 1984. London.
74. Chalmers, D.W., Osborn, R.J. and Bunney. A., "Hull Construction of MCMV's in the United Kingdom", in RINA Symposium on Mine Warfare Vessels and Systems. 1984. London.
75. Norwood, L., Caulier, C. and S. Bader., "Testing the Effectiveness of Tough Resin Systems for Improving the Structural Performance of Joints in GRP Ships" in Nautical Construction with Composite Materials. 1992. Paris (France): Service de la Documentation et des Publications (S.D.P.).
76. Green, A.K. and Bowyer, W.H., "The Testing and Analysis of Novel Top-Hat Stiffener Fabrication Methods for use in GRP Ships", I.H. Marshall, Editor. 1981, Fulmer Research Laboratories: Slough. p. 182-201.
77. Green, A.K. and Bowyer, W.H. "The development of improved attachment methods for stiffening frames on large GRP panels. Composites", 1981. **12**(1): p. 49-55.
78. Systems, S., Resin Properties for Composite Materials. 2005, http://www.azom.com/Suppliers.asp?SupplierID=221: Isle of Wight.
79. Yunus, S.M. and Kohnke, P.C., "An Efficient Through-Thickness Integration Scheme in an Unlimited Layer Doubly Curved Isoparametric Composite Shell Element", International Journal for Numerical Methods in Engineering, 1989. **28**: p. 2777-2793.

80. Hawkins, G.L., "The Behaviour of Bonded Out-of-Plane Joints in Fibre Reinforced Plastics Structures", in Faculty of Engineering and Applied Science. 1995, University of Southampton: Southampton.

81. Qiao, P., Davalos, J.F. and Barbero, E.J., "Design Optimization of Fibre Reinforced Plastic Composite Shapes", 1996, West Virginia University: West Virginia.

82. Padhi, G.S., Shenoi, R.A., Moy, S.S.J. and Hawkins, G.L., "Progressive Failure and Ultimate Collapse of Laminated Composite Plates in Bending", Composite Structures, 1998. **40**(3-4): p. 277-291.

83. Feng, Z.N., Allen, H.G., and Moy, S.S.J., "Theoretical and Experimental Investigation of Progressive Failure of Woven Composite Panels. Journal of Composite Materials", 1999. **33**(11).

84. Barbero, E., "Computer Aided Design Environment for Composites (CADEC)", 1998, West Virginia University: West Virginia.

85. ASTM Standards and Literature References for Composite Materials. 1990.

86. ANSYS 5.0 User manual volume IV, theory. Swanson Analysis Systems Inc. 1992.

87. Wilson. E.L., Taylor. L.R, Doherty, W.P., and Ghaboussi. J., "Incompatible Displacement Models", Numerical and Computer Methods in Structural Mechanics, Eds. by Fenves, S.J, Academic Press Inc. N.Y. and London pp:43-57, 1977.

Appendix A ENERGY ABSORPTION OF THE TOP HAT STIFFENERS

A.1 Introduction

The load/deflection curves of the failure test have been integrated to determine the energy absorption of each to allow comparison of work done to failure. The calculation performed within the framework of this study refers to the top hat stiffeners in chapter 4. The integration was calculated automatically in the popular design software AutoCAD.

A.2 Integration Results for Top Hat Stiffener Specimens

Two different types of top hat stiffeners which referred to as stiffeners A and B, have been tested under four point bending load. They were three specimens of each type (denominated 1, 2 and 3). Integration results from the load/deflection plots for each specimen are given Figures A1 to A6.

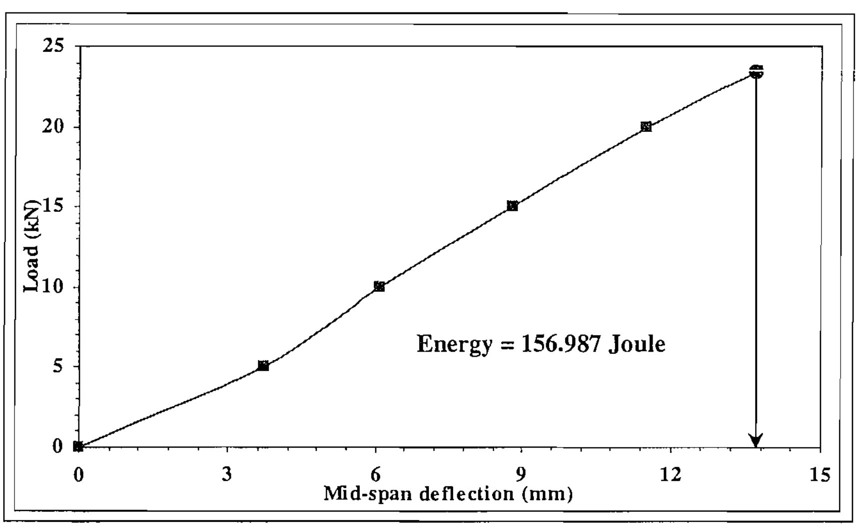

Figure A 1 Integration results for stiffener-A1

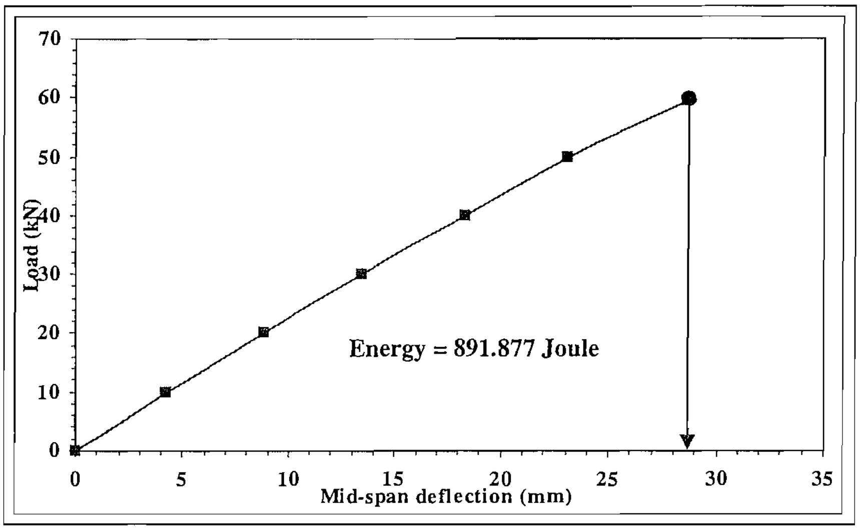

Figure A 2 Integration results for stiffener-A2

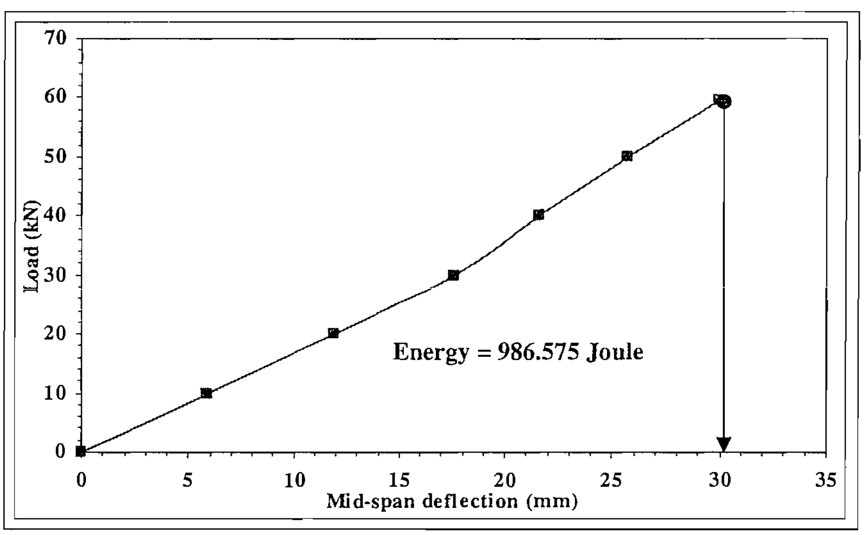

Figure A 3 Integration results for stiffener-A3

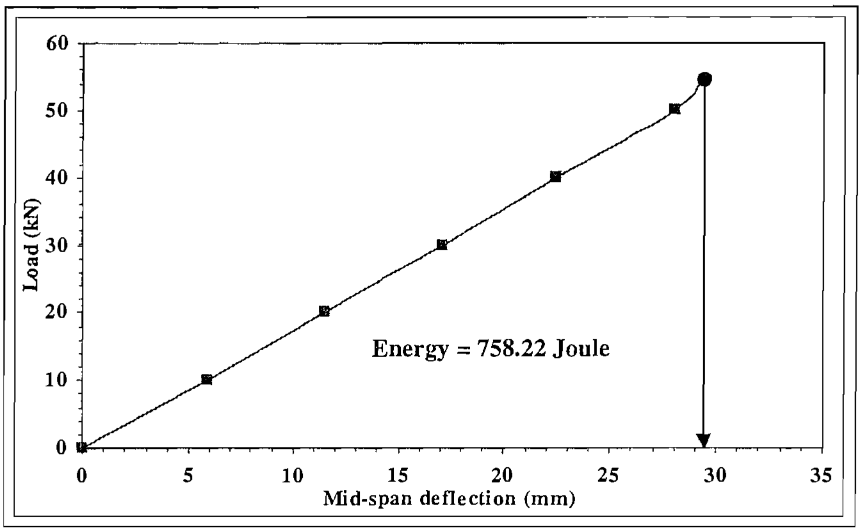

Figure A 4 Integration results for stiffener-B1

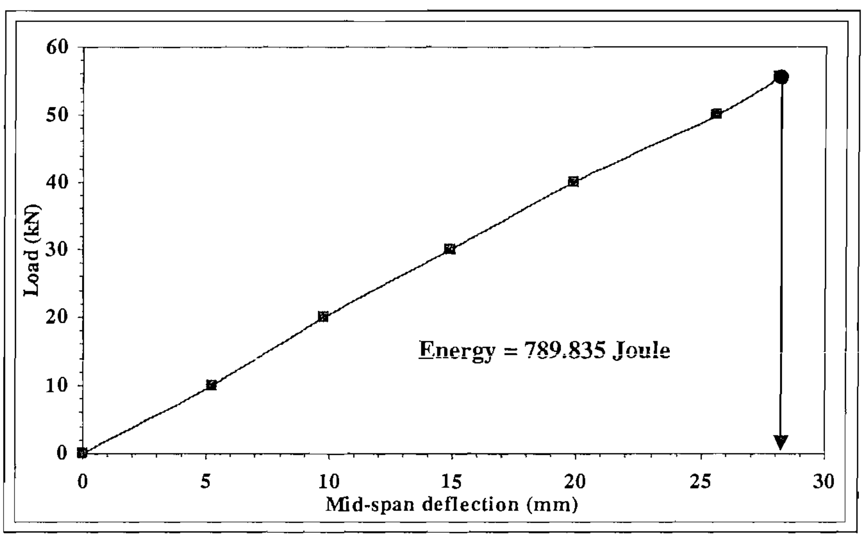

Figure A 5 Integration results for stiffener-B2

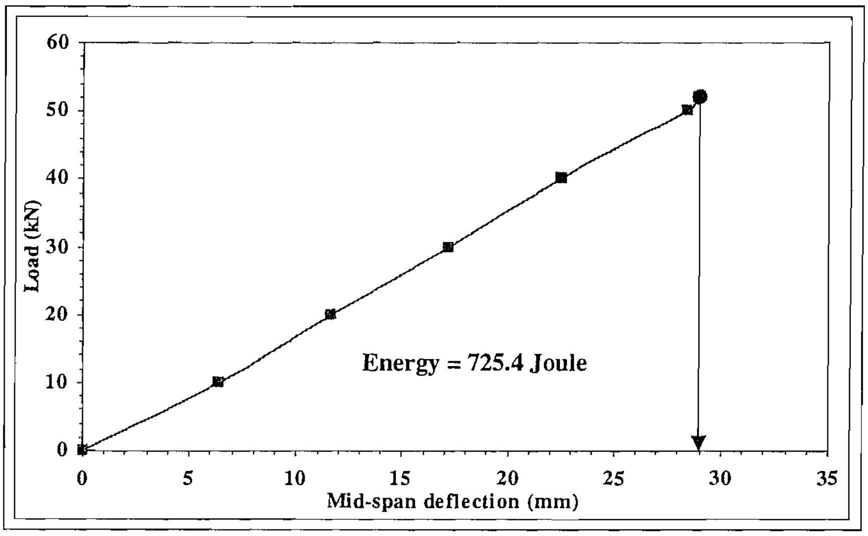

Figure A 6 Integration results for stiffener-B3

Appendix B MATERIAL CHARACTERISATION AND PROPERTIES

B.1 Introduction

Experiments on composite coupons can provide important information such as fibre content, overall stiffness and strength of composite. The laminated specimens were fabricated by the boatyard by using hand lay-up method. Experimental works were conducted to investigate the flexural stiffness and strength and fibre content of the laminated specimens. The material properties of the unidirectional layer and Bias layer were calculated by using Computer Aided Design Environment for Composites (CADEC) [84].

B.2 Bending Test

An Instron universal machine was used for the entire coupon test. They were four laminated specimens which are denominated laminate A,B,C and D. The lamination schemes for the specimens are given in Table B.1. The objective of static bending test is to determine the moduli of elasticity in two orthogonal directions of the composite specimens, E_x and E_y, both in flexural modes. The test is carried out as much in accordance as to ASTM standard D 790M [85]. *Standard test methods for flexural properties of unreinforced and reinforced plastics and electrical insulating materials [Metrics]*. The discrepancies in applying this standard in practise were mainly due to limitation on specimens and equipment, which will be described later. The standard provides two options of test set up, namely three-point and four-point bending. The former has been chosen because of its simplicity in equipment and execution. The test set up can be described as in Figure B.1.

The loading nose and supports are suggested cylindrical, with diameters of at least 6 mm for the loading nose and supports. For specimens with less than 3mm thickness, the diameter of loading nose could be up to 8 times the specimen thickness. For thicker specimens, the maximum loading nose diameter is 1.5 times the specimen thickness. In this test set up, the diameter of the loading nose and supports are 12.55 and 6.3 mm, respectively. The specimens comprise composite plates with thickness between 1.5 to 4.7 mm. Therefore, the rollers meet the standard recommendation.

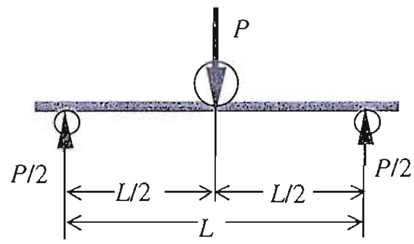

Figure B.1 Loading diagram of three-point bending test. L is the support span, P is the load

The standard recommends the following load-span to thickness ratio, 16, 32, 40 and 60. The latter is especially recommended for highly anisotropic specimens. Most of the specimens tested were of 16 ratio, with the rest were of higher ratio in order to see the effect of different span-to-thickness, or in other term, aspect ratio, particularly that it is suspected that lower ratio specimens give an inaccurate result due to the presence of shear deformation. This effect might be worse since three-point bending tests is used, which introduces shear stress in the entire specimen span. Dimensions for each specimen are presented in Table B.2 along with the corresponding result. Other suggested dimensions for specimens include the width and the overall specimen length.

The measurement is carried out on both the load, L, and deflection at the point of loading, δ. The three-point bending test set up allows the measurement of the two data directly from the test machine, that is the load is measured by a load cell placed between the machine support and the lower fixture, whilst the measured deflection is from the test machine reading of the movement of the cross head the leading to the loading nose.

Table B.1 Lay-up of the laminated specimens

Laminate	Reinforcement E-Glass	Resin Polyester	Accelerator	Young's Modulus (MPa)
A Hand lay-up	3 plies 600 g/m^2 CSM	Scott Bader 7959PA	Scott Bader Axo Butanox M50	6788
B Hand lay-up	3 plies 225/600 g/m^2 CSM/Bias	Scott Bader 7959PA	Scott Bader Axo Butanox M50	8000
C Hand lay-up	3 plies 600 g/m^2 woven rowing	Scott Bader 7959PA	Scott Bader Axo Butanox M50	14800
D Hand lay-up	6 plies 300 g/m^2 CSM	Scott Bader 489PA	Scott Bader Axo Butanox M50	8000

B.3 Bending Test Results

It is suggested that each set of experiment consist of at least 5 specimens. Moreover, specimens with higher thickness ratio (*a/h*) are preferable in order to minimise the contribution of transverse shear moduli, so that more accurate prediction the in-plane modulus of elasticity. The need for higher thickness ratio is even more so for highly anisotropic specimens. However, due to the limitation in material, the number of specimens and requirement of higher thickness ratio cannot be fulfilled. Only four specimens are used for each main orientation of specimen, therefore 8 for each specimen, with variation of thickness ratio. Table B.2 shows the variation of specimen dimensions and the corresponding result, the variation of which can be used as a comparison for the characterisation purposes.

B.4 Tensile Test

Coupons with dimensions of 30*300 mm (or shorter). All the test specimens were accurately measured for thickness and width at three points along the length. Before the test, all the equipment were set up and calibrated. The test set up can be described as in Figure B.2. The coupons have been tested until failure to investigate the ultimate tensile strength of the laminated specimens. The ultimate tensile strength values are listed in Table B.3. It can be seen from this table amongst the laminated specimens, laminate C (3 layers of 600 g/m^2 woven roving) has the biggest strength. Figure B.3 shows the failure photographs of the specimen.

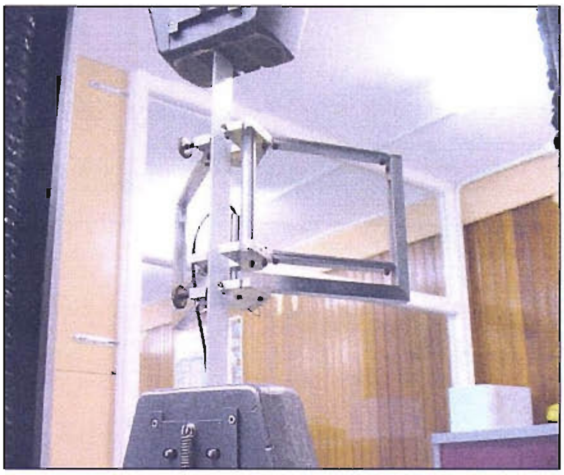

Figure B.2 Test set-up for a coupon test on a laminate A

Table B.2 Dimension of specimens and results of static bending tests, where h_{act}, w, L_{act} are measured thickness, width and length of each specimen, all in mm, and E is the modulus of elasticity, in MPa.

	Orientation 1					Orientation 2				
	Specimen	h_{act}	w_{act}	L_{act}	E	Specimen	h_{act}	w_{act}	L_{act}	E
Laminate A	11	3.812	9.75	**140**	6685	15	3.688	8.84	**140**	7406
	12	3.916	10.24	**140**	7037	16	3.594	13.24	**140**	6976
	13	3.766	10.19		8859	17	3.412	10.39		7555
	14	3.636	10.00	**150**	7253	18	3.124	8.34	**140**	8681
					7458					**7655**
				140					**140**	
				$\bar{E}$					$\bar{E}$	
Laminate B	21	2.814	23.95	**55**	7194	25	2.918	24.97	**55**	6208
	22	2.686	22.73	**55**	7389	26	3.007	25.28	**55**	6533
	23	2.865	24.38		6987	27	2.974	25.45		6535
	24	2.920	24.82	**55**	7517	28	2.952	22.27	**50**	8218
					7272					**6873**
				100					**180**	
				$\bar{E}$					$\bar{E}$	
Laminate C	31	1.590	21.6	55	14270	35	1.708	23.67	40	14858
	32	1.578	23.23	55	14779	36	1.680	23.52	40	14798
	33	1.482	23.26	55	15332	37	1.644	23.78	55	14476
	34	1.600	23.89	100	16351	38	1.632	25.28	75	16119
				$\bar{E}$	**14793**	39	1.648	25.09	75	17044
									$\bar{E}$	**14711**
Laminate D	41	1.528	27.77	*70*	7517	45	1.588	26.43	**120**	6199
	42	1.464	27.90	*70*	6965	46	1.500	24.91	**50**	5738
	43	1.312	26.73		6384	47	1.632	24.84		7332
	44	1.226	27.15	*70*	7452	48	1.522	24.81	**50**	6435
					7079					**6426**
				70					**56**	
				$\bar{E}$					$\bar{E}$	

Table B.3 Tensile test results of the composite

Laminate	Tensile Strength (MPa)
A	130
B	100
C	300
D	107

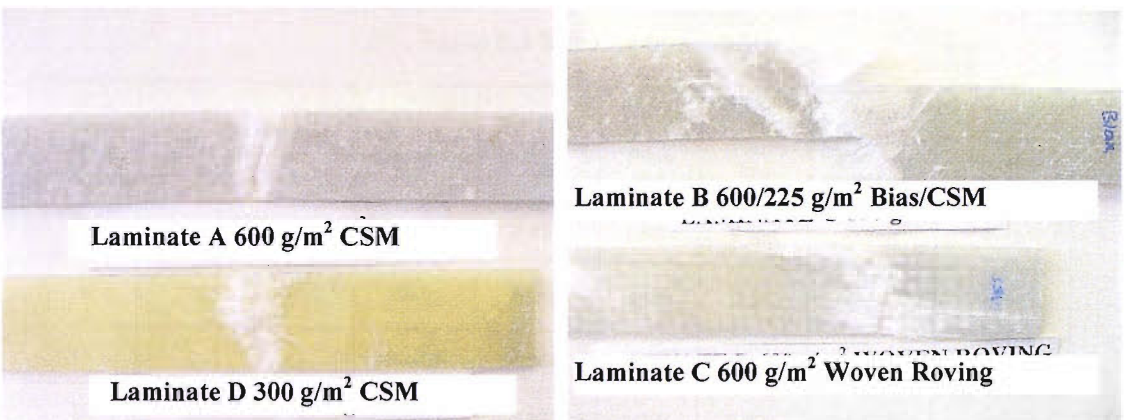

Figure B.3 The tested samples of laminates A,B,C and D

B.5 Burning Test Results

In order to obtain the detailed make-up of the composite materials, pieces were cut from coupons. For laminate A, B, C and D samples with dimensions of 30 mm × 50 mm were used. These were weighed, placed in crucibles, weighed again held for 4 hours in a muffle furnace at 550 C^0 and then weighed again. This established the weight of the resin lost during the burning process, in comparison with the weight of the original samples. Thus the fibre content by volume V_f and resin content by volume V_m can be calculated. In the calculation a nominal specific gravity of glass fibre 2.55 g/cm^3, orthopthalic resin 1.23 g/cm^3 and isopthalic resin 1.21 g/cm^3 were used.

- Laminate A is a 600 g/m^2 3-layer CSM is made of orthopthalic resin. The overall fibre content by volume (V_f) is 0.18.

- Laminate B is a made of 3 layers of 225/625 g/m^2 CSM/Bias with a orthopthalic resin. The overall fibre content by volume (V_f) is 0.33.
- Laminate C is a balanced 600 g/m^2 3-layer woven roving is made of orthopthalic resin. The fibres are aligned only placed in 0 and 90 degrees. It is assumed that in each layer, the weight of fibres in the warp direction is the same as that in the weft direction. The overall fibre content by volume (V_f) is 0.46.
- Laminate D is a 300 g/m^2 3-layer CSM is made of isopthalic resin. The overall fibre content by volume (V_f) is 0.19.

The details about burning test results are given in Table B.4.

Table B.4 Burning test results

Laminate ID	Material ID	Geometry (mmxmm)	Weight of Composite (gr)	Weight of Fibre (gr)	Weight of Resin lost (gr)	Fibre Weight Fraction (W_f)	Fibre Volume Fraction (V_f)
A	3 layers 600 g/m^2 CSM	30x50	8.624	2.693	5.931	0.312	0.18
B	3 layers 225/600 g/m^2 CSM/Bias	30x50	6.229	3.169	3.06	0.509	0.33
C	3 layers 600 g/m^2 WR	30x50	4.056	2.587	1.468	0.638	0.46
D	3 layers 300 g/m^2 CSM	30x50	3.953	1.328	2.625	0.336	0.19

B.6 Elastic Properties of Unidirectional and Bias Layer

Laminated composite containing stacks of unidirectional laminae are one of the most commonly used composite forms. Under the assumption that fibres in the composite are regularly spaced and aligned in the matrix. Various theoretical models were developed to calculate material properties. CADEC software was used to calculate the GRP unidirectional layer for a 0.3 fibre content. Based on this data GRP Bias layer was discretized the unidirectional layers and elastic properties of the laminate calculated based on the CLPT theory. For the Unidirectional layer it was assumed E_y=E_z and G_{xy}=G_{xz}. Results are given in Table B.5.

Table B.5 Elastic Material Properties

	GRP Laminates (V_f=0.3)	
	Unidirectional	**Biaxial**
E_x (GPa)	24.6	9.9
E_y (GPa)	7.3	9.9
G_{xy} (GPa)	2.3	6.6
ν_{xy}	0.395	0.494

Appendix C BENDING OF BEAMS

C.1 Elastic Bending of Beams

When a 'beam' experiences a bending moment it will change its shape and internal stresses (forces) will be developed. The Figure C.1 illustrates the shape change of elements of a beam in bending. Note that the material is in compression on the inside of the curve and tension on the outside of the curve, and that transverse planes in the material remain parallel to the radius during bending

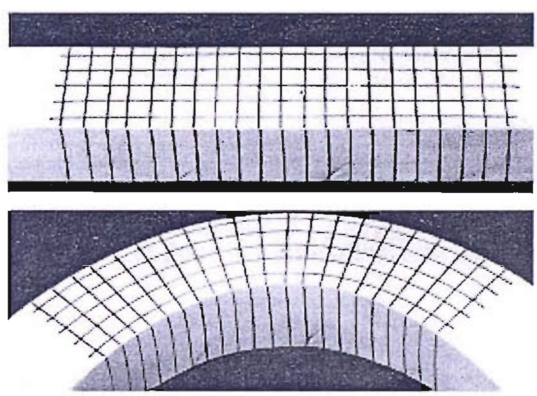

Figure C.1 Beam bending

The basic differential equation used for most of the beam bending problem is

$$EI\frac{d^2y}{dx^2} = M \tag{C.1}$$

and

$$\frac{dy}{dx} = \int\frac{M}{EI}dx + A \tag{C.2}$$

$$y = \iint\left[\frac{M}{EI}dx\right]dx + Ax + B \tag{C.3}$$

Where A and B are constants of integration evaluated from known conditions of slope and deflection for a particular of x.

C.2 Four Point Bending Case

The pure bending shown in the diagram can be produced by applying four forces to the beam, two of opposite direction at each end. This configuration is known as 'four-point bending' and produces a uniform bending moment over the centre section of the beam as illustrated in Figure C.2.

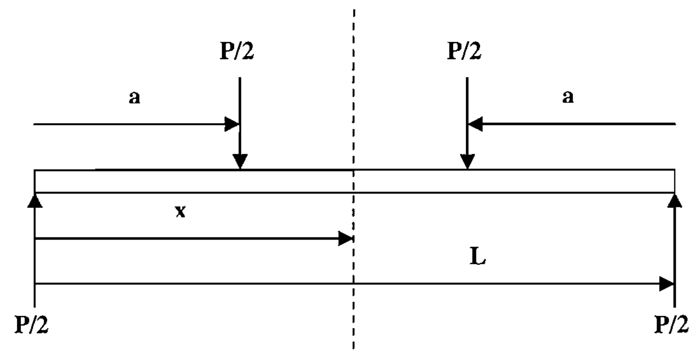

Figure C.2 Four point bending configuration

deflection at any point between the inner loading points is given by

$$\delta = \frac{Pa\left[3Lx - 3x^2 - a^2\right]}{12EI} \tag{C.4}$$

Putting x=L/2 for maximum deflection becomes

$$\delta = \frac{Pa\left[3L^2 - 4a^2\right]}{48EI} \tag{C.5}$$

C.3 Bending Stress

Under four-point bending loading the maximum bending stresses can be obtained by beam theory

$$\sigma_x = \frac{M}{I} y \tag{C.6}$$

C.4 Shear Stress

From the shear force Q acting on a beam cross-section the shear stress τ is obtained

$$\tau = \frac{Q}{It} \int \bar{y} dA \tag{C.7}$$

Where:

M - applied bending moment, Nm

I - second moment of area, m^4

σ_x - normal stress, Nm^{-2}

y - distance from neutral axis to point in question, m

E - Young's modulus, Nm^{-2}

τ - Shear stress Nm^{-2}

Q - Shear force N

t - thickness of the cross-section mm

$\int \bar{y} dA$ - first moment about the neutral axis of the area above the level where the shear stress is required mm^3

Under four-point bending loading the shear force and moment diagram is given in Figure C.3

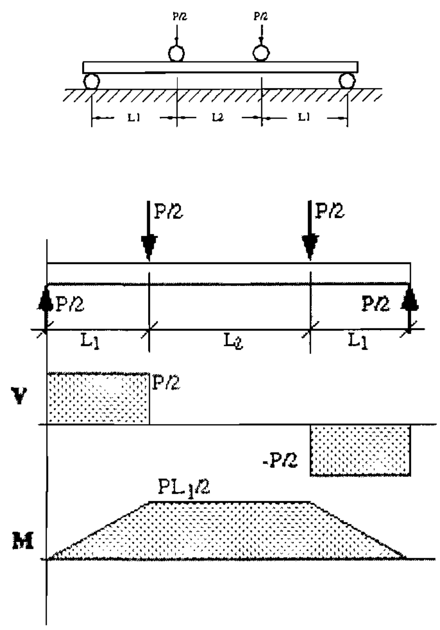

Figure C.3 Shear force and bending moment diagram

C.5 Calculation of I value for Stiffener A

Calculation of the second moment of area of top hat stiffener is presented in a tabular form is shown at below. An assumed neutral axis is taken near the mid-depth which is shown at Figure C.4

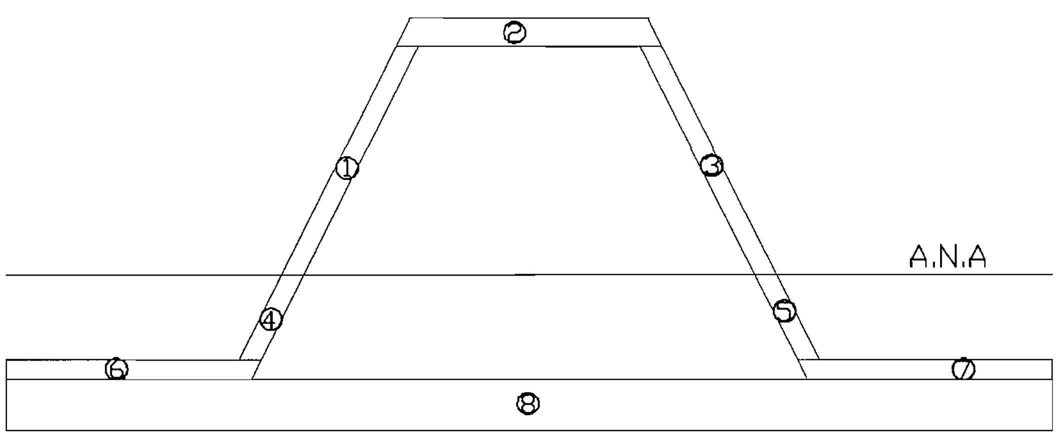

Figure C.4 Assumed neutral axis for top hat stiffener

Table C.1 Calculation of I value in tabular form

1	2	3	4	5	6	7
Item	**A (mm^2)**	**h (mm)**	**A*h (mm^3)**	**A*h^2 (mm^4)**	**k^2 (mm^2)**	**A*k^2 (mm^4)**
Each item above A.N.A						
Totals above A.N.A	ΣA_1		$\Sigma A_1 h_1$	$\Sigma A_1 h_1^2$		$\Sigma A_1 k_1^2$
Each item above A.N.A						
Totals above A.N.A	ΣA_2		$\Sigma A_2 h_2$	$\Sigma A_2 h_2^2$		$\Sigma A_2 k_2^2$

Where:

A = cross-sectional area of item,

h = distance from A.N.A

k = radius of gyration of the structural element about its own NA.

Distance of true N.A. above A.N.A $d = \dfrac{\sum A_1 h_1 + \sum A_2 h_2}{\sum A_1 + \sum A_2}$ (C.8)

Second moment of area about true NA

$$I = \sum A_1 h_1^2 + \sum A_2 h_2^2 + \sum A_1 k_1^2 + \sum A_2 k_2^2 - \left(\sum A_1 + \sum A_2\right) d^2 \quad \text{(C.9)}$$

Table C.2 Second moment of area calculation

	A (mm^2)	h1 (mm)	A*h1 (mm^3)	A*h1^2 (mm^4)	k1^2 (mm^2)	Ak1^2 (mm^4)
	200.86	19.96	4009.17	80022.95	132.67	26647.59
	369.30	43.40	16027.62	695598.71	27.02	9978.57
	200.86	19.96	4009.17	80022.95	132.67	26647.59
Totals above A.N.A	771.02		24045.95	855644.60		63273.76

	A (mm^2)	h2 (mm)	A*h2 (mm^3)	A*h1^2 (mm^4)	k1^2 (mm^2)	A*k1^2 (mm^4)
	307.64	15.28	4700.74	71827.29	77.88	23958.10
	505.00	32.87	16599.35	545620.63	1.69	852.19
	2667.25	40.75	108690.44	4429135.33	10.74	28633.48
Totals below A.N.A	3479.89		129990.53	5046583.26		53443.78

C.6 Results

Distance of true N.A. above A.N.A $d = -24.92$

N.A from base = 21.5 mm (Analytical)

N.A from base = 21.48 mm (ANSYS)

Second moment of area $I_y = 3378510\ mm^4$ (Analytical)

Second moment of area $I_y = 3354710\ mm^4$ (ANSYS)

Young modulus of Stiffener $E = 8000\ Nmm^{-2}$

Load $P = 29750$ N

Span of Beam $L = 890$ mm

$a = 245$ mm

The maximum deflection $\delta = 24.3$ mm (Analytical)

The maximum deflection $\delta = 27.9$ mm (ANSYS)

The maximum deflection $\delta = 28.6$ mm (Experimental)

Bending moment M = 7288750 Nmm

Distance between crown and NA y = 71.37 mm

Bending Stress σ_x = 155.5 Nmm^{-2} (Analytical)

Bending Stress σ_x = 160.3 Nmm^{-2} (ANSYS)

first moment about the neutral axis

of the area above the level where the

shear stress is required mm^3 $\int \bar{y} dA$ = 46371.6 mm^3

thickness of the cross-section t = 9 mm

Maximum shear stress τ_{xy} = 45.8 Nmm^{-2} (Analytical at Neutral axis=21.45 mm from the base)

Maximum shear stress τ_{xy} = 47.2 Nmm^{-2} (ANSYS maximum shear stress occurred 19.9 mm from base)

In a similar manner I value was calculated for stiffener B

Second moment of area I_y = 2340341 mm^4 (Analytical)

Second moment of area I_y = 2337400 mm^4 (ANSYS)

Young modulus of Stiffener E = 11000 Nmm^{-2}

C.7 Comparison of Different Element Types

Three elements with composite capabilities are available within ANSYS, two eight node shell elements (SHELL91 and SHELL99) and one eight node solid element (SOLID46). As mentioned in the chapter 5 shell element formulation is not suitable to model the out-of-plane joint problem as some stacking in the through thickness direction is always required and using Solid46 element causes inaccurate through thickness stress distributions between layers (through-thickness stress is calculated from the nodal forces and the effective material properties making it constant through the thickness) which does not allow for the introduction of delaminations between layers of overlaminate in to the model. Therefore model containing one element per layer generated here by using SOLID45 elements. This allows improving internal stress distributions most importantly in the through-thickness direction. Two problems were considered to compare the results from simple 2-D elastic beam theory and those obtained from the SOLID45 elements.

A beam aspect ratio 12:1 made up isotropic in three point bending. The FE results were compared to analytical solution and listed in Table C.3. The co-ordinate system for FE model is given in Figure C.5. The location for values of deflection and stresses are given at below

δ_{FE} : (a=120,b/2=5,h=0) At the mid-point of the beam

$\delta_{ANALYTICAL}$: (a,b,h=0) At the mid-point of the beam

$\sigma_{x\ FE}$: (a/2=60,b/2=5,h=12)

$\sigma_{x\ ANALYTICAL}$: (a,b,h=12)

$\tau_{xy\ FE}$: (a,b=0,h=6)

$\tau_{xy\ ANALYTICAL}$: (a,b=0,h=6)

Table C.3 Comparison between FE and analytical results in three point bending

	SOLID45	BEAM THEORY
Deflection δ (mm)	0.235	0.242
Max.Stress σ_x (MPa)	10.18	10
Shear Stress τ_{xy} (MPa)	0.584	0.5

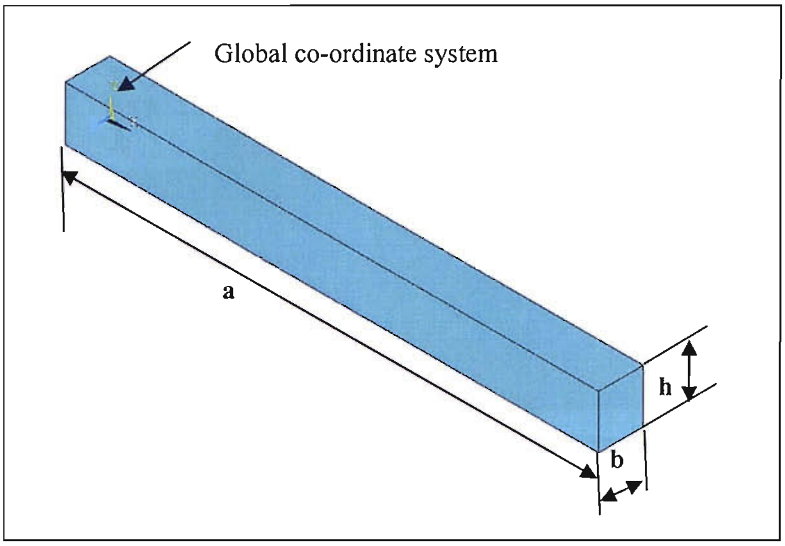

Figure C.5 Co-ordinate system for rectangular section beam

Top hat stiffener A (a geometry defined in Chapter 4) made up assumed isotropic material properties in four point bending. The FE results were compared to analytical solution and listed in Table C.4. The co-ordinate system for FE model is given in Figure C.6. The location for values of deflection and stresses are given at below.

δ_{FE} : (a=625,b=117.5,h=92.85) At the mid-point of the stiffener

$\delta_{ANALYTICAL}$: (a,b,h=92.85) At the mid-point of the stiffener

$\sigma_{x\ FE}$: (a=625,b=117.5,h=92.85) At the mid-point of the stiffener (on the crown)

$\sigma_{x\ ANALYTICAL}$: (a,b,h=92.85) At the mid-point of the stiffener (on the crown)

$\tau_{xy\ FE}$: (a=278,b=54.29,h=19.99) In the web of the stiffener

$\tau_{xy\ ANALYTICAL}$: (a,b,h=21.48) In the web of the stiffener

Table C.4 Comparison between FE and analytical solution in four point bending

	FE (SOLID45)	**BEAM THEORY**
Deflection δ (mm)	**27.3**	**24.3**
Max. Stress σ_x (MPa)	**156.2**	**155.5**
Shear Stress τ_{xy} (MPa)	**47.2**	**45.8**

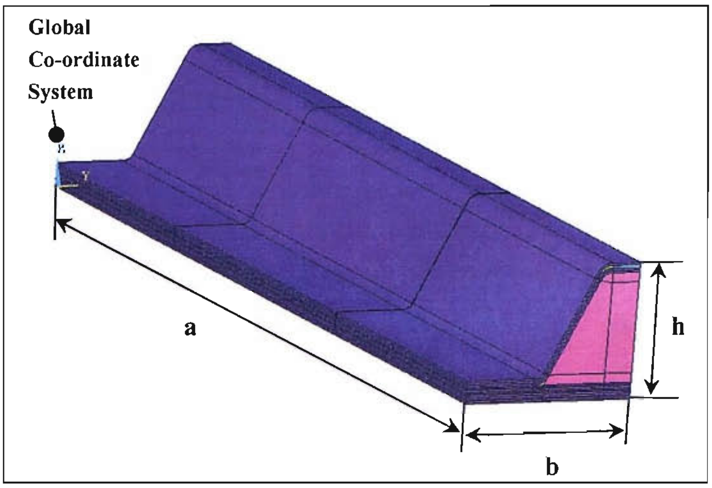

Figure C.6 Geometry of top hat stiffener

The results above indicate that correlation between FE results and 2-D elastic beam theory very close in the case of rectangular section beam compared to hat section beam. This might be due to 2-D elastic beam theory neglects the shear deflection and three dimensional effect which is apparent when the considering complex cross-section.

C.8 SOLID45 (3-D Isoparametric Solid Element)

SOLID45 is used for the three-dimensional modelling of solid structures. The element is defined by eight nodes having three degrees of freedom at each node: translations in the nodal x, y, and z directions. The geometry, node locations, and the coordinate system for this element are shown in Figure C.7. The element is defined by eight nodes and the orthotropic material properties. Orthotropic material directions correspond to the element coordinate directions. The element coordinate system orientation is as described in coordinate systems [86].

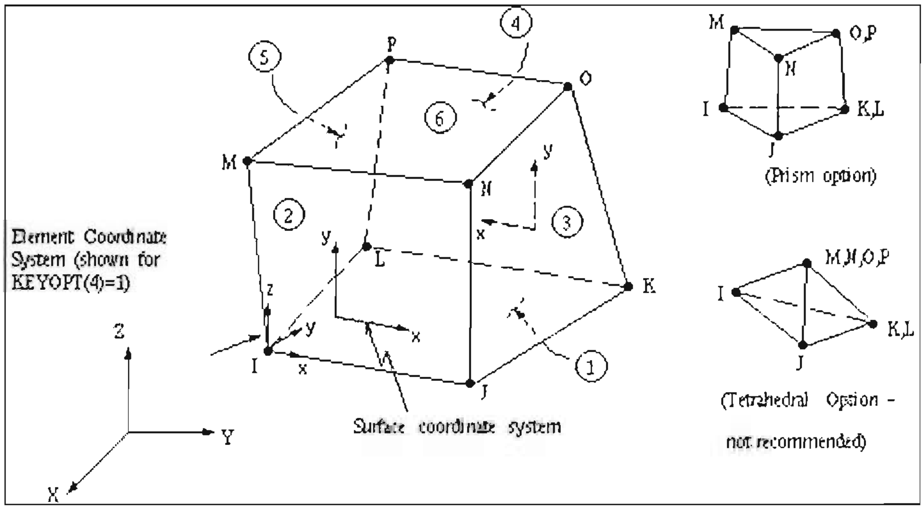

Figure C.7 Geometry and node location for SOLID45 elements

The element has plasticity, creep, swelling, stress stiffening, large deflection, and large strain capabilities.

C.8.1 Stress-Strain Relationship

This section discusses material relationship for linear materials. The stress is related the strain by:

$$\{\sigma\}=[D](\{\varepsilon\}-\{\varepsilon^{th}\}) \tag{C.10}$$

$\{\sigma\}=$ stress vector $=[\sigma_x,\sigma_y,\sigma_z,\sigma_{xy},\sigma_{yz},\sigma_{xz}]^T$

$[D]$=elasticity matrix

$\{\varepsilon\}=$ strain vector $[\varepsilon_x,\varepsilon_y,\varepsilon_z,\varepsilon_{xy},\varepsilon_{yz},\varepsilon_{xz}]^T$

$\{\varepsilon^{th}\}=$ thermal strain vector

Equation B.1 may also be inverted to:

$$\{\varepsilon\}=\{\varepsilon^{th}\}+[D]^{-1}\{\sigma\} \tag{C.11}$$

For the 3-D case, the thermal strain vector is:

$$\{\varepsilon^{th}\}=\Delta T[\alpha_x,\alpha_y,\alpha_z,0,0,0]^T \tag{C.12}$$

$[D]^{-1}$ is "column normalized" format, is:

$$[D]^{-1} = \begin{bmatrix} 1/E_x & -\nu_{xy}/E_y & -\nu_{xz}/E_z & 0 & 0 & 0 \\ -\nu_{yx}/E_x & 1/E_y & -\nu_{yz}/E_z & 0 & 0 & 0 \\ -\nu_{zx}/E_x & -\nu_{zy}/E_y & 1/E_z & 0 & 0 & 0 \\ 0 & 0 & 0 & 1/G_{xy} & 0 & 0 \\ 0 & 0 & 0 & 0 & 1/G_{yz} & 0 \\ 0 & 0 & 0 & 0 & 0 & 1/G_{xz} \end{bmatrix} \tag{C.13}$$

E_x= Young's modulus in the x direction

ν_{xy} =Poisson's ratio relating ε_x to σ_y / E_y

The $[D]^{-1}$ matrix is presumed to be symmetric, so for orthotrophic materials

$$\frac{\nu_{yx}}{E_x} = \frac{\nu_{xy}}{E_y}, \quad \frac{\nu_{zx}}{E_x} = \frac{\nu_{xz}}{E_z}, \text{ and } \quad \frac{\nu_{zy}}{E_y} = \frac{\nu_{yz}}{E_z} \tag{C.14}$$

Expanding the equations C.11 with equations C.12, C.13 and C.14 and writing out the six equations explicitly,

$$\varepsilon_x = \alpha_x \Delta T + \frac{\sigma_x}{E_x} - \frac{\nu_{xy}\sigma_y}{E_y} - \frac{\nu_{xz}\sigma_z}{E_z} \tag{C.15}$$

$$\varepsilon_y = \alpha_y \Delta T + \frac{\sigma_y}{E_y} - \frac{\nu_{xy}\sigma_x}{E_y} - \frac{\nu_{yz}\sigma_z}{E_z} \tag{C.16}$$

$$\varepsilon_z = \alpha_z \Delta T + \frac{\sigma_z}{E_z} - \frac{\nu_{xz}\sigma_x}{E_z} - \frac{\nu_{yz}\sigma_y}{E_z} \tag{C.17}$$

$$\varepsilon_{xy} = \frac{\sigma_{xy}}{G_{xy}} \tag{C.18}$$

$$\varepsilon_{yz} = \frac{\sigma_{yz}}{G_{yz}} \tag{C.19}$$

$$\varepsilon_{xz} = \frac{\sigma_{xz}}{G_{xz}} \tag{C.20}$$

where typical terms are

ε_x = direct strain in x direction

ε_{xy} = shear strain in the x-y plane

σ_x = direct stress in the x direction

σ_{xy} = shear stress on the x-y plane

Alternatively equation C.10 may be expanded by first inverting the equation C.13 and then combining that result with equations C.12 and C.14

$$\sigma_x = \frac{E_x}{h}\left(1-(\nu_{yz})^2\frac{E_y}{E_z}\right)(\varepsilon_x-\alpha_x\Delta T)+\frac{E_x}{h}\left(\nu_{xy}+\nu_{xz}\nu_{yz}\frac{E_y}{E_z}\right)(\varepsilon_y-\alpha_y\Delta T) + \frac{E_x}{h}\left(\nu_{xz}+\nu_{xy}\nu_{yz}\frac{E_y}{E_z}\right)(\varepsilon_z-\alpha_z\Delta T) \tag{C.21}$$

$$\sigma_y = \frac{E_x}{h}\left(\nu_{xy}+\nu_{xz}\nu_{yz}\frac{E_y}{E_z}\right)(\varepsilon_x-\alpha_x\Delta T)+\frac{E_y}{h}\left(1-(\nu_{xz})^2\frac{E_x}{E_z}\right)(\varepsilon_y-\alpha_y\Delta T) + \frac{E_y}{h}\left(\nu_{yz}+\nu_{xy}\nu_{xz}\frac{E_x}{E_y}\right)(\varepsilon_z-\alpha_z\Delta T) \tag{C.22}$$

$$\sigma_z = \frac{E_x}{h}(\nu_{xz}+\nu_{xz}\nu_{yz})(\varepsilon_x-\alpha_x\Delta T)+\frac{E_y}{h}\left(\nu_{yz}+\nu_{xy}\nu_{xz}\frac{E_x}{E_y}\right)(\varepsilon_y-\alpha_y\Delta T) + \frac{E_z}{h}\left(1-(\nu_{xy})^2\frac{E_x}{E_y}\right)(\varepsilon_z-\alpha_z\Delta T) \tag{C.23}$$

$$\sigma_{xy} = G_{xy}\varepsilon_{xy} \tag{C.24}$$

$$\sigma_{yz} = G_{yz}\varepsilon_{yz} \tag{C.25}$$

$$\sigma_{xz} = G_{xz}\varepsilon_{xz} \tag{C.26}$$

where:

$$h = 1-(\nu_{xy})^2\frac{E_x}{E_y}-(\nu_{yz})^2\frac{E_y}{E_z}-(\nu_{xz})^2\frac{E_x}{E_z}-2\nu_{xy}\nu_{yz}\nu_{xz}\frac{E_x}{E_z} \tag{C.27}$$

C.8.2 Derivation of Structural Matrices

The principal of virtual work states that a virtual (very small) change of the internal stress energy must be offset by an identical change in external work due to the applied loads or:

$$\delta U = \delta V \tag{C.28}$$

where:

U = Strain energy $U_1 + U_2$

V = External work $V_1 + V_2 + V_3$

δ = Virtual operator

The virtual energy is

$$\delta U_1 = \int_{vol} \{\delta \varepsilon\}^T \{\sigma\} d(vol) \tag{C.29}$$

where:

$\{\varepsilon\}$ = strain vector

$\{\sigma\}$ = stress vector

vol = volume element

Continuation the derivation assuming linear materials and geometry, equations C.10 and C.29 are combined to give:

$$\delta U_1 = \int_{vol} \left(\{\delta \varepsilon\}^T [D]\{\varepsilon\} - \{\delta \varepsilon\}^T [D]\{\varepsilon^{th}\}\right) d(vol) \tag{C.30}$$

The strains may be related to the nodal displacement by:

$$\{\varepsilon\} = [B]\{u\} \tag{C.31}$$

where

$[B]$ = strain-displacement matrix, based on the element shape functions

$\{u\}$ = nodal displacement vector

Combining equation C.30 with equation C.31:

$$\delta U_1 = \{\delta u\}^T \int_{vol} [B]^T [D][B] d(vol)\{u\} - \{\delta u\}^T \int_{vol} [B]^T [D]\{\varepsilon^{th}\} d(vol) \tag{C.32}$$

Another form of virtual strain energy is when a surface moves against a distributed resistance, as in foundation stiffness. This may be written as:

$$\delta U_2 = \int_{area_f} \{\delta w_n\}^T \{\sigma\} d(area_f) \tag{C.33}$$

where

$\{w_n\}$ = motion normal to the surface

$\{\sigma\}$ = stress carried by the surface

$area_f$ = area of the distributed resistance

Both $\{w_n\}$ and $\{\sigma\}$ will usually have only one non-zero component. The point-wise normal displacement is related to the nodal displacement by:

$$\{w_n\}=[N_n]\{u\} \tag{C.34}$$

where:

$[N_n]$ = matrix of shape functions for normal motions at the surface

The stress, $\{\sigma\}=k\{w_n\}$ (C.35)

Where k = the foundation stiffness in units of force per length per unit area. Combining equations C.33 through C.35 and assuming that k is constant over the area ,

$$\delta U_2=\{\delta u\}^T k \int_{area_f}[N_n]^T[N_n]d(area_f)\{u\} \tag{C.36}$$

Next the external virtual work will be considered. The inertial effects are given:

$$\delta V_1=-\int_{vol}\{\delta w\}^T\frac{\{F^a\}}{vol}d(vol) \tag{C.37}$$

where

$\{w\}$ = vector of displacement of a general point

$\{F^a\}$ = Acceleration (D'Alembert) force vector

According to the Newton's second law

$$\frac{[F^a]}{vol}=\rho\frac{\partial^2}{\partial t^2}\{w\} \tag{C.38}$$

where: ρ = density and t = time

The displacements within the element are related to the nodal displacements by:

$$\{w\} = [N]\{u\} \tag{C.39}$$

where [N] matrix of shape functions. Combining the equations C.28, C.29 and C.30 and assuming that ρ is constant over the volume,

$$\delta V_1 = -\{\delta u\}^T \rho \int_{vol} [N]^T [N] d(vol) \frac{\partial^2}{\partial t^2}\{u\} \tag{C.40}$$

The pressure force vector formulation starts with:

$$\delta V_2 = \{\delta u\}^T \int_{area_p} [N_n]^T \{P\} d(area_p) \tag{C.41}$$

{P}= Applied pressure vector

$area_p$ = area over which pressure acts

Combining the equations C.39 and C.41,

$$\delta V_2 = \{\delta u\}^T \int_{area_p} [N_n]^T \{P\} d\{area_p\} \tag{C.42}$$

Nodal forces applied to the element can be accounted for by:

$$\delta V_3 = \{\delta u\}^T \{F_e^{nd}\} \tag{C.43}$$

where $\{F_e^{nd}\}$ = nodal forces applied to the element

All material properties for stress analysis elements are evaluated at the average temperature of each element. Finally, equations C.28, C.32, C.36, C.40, C.42 and C.43 may be combined to give:

$$\begin{aligned} &\{\delta u\}^T \int_{vol} [B]^T [D][B] d(vol)\{u\} - \{\delta u\}^T \int_{vol} [B]^T [D]\{\varepsilon^{th}\} d(vol) \\ &+ \{\delta u\}^T k \int_{area_f} [N_n]^T [N_u] d(area_f)\{u\} \\ &= -\{\delta u\}^T \rho \int_{vol} [N]^T [N] d(vol) \frac{\partial^2}{\partial t^2}\{u\} + \{\delta u\}^T \int_{area_p} [N]^T \{P\} d(area_p) + \{\delta u\}^T \{F_e^{nd}\} \end{aligned} \tag{C.44}$$

Nothing that the $\{\delta u\}^T$ vector is a set of arbitrary virtual displacements common in all of the above terms the condition required to satisfy equation C.44 reduced to

$$([K_e] + [K_e^f])\{u\} - \{F_e^{th}\} = [M_e]\{\ddot{u}\} + \{F_e^{pr}\} + \{F_e^{nd}\} \tag{C.45}$$

where

$[K_e] = \int_{vol} [B]^T [D][B] d(vol)$ = element stiffness matrix

$[K_e^f] = k \int_{area_f} [N_n]^T [N_n] d(area_f)$ = element foundation stiffness matrix

$[F_e^{th}] = \int_{vol} [B]^T [D] \{\varepsilon^{th}\} d(vol)$ = element thermal load vector

$[M_e] = \rho \int_{vol} [N]^T [N] d(vol)$ = element mass matrix

$\{\ddot{u}\} = \frac{\partial^2}{\partial t^2}\{u\}$ = acceleration vector (such as gravity effects)

$\{F_e^{pr}\} = \int_{area_p} [N_n]^T [P] d(area_p)$ = element pressure vector

Equation C.45 represents the equilibrium equation on a one element basis

C.8.3 Shape Functions

The SOLID45 element [29,87] is in three dimensional form, and has a linear displacement function (to which extra quadratic shape functions can be added) which is the same in all orthogonal directions. The shape function for SOLID45 8 node brick elements with extra shape functions as shown at below

$$u = \frac{1}{8}\begin{pmatrix} u_I(1-s)(1-t)(1-r) + u_J(1+s)(1-t)(1-r) \\ + u_K(1+s)(1+t)(1-r) + u_L(1-s)(1+t)(1-r) \\ + u_M(1-s)(1-t)(1+r) + u_N(1+s)(1-t)(1+r) \\ + u_O(1+s)(1+t)(1+r) + u_P(1-s)(1+t)(1+r) \end{pmatrix} \tag{C.46}$$
$$+ u_1(1-s^2) + u_2(1-t^2) + u_3(1-r^2)$$

$v = \frac{1}{8}\left(v_I(1-s)...\right)$ analogous to u

$w = \frac{1}{8}\left(w_I(1-s)...\right)$ analogous to u

C.8.4 Structural Strain and Stress Evaluations

The element integration point strains and stresses are computed by combining the equations C.10 and C.31 to get:

$$\{\varepsilon^{el}\}=[B]\{u\}-\{\varepsilon^{th}\}$$

$$\{\sigma\}=[D]\{\varepsilon^{el}\}$$

where:

$\{\varepsilon^{el}\}$= strains that cause stresses

$[B]$ = strain-displacement matrix, evaluated at integration point

$\{u\}$ = nodal displacement vector

$\{\varepsilon^{th}\}$= thermal strain vector

$\{\sigma\}$ = stress vector = $[\sigma_x, \sigma_y, \sigma_z, \sigma_{xy}, \sigma_{yz}, \sigma_{xz}]^T$

$[D]$ = elasticity matrix

C.9 Sensitivity study on support span

In the cases of where the difference between stiffness of the FE structural model is significantly large a sensitivity study has been carried out to account for these discrepancies.

C.10 Effect of Support on Stiffness of Beams

The support span has effect on FE model stiffness. A sensitivity study has been carried out to account for the difference in the stiffness of the FE model and the tested specimen. Two different FE model have been investigated in different three support span under four point bending loading. Top hat composite beam panel were modelled by using SHELL99 & SOLID95 and SOLID45 elements available within the ANSYS and those results compared with results from Beam theory for maximum deflection. The geometry of wooden support and three support spans are shown in Figures C.8 and C.9. The results of this study are given Table C.6.

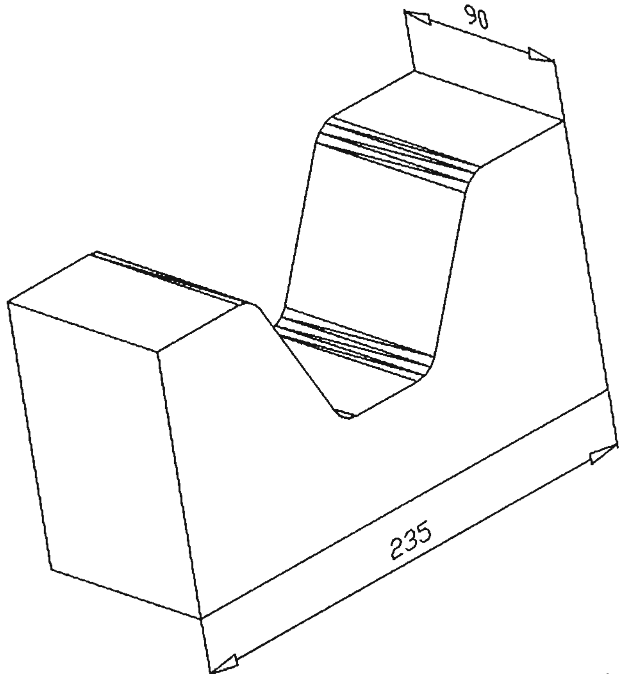

Figure C.8 Geometry of Wooden Support

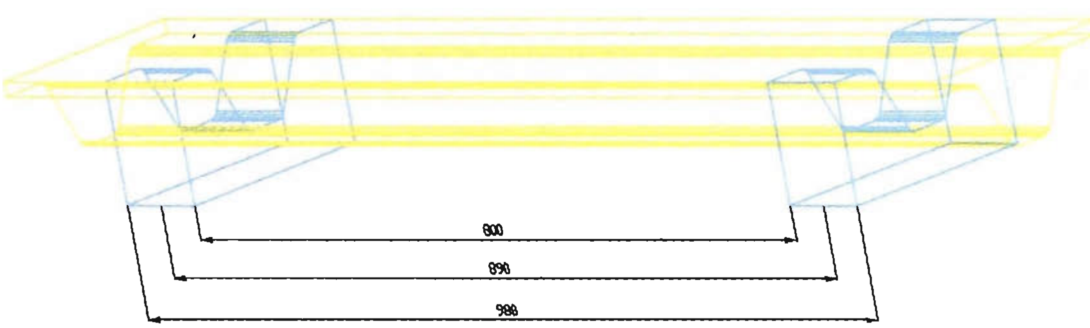

Figure C.9 Different support spans for FE models

Table C.5 Results of sensitivity study on a support span

	SHELL99 & SOLID95	SOLID45	BEAM THEORY	SUPPORT SPAN (mm)
Deflection (mm)	27.3	18.2	16.3	800
Deflection (mm)	40.9	26.1	24.2	890
Deflection (mm)	53.3	35.6	34.2	980

The results from Table C.5 clearly show that SOLID45 element gave close correlation compared to those results obtained from 2-D elastic beam theory and experimental deflection (δ_{max}=28.6mm) considering the 890 mm support span. Hence SOLID45 was used for numerical modeling of the top hat stiffener and top hat stiffened panels.

Appendix D ENERGY ABSORPTION OF THE TOP HAT STIFFENED PANELS

D.1 Introduction

The load/deflection curves of the failure test have been integrated to determine the energy absorption of each to allow comparison of work done to failure. The calculation performed within the framework of this study refers to the top hat stiffened panels in chapter 6. The integration was calculated automatically calculated in the popular design software AutoCAD.

D.2 Integration Results for Top Hat Stiffened Panels

A total of 11 top hat stiffened panels were tested under uniform pressure. Four different designs were used. There were three specimens of each type (denominated as A, B and C). Integration results from the load/deflection plots for each specimen are given Figures D.1 to D11.

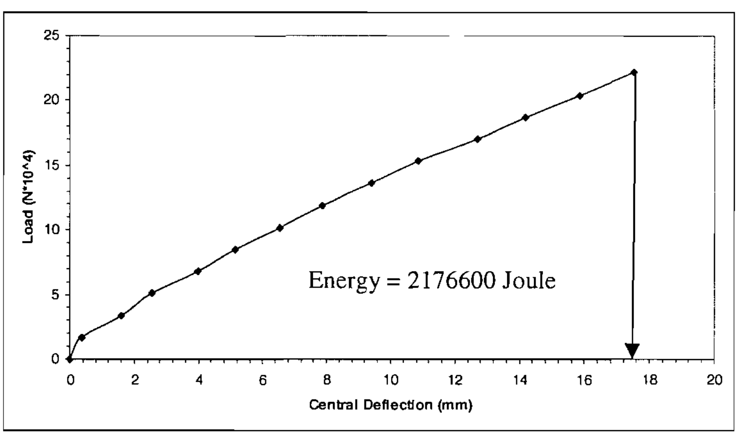

Figure D.1 Integration results for Panel-1A

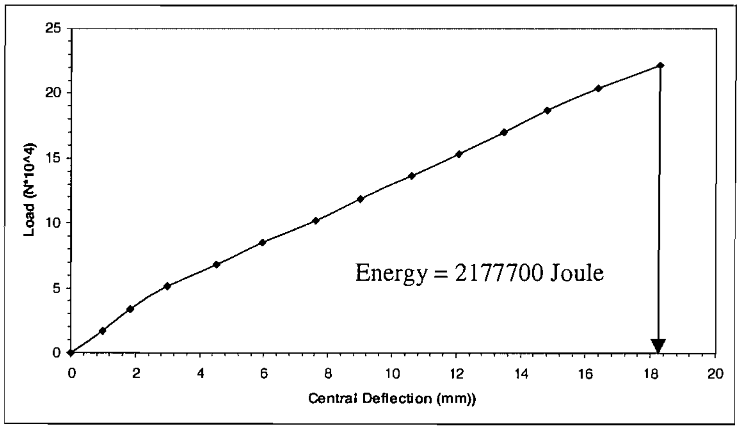

Figure D.2 Integration result for Panel-1B

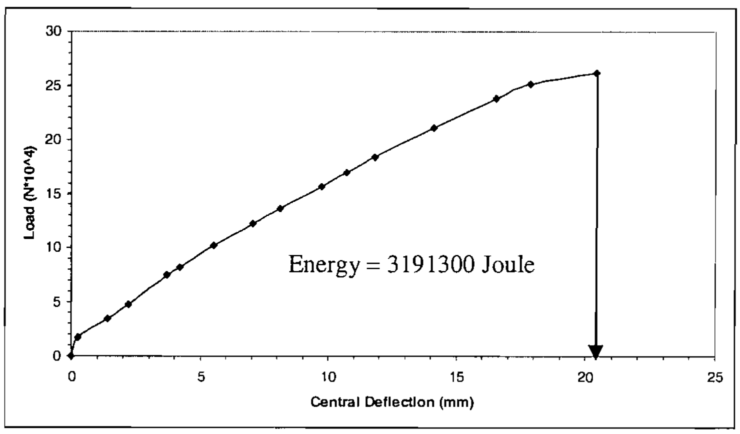

Figure D.3 Integration results for Panel-1C

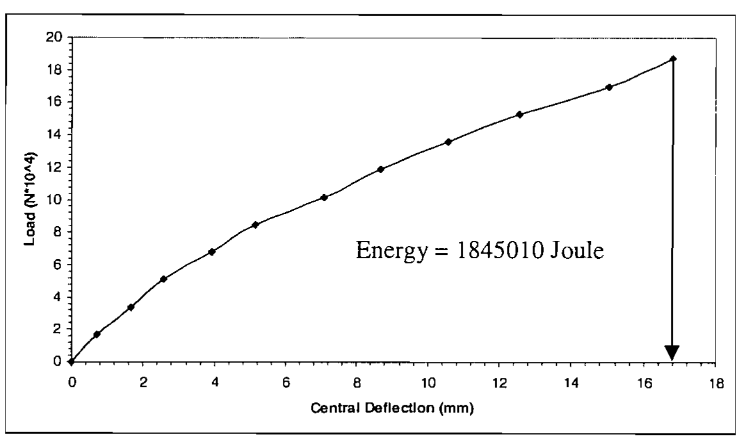

Figure D.4 Integration result for Panel-2A

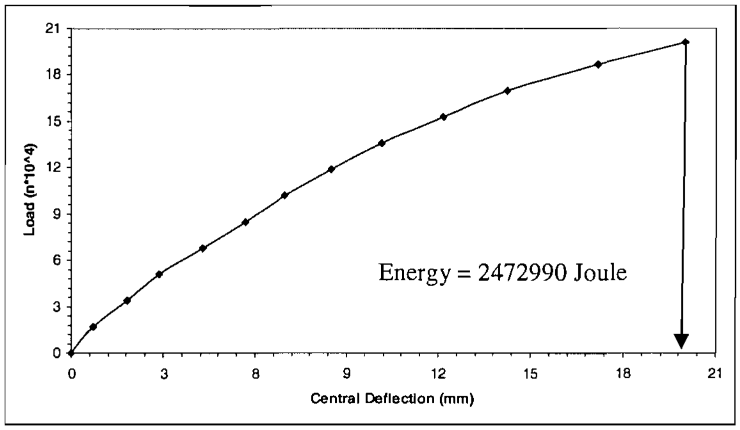

Figure D.5 Integration results for Panel-2B

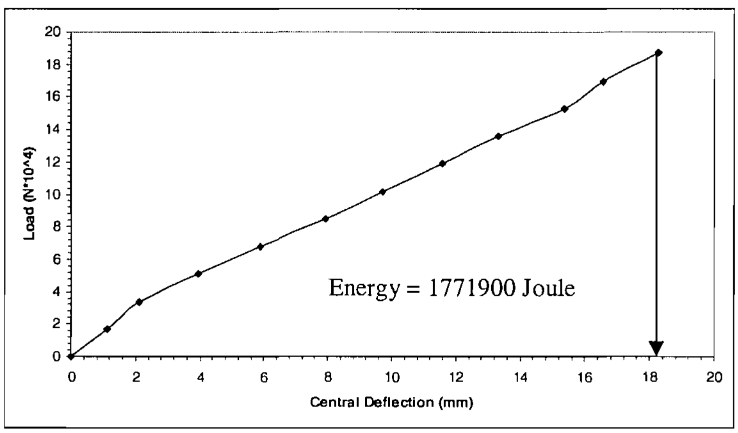

Figure D.6 Integration results for Panel-2C

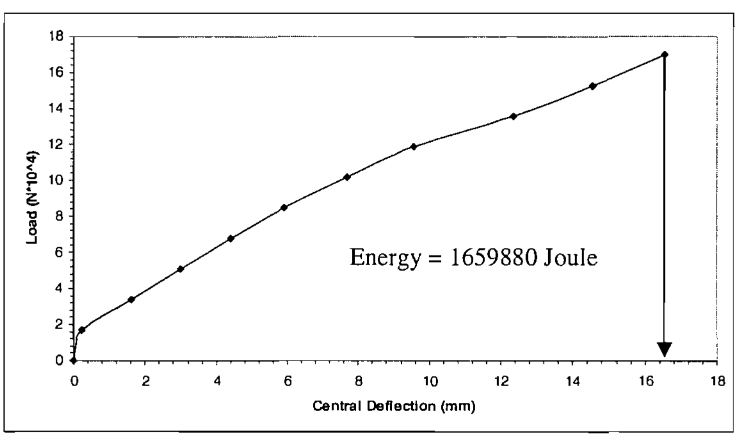

Figure D.7 Integration results for Panel-3A

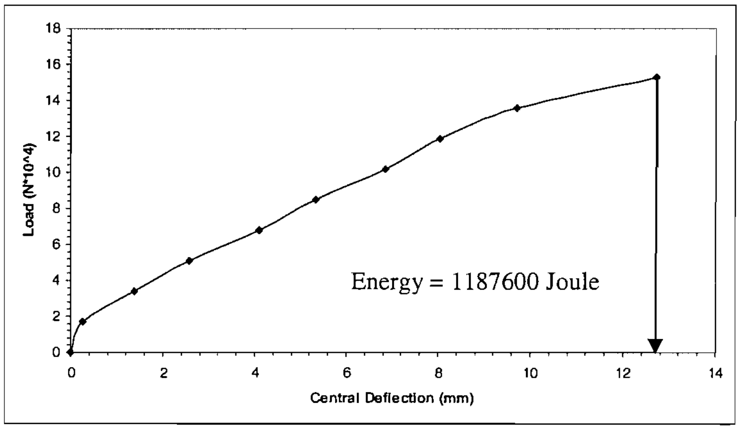

Figure D.8 Integration results for Panel-3C

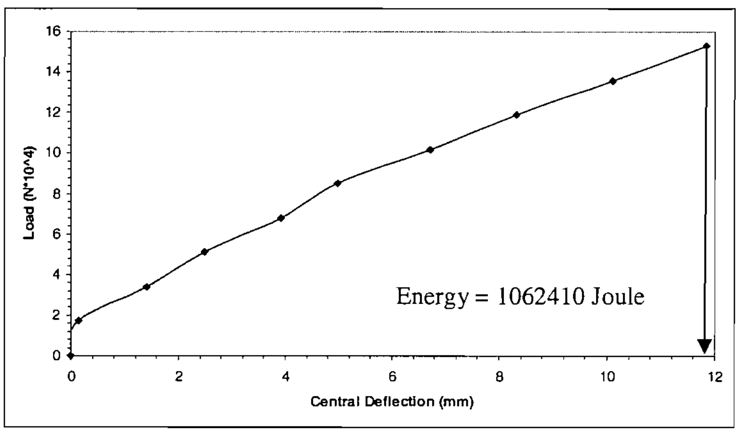

Figure D.9 Integration results for Panel-4A

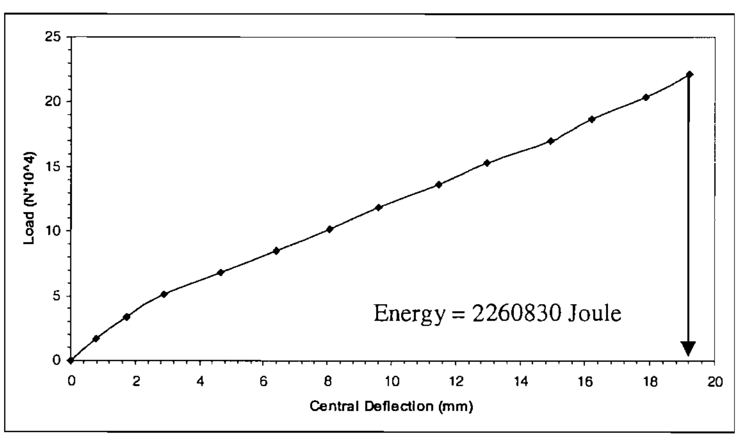

Figure D.10 Integration result for Panel-4B

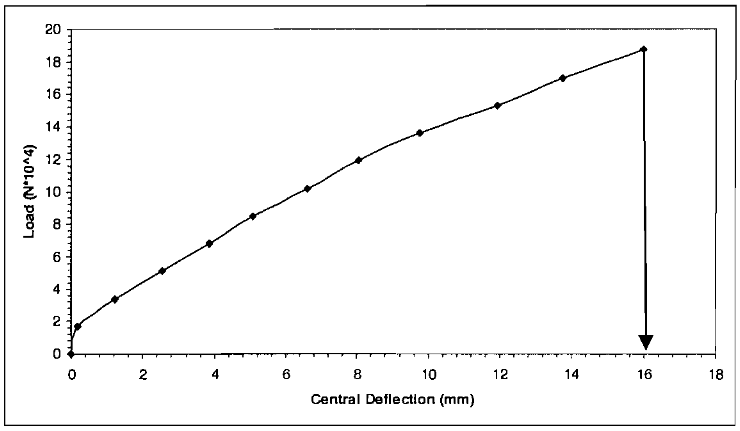

Figure D.11 Integration results for Panel-4C